

AD-A103 069

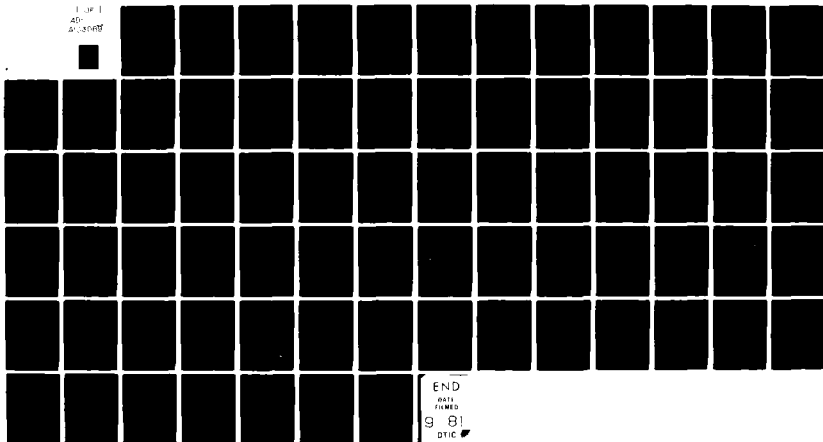
NORWEGIAN DEFENCE RESEARCH ESTABLISHMENT KJELLER
SPACECRAFT AND STELLAR OCCULTATIONS BY TURBULENT PLANETARY ATMOS--ETC(U)
MAY 81 B S HAUGSTAD
NDRE/PUBL-81/1002

F/G 3/2

UNCLASSIFIED

NL

1 OF 1
AD-
AUGUST



END

DATA

FILED

9 81

DTIC

AD A1C3069

**SPACECRAFT AND STELLAR OCCULTATIONS
BY TURBULENT PLANETARY ATMOSPHERES**

**A theoretical investigation of various wave propaga-
tion effects and their impact on derived profiles of
refractivity, temperature and pressure**

BY

BJARNE S HAUGSTAD

NDRE/PUBL-81/1002

ISSN 0085-4301

DTIC
ELECTE
AUG 19 1981
A

FORSVARETS FORSKNING SINSTITUTT
NORWEGIAN DEFENCE RESEARCH ESTABLISHMENT
P O Box 25 - N-2007 Kjeller, Norway

DTIC FILE COPY

81 8 19 040

A theoretical investigation of various wave propagation effects and their impact on derived profiles of refractivity, temperature and pressure

by

Bjarne S Haugstad

ISSN 0085 4301

NORWEGIAN DEFENCE RESEARCH ESTABLISHMENT

May 1981

...and sale; its
...is unlimited.

Special

A

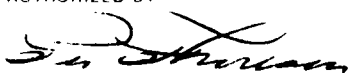
NORWEGIAN DEFENCE RESEARCH ESTABLISHMENT (NDRE)
FORSVARETS FORSKNINGSinSTITUTT (FFI)

POST OFFICE BOX 25
N-2007 KJELLER, NORWAY

UNCLASSIFIED

SECURITY CLASSIFICATION OF THIS PAGE
(when data entered)

REPORT DOCUMENTATION PAGE

1) PUBL REPORT NUMBER NDRE/PUBL -81/1002 1a) DOD REFERENCE 428 -VM/130	2) SECURITY CLASSIFICATION UNCLASSIFIED 2a) DECLASSIFICATION/DOWNGRADING SCHEDULE --	3) NUMBER OF PAGES 75												
4) TITLE SPACECRAFT AND STELLAR OCCULTATIONS BY TURBULENT PLANETARY ATMOSPHERES A theoretical investigation of various wave propagation effects and their impact on derived profiles of refractivity, temperature and pressure														
5) NAMES OF AUTHOR(S) IN FULL (surname first) HAUGSTAD, Bjarne Sigurd														
6) DISTRIBUTION STATEMENT Approved for public release. Distribution unlimited. (Offentlig tilgjengelig)														
7) INDEXING TERMS <table border="0"> <tr> <td>IN ENGLISH</td> <td>IN NORWEGIAN</td> </tr> <tr> <td>a) <u>Radio occultation</u></td> <td>a) <u>Radio formorkning</u></td> </tr> <tr> <td>b) <u>Scintillations</u></td> <td>b) <u>Scintillasjoner</u></td> </tr> <tr> <td>c) <u>Planetary atmospheres</u></td> <td>c) <u>Planeters atmosfærer</u></td> </tr> <tr> <td>d) _____</td> <td>d) _____</td> </tr> <tr> <td>e) _____</td> <td>e) _____</td> </tr> </table> THE SAURUS REFERENCE			IN ENGLISH	IN NORWEGIAN	a) <u>Radio occultation</u>	a) <u>Radio formorkning</u>	b) <u>Scintillations</u>	b) <u>Scintillasjoner</u>	c) <u>Planetary atmospheres</u>	c) <u>Planeters atmosfærer</u>	d) _____	d) _____	e) _____	e) _____
IN ENGLISH	IN NORWEGIAN													
a) <u>Radio occultation</u>	a) <u>Radio formorkning</u>													
b) <u>Scintillations</u>	b) <u>Scintillasjoner</u>													
c) <u>Planetary atmospheres</u>	c) <u>Planeters atmosfærer</u>													
d) _____	d) _____													
e) _____	e) _____													
8) ABSTRACT (continue on reverse side if necessary) <p>The long propagation paths involved in radio and stellar occultations by turbulent planetary atmospheres require that the classical, weak scattering scintillation theory be expanded to account for the inhomogeneous ambient atmosphere upon which the turbulence is superimposed. Such coupling between the turbulent and the ambient components of refractivity reduces the scintillation index by less than a factor of two in shallow radio occultations. For stellar occultations the reduction varies between this value for very small projected stellar radii, to approximately a factor of 3.6 when the projected stellar radius above the planetary limb greatly exceeds the radius of the free-space Fresnel zone at this distance. More profound changes are found in the scintillation power spectrum, the shape of which depends strongly on both occultation depth and geometry when coupling to the inhomogeneous background is properly accounted for.</p> <p>Second-order, systematic propagation effects calculated from both geometrical optics and a wave-optical formulation show that the average phase velocity is <i>increased</i> in the presence of turbulence. The finite ($\lambda^{-1/6}$) wavelength dependence of the phase path bias implies that an initially non-dispersive medium becomes slightly dispersive by the addition of turbulence.</p>														
9) DATE 8 May 1981	THIS PAGE AUTHORIZED BY 	POSITION Superintendent												

UNCLASSIFIED

SECURITY CLASSIFICATION OF THIS PAGE
(when data entered)

UNCLASSIFIED

SECURITY CLASSIFICATION OF THIS PAGE
(when data entered)

ABSTRACT (continued)

Atmospheric profiles derived from occultations by turbulent planetary atmospheres differ only slightly from those of the corresponding non-turbulent atmosphere when the weak scattering condition is satisfied. Even so, there is strong indication that profiles obtained from radio Doppler measurements are much less affected by turbulence than those from radio or stellar intensity measurements. Systematic errors in refractivity, temperature and pressure are all small for either kind of measurement in the limit of weak scattering.

Radio and stellar occultations, when properly conducted and interpreted, are a potential source of information also on turbulence strength, bulk flow scales, planetary rotation and atmospheric winds.

UNCLASSIFIED

SECURITY CLASSIFICATION OF THIS PAGE
(when data entered)

CONTENTS

	Page
1 INTRODUCTION	7
1.1 Historical perspective	7
1.2 Objective and outline	11
2 RADIO AND STELLAR OCCULTATIONS; FORMAL THEORY	13
2.1 Profiles of refractivity, temperature and pressure	13
2.2 Effects of boundary conditions and various measurement errors	16
3 ELECTROMAGNETIC WAVE PROPAGATION IN A NON-TURBULENT PLANETARY ATMOSPHERE	17
3.1 General formulation	17
3.2 Geometrical optics	19
3.3 Wave-optical effects	22
4 PROPAGATION IN A TURBULENT PLANETARY ATMOSPHERE	23
4.1 Phase and intensity in the weak scattering approximation	23
4.2 An atmospheric model	26
4.3 Radio and stellar intensity scintillations	28
4.4 Temporal power spectra	31
4.4.1 Theoretical phase and intensity power spectra	31
4.4.2 Observed power spectra	36
4.5 The weak scintillation approximation in planetary occultations	40
5 PROFILE ERRORS DUE TO TURBULENCE	42
5.1 Random errors in atmospheric profiles from radio or stellar intensity measurements	42
5.2 Random errors in atmospheric profiles from Doppler measurements	43
5.3 Systematic profile errors	45
5.3.1 The second-order phase bias	45
5.3.2 Systematic errors in atmospheric profiles from Doppler or intensity measurements	48
6 TURBULENCE IN DEEP RADIO OCCULTATIONS	50
6.1 General considerations	50
6.2 Scintillation index and power spectrum close to the focus	50
6.3 Applications	53
6.3.1 The Voyager 1 Jupiter encounter	53
6.3.2 The gravitational lens of the sun	54
7 DIAGNOSTICS OF SMALL-SCALE ATMOSPHERIC STRUCTURES	56
7.1 General considerations	56
7.2 Estimation of the turbulence strength	57

	Page
7.3 Estimation of the outer scale	59
7.4 Planetary rotation and atmospheric winds	60
7.5 Practical considerations	61
8 DISCUSSION AND FURTHER PERSPECTIVES	62
Acknowledgements	65
References	65

SPACECRAFT AND STELLAR OCCULTATIONS BY TURBULENT PLANETARY ATMOSPHERES

A theoretical investigation of various wave propagation effects and their impact on derived profiles of refractivity, temperature and pressure

ABSTRACT

The long propagation paths involved in radio and stellar occultations by turbulent planetary atmospheres require that the classical, weak scattering scintillation theory be expanded to account for the inhomogeneous ambient atmosphere upon which the turbulence is superimposed. Such coupling between the turbulent and the ambient components of refractivity reduces the scintillation index by less than a factor of two in shallow radio occultations. For stellar occultations the reduction varies between this value for very small projected stellar radii, to approximately a factor of 3.6 when the projected stellar radius above the planetary limb greatly exceeds the radius of the free-space Fresnel zone at this distance. More profound changes are found in the scintillation power spectrum, the shape of which depends strongly on both occultation depth and geometry when coupling to the inhomogeneous background is properly accounted for.

Second-order, systematic propagation effects calculated from both geometrical optics and a wave-optical formulation show that the average phase velocity is *increased* in the presence of turbulence. The finite ($\lambda^{-1/6}$) wavelength dependence of the phase path bias implies that an initially non-dispersive medium becomes slightly dispersive by the addition of turbulence.

Atmospheric profiles derived from occultations by turbulent planetary atmospheres differ only slightly from those of the corresponding non-turbulent atmosphere when the weak scattering condition is satisfied. Even so, there is strong indication that profiles obtained from radio Doppler measurements are much less affected by turbulence than those from radio or stellar intensity measurements. Systematic errors in refractivity, temperature and pressure are all small for either kind of measurement in the limit of weak scattering.

Radio and stellar occultations, when properly conducted and interpreted, are a potential source of information also on turbulence strength, bulk flow scales, planetary rotation and atmospheric winds.

1 INTRODUCTION

1.1 Historical perspective

Theoretical interpretation of the occultation of stars by planetary atmospheres appears to have originated with Pannekoek (1903), who observed the occultation of a star by Jupiter on September 19 of that year. He recommended that such observations be made carefully: "Because they can give a determination of the temperature distribution in the outermost layers of the planetary atmosphere, or more directly, the way in which the horizontal refraction varies with height". The theoretical problem of deriving a refractivity profile from a luminosity record of the occulted star was later reviewed by Fabry (1929), by Baum and Code (1953), and finally by Link (1969), who was the first to employ numerical inversion techniques to the optical data.

To date observations of stellar occultations have yielded information on the atmosphere of Jupiter through the occultation of σ Arietis (Baum and Code 1953) and the β -Scorpii system (e.g. Hubbard *et al* 1972, Veverka *et al* 1974b). For a review of stellar occultations by Jupiter, see Hunten and Veverka (1976). Structural information on the upper atmosphere of Neptune was similarly obtained by the occultation of BD-17°4388 on 7 April 1968 (Osawa *et al* 1968, Kovalevsky and Link 1968, Freeman and Lynga 1970, Rages *et al* 1974, Veverka *et al* 1974a). Stellar occultations by Mars (Texas-Arizona Occultation Group 1977, Elliot *et al* 1977b, Young 1977), by Venus (de Vaucouleurs and Menzel 1960, Veverka and Wasserman 1974) and by Uranus (Elliot *et al* 1977a, Millis *et al* 1977, Hubbard *et al* 1977) have also been recorded.

With the advent of spacecraft missions to the planets, occultation of the spacecraft itself has become a very important and complementary source of information of the structure of planetary atmospheres. While stellar occultations are limited to fairly tenuous atmospheric regions, spacecraft occultations, by virtue of their much higher signal-to-noise ratio, smaller planet-to-spacecraft distance, and the Doppler frequency as a new data source, have opened up for study much deeper atmospheric regions not accessible to earth-based optical observations. This subject was one of several related bistatic radar experiments introduced by V R Eshleman at the 1962 Review of Space Research conducted at the State University of Iowa by the US National Academy of Sciences (Publication 1079), and early reports by Fjeldbo (1964), Eshleman (1964), and Kliore *et al* (1964) describe details of its scientific and engineering aspects. Since the first encounter of Mars by Mariner 4 on 15 July 1965 (Kliore *et al* 1965, Fjeldbo *et al* 1966a, Fjeldbo and Eshleman 1968), the subsequent occultations of Mariner 5 and 10 by Venus (*e.g.* Kliore *et al* 1967, Mariner Stanford Group 1967, Fjeldbo and Eshleman 1969, Fjeldbo *et al* 1971, Howard *et al* 1974, Fjeldbo *et al* 1975), of Pioneer 10 and 11 by Jupiter (*e.g.* Kliore *et al* 1974, Kliore *et al* 1975, Kliore and Woiceshyn 1976, Fjeldbo *et al* 1975), of Pioneer 11 at Saturn (Kliore *et al* 1980) and the occultations of Voyager 1 and 2 by Jupiter (Eshleman *et al* 1979b) have yielded important new results on the structure of both the atmosphere and ionosphere of these very planets. Additional *in situ* information on temperature, pressure and chemical composition have been provided by the Venera landers descending into the atmosphere of Venus (*e.g.* Vakhnin 1968, Vinogradov *et al* 1968) and recently also by the Pioneer Venus entry probes (Seiff *et al* 1979).

As the potential viability of the occultation technique has been demonstrated in a number of both optical and radio occultations, a question of utmost importance concerns the *accuracy* of the information on atmospheric structure obtained in this way. As it turns out, the answer to this question is far from simple: sources of widely different character and magnitude contribute to the ultimate error. It is remarkable that not until the early analyses of the Pioneer 10 and 11 occultations by Jupiter produced grossly unrealistic results, was the question of accuracy raised on a serious and systematic basis (*e.g.* Eshleman 1975, Hubbard *et al* 1975).

Prior to these difficulties, to which I shall return shortly, stellar occultation profiles had long been suspected of containing substantial errors. An outstanding and contributing factor has here been the large *spikes* in intensity that appear to be a regular feature of stellar occultation light curves. Without doubt, these features, caused by some as yet unknown vertical microstructure in the atmosphere, have hampered the derivation of a refractivity profile from the occultation data, in particular in the earlier days before the numerical inversion technique was introduced by Kovalevsky and Link (1968) to facilitate the analysis of the BD-17°4388 occultation by Neptune. But it is also clear that other major sources of error are present. Perhaps the most dramatic example of the difficulties associated with this technique is provided by the discrepant refractivity profiles obtained by several research groups for the β -Scorpii occultation by Jupiter. Of the six recorded profiles only three seem to approach the factual temperature distribution in the upper Jovian atmosphere (Vapillon *et al* 1973, Hubbard *et al* 1972, Veverka *et al* 1974b). For a review of the β -Scorpii occultations, see Hunten and Veverka (1976). It is clear that meaningful results demand extreme care in both the experimental design phase and also during the recording of data. It is also essential that due regard be paid to the different potential sources of error that may arise in the subsequent data reduction to obtain profiles of refractivity, temperature and pressure (see *e.g.* Wasserman and Veverka 1973, French *et al* 1978).

When the first radio occultation profiles from the Mariner 4 Mars encounter appeared (Kliore *et al* 1965, Fjeldbo *et al* 1966a,b, Fjeldbo and Eshleman 1968), there was no reason to doubt their general validity, except that the upper few scale heights of these profiles were somewhat indeterminate because of partially unknown boundary

conditions, a problem common to both radio and optical occultations. The subsequent occultations of Mariner 5 and 10 by Venus on 19 October 1967 and 5 February 1974, respectively, also yielded results that were in all major respects reasonable (Kliore *et al* 1967, Mariner Stanford Group 1967, Howard *et al* 1974). Indeed, comparisons between the Mariner 5 profiles and that of the Venera 4 landing module (Eshleman *et al* 1968, Eshleman 1970), and between the Mariner 5 and 10 profiles and the Venera 8, 9 and 10 data (Nicholson and Muhleman 1978), display a substantial degree of consistence, both between the individual radio occultation profiles and between these profiles and those of the landers where a comparison could be made. On a finer level it is nevertheless clear that the small differences that still do exist between the different Mariner 10 profiles are not due to either statistical fluctuations in the data processing, or in differing assumptions regarding the initial conditions for the profile computations (Lipa and Tyler 1979). Differences by as much as 10 K between the profile computations of Nicholson and Muhleman (1978) and Lipa and Tyler (1979) and the initial profile of Howard *et al* (1974) probably require an explanation in terms of the difference in computational procedures used to obtain these profiles (Lipa and Tyler 1979).

The high confidence in the radio occultation technique, as a tool for probing planetary ionospheres and atmospheres to depths not accessible to optical occultations, was seriously shaken by the publication of the preliminary temperature-pressure profiles obtained from the Pioneer 10 and 11 encounters with Jupiter on 3 December 1973 and 4 December 1974, respectively (Kliore *et al* 1974, Kliore *et al* 1975). Analysis of the ionospheric part was hampered by multipath propagation until the several simultaneous signals were laboriously sorted out by hand (Fjeldbo *et al* 1975). In the lower neutral atmosphere, temperatures were far in excess of those obtained from radiative-convective balance calculations and on-board radiometric observations (Trafton 1973, Wallace *et al* 1974, Orton and Ingersoll 1976). The radiometric observations fixed the effective atmospheric temperature at 125 ± 2 K at the 500 mb level, far below the ≈ 400 K computed from the first analyses of the Pioneer 10 and 11 occultation data. This circumstance, further aggravated by Gulkis' (Berge and Gulkis 1976) argument that the 13 cm S-band radio signal could not propagate below the 280 K level corresponding to the 13 cm atmospheric brightness temperature of Jupiter, led one to conclude that the Pioneer 10 and 11 radio occultation profiles were in all probability wrong.

This unexpected situation spurred hectic efforts to uncover the problem with the Pioneer occultation profiles. A major source of error, the neglect of planetary oblateness in the inversion calculation to obtain a refractivity profile from the atmospheric phase perturbations, was identified by Hubbard *et al* (1975); see also Hubbard (1976). Almost simultaneously Eshleman (1975) performed a general parametric sensitivity analysis of radio occultation experiments, showing that small errors in either Doppler rate, spacecraft-limb distance or in spacecraft velocity, were magnified by a potentially large factor in such experiments. In the Pioneer 10 entry occultation this factor became as large as ≈ 70 . Eshleman also showed that there was more than one source of major error in the original profiles, although correction for the oblateness or velocity factor did make it possible to produce several temperature-pressure profiles that are both mutually consistent and in reasonable agreement with the Pioneer radiometer observations, in particular in deeper regions of the atmosphere, below about 10 mb, where the effect of partially unknown boundary conditions is rapidly decreasing (Kliore *et al* 1976, Kliore and Woiceshyn 1976).

Simultaneously, and independently of the events described above, a different line of development, from which also the present work arose, sought the explanation for the erroneous Pioneer profiles in terms of *smaller scale* refractive anomalies, such as turbulence, in the Jovian atmosphere. While layers, vertically propagating internal

gravity waves or turbulence had long been suspected of causing the large spikes seen in stellar occultation light curves, virtually no systematic effort was expended up to the year of 1976 to explore these possibilities. For radio occultation a first quantitative step was taken by Hubbard and Jokipii (1975), who calculated the second-order, systematic effect of turbulence on radio occultation profiles derived from Doppler measurements. Hubbard and Jokipii showed that if exponential turbulence was imbedded in an otherwise isothermal atmosphere, the average radio phase would be retarded, progressively with increasing atmospheric depth, and yield a resulting temperature profile that is slightly offset from the true profile of the quiescent atmosphere. The Hubbard-Jokipii calculation was later criticized by Eshleman and Haugstad (1977, 1978) and Haugstad (1976), who showed that the average phase bias caused by the turbulence was in the opposite direction (*i.e.*, the average phase was *advanced*), and furthermore that the analysis, contrary to their claim, was valid only in the limit of geometrical optics which is never realized in radio occultation experiments. It was also demonstrated that taking proper account of diffraction effects both yielded a wavelength dependence of the phase path bias and reduced its magnitude far below the value calculated from geometrical optics (Eshleman and Haugstad 1978, Haugstad 1978b,c,d, Haugstad and Eshleman 1979). While the precise form of this systematic effect of turbulence, its magnitude and the question of wavelength dependence, is still under debate, both parties appear to agree that this propagation effect is too small to be of any practical concern (Hubbard and Jokipii 1977a,b, Haugstad and Eshleman 1979, Hubbard and Jokipii 1979, Hubbard 1979, Eshleman and Haugstad 1979).

Another, and in retrospect more important step to clarify the effect of turbulence, was taken by A T Young (1976). Young considered the larger, first-order random effects of turbulence and argued forcefully that the intensity spikes typical of stellar occultation luminosity curves were uncorrelated on a planetary scale and were in all probability manifestations of turbulence rather than layers or other horizontally extended structures. Developing a hybrid geometrical optics – wave optics scintillation theory that accounted for "coupling" between the turbulence and the inhomogeneous background upon which it is superimposed, Young argued that also radio occultation experiments should be severely contaminated by turbulence effects. Although Young's heuristic approach did not yield the correct form of this coupling effect, which appears as a result of propagation over very long distances, his paper did bring into focus turbulence as a major concern and undoubtedly stimulated other, independent attempts to develop the correct theoretical basis for the first-order, random effects of turbulence (Ishimaru 1977, Haugstad 1977, Haugstad 1978b,c,d,e, Hubbard *et al* 1978, Haugstad 1979a, Woo *et al* 1980). These analyses showed that Young's heuristic model seriously overestimated the effect of turbulence and furthermore indicated that previous spacecraft occultation profiles may not have been seriously affected by turbulence (Haugstad 1978d,e).

Along a parallel line of development, interest was shifted from the possible degrading effect of turbulence on radio occultation profiles, to the possibility of extracting from the radio signal characteristics of the underlying turbulence. As stressed by Woo *et al* (1974), information on the strength and spatial extent of turbulence is important as a means of constraining theoretical circulation models of planetary atmospheres. Not surprisingly, developing procedures for extracting such information turned out to be but another aspect of the general problem of electromagnetic wave propagation in a randomly inhomogeneous medium with inhomogeneous (and possibly anisotropic) mean characteristics. The pioneering work here was done by R Woo and A Ishimaru, who applied standard weak scintillation theory to conditions typical of radio occultations of planetary spacecraft (Woo and Ishimaru 1973, Woo and Ishimaru 1974). The theory, not yet accounting for the coupling effect discussed earlier, was subsequently applied to the Mariner 5 and 10 occultations

to yield rough estimates of the scintillation index and structure constant in regions where turbulence could be reliably identified (Woo *et al* 1974, Woo 1975a); see also Gurvich (1969), and Golitsyn and Gurvich (1971). The theory was later expanded by Haugstad (1978c,d,e), Hubbard *et al* (1978), and by Woo *et al* (1980) to include effects of coupling to the inhomogeneous ambient atmosphere. Power spectra of phase (Haugstad 1979a) and intensity scintillations (Haugstad 1979a, Woo *et al* 1980) were calculated for a range of different occultation geometries and discussed in terms of their potential usefulness for deriving turbulence characteristics from the radio occultation data.

Even though the past 5–6 years have seen major advances in the theory of turbulence effects in radio and optical occultations, fundamental problems still remain unsolved. A common feature of all the turbulence theories quoted here, for example, is their limitation to weak scattering conditions. While strong scattering theories suitable for short-path, terrestrial propagation conditions have been successfully formulated during the past decade (for a review, see *e.g.* Fante 1975), inclusion of the inhomogeneous background essential to radio and optical occultation conditions, still poses an unsolved problem in the context of strong scattering. This and other related problems, to be considered in the next section, undoubtedly constitute a principal challenge to future theoretical work in this field.

1.2 Objective and outline

The general problem to be addressed in this report is twofold:

- a) To establish, by theoretical analysis, the effect of turbulence on radio and stellar occultation temperature and pressure profiles
- b) To provide a theoretical basis from which the characteristics of turbulence in planetary atmospheres can be derived from occultation measurements

In order to uncover the various facets of this extensive problem and, at the same time, provide a justification for the particular aspects of this problem that will be subjected to detailed examination here, it is convenient to consult the schematic illustration in Figure 1.1. In order to solve the problem specified above, an essential first step will be to formulate a realistic model of both the quiescent, ambient

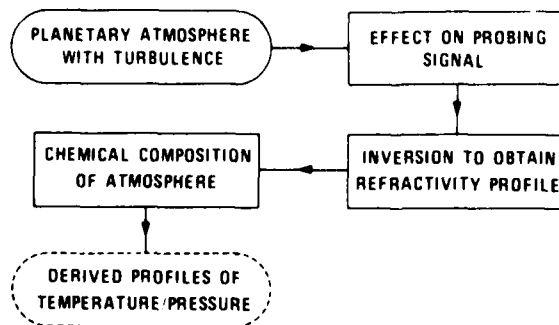


Figure 1.1 Schematic illustration of the effect of turbulence on atmospheric profiles derived from occultation measurements

atmosphere and the turbulence. Once established, the problem consists of calculating its effect on the probing electromagnetic signal. The resulting signal, contaminated by effects due to turbulence, is then subjected to the standard inversion algorithm (*i.e.* to its mathematical representation), by which a profile of refractivity versus height is constructed from the probing signal. Knowing the effect of the turbulence on this signal allows one, at least in principle, to calculate also the corresponding effect of the turbulence on the refractivity profile. If, furthermore, the chemical composition of the atmosphere is known, also profiles of temperature and pressure may be computed and separated, at

least in principle and in an average sense, into an ambient part and a fictitious component caused by turbulence.

While this procedure is in principle complete and will solve the stated problem, difficulties arise on different levels when *practical* solutions are sought. For instance, when applying the result of an analysis of this sort to any specific occultation, a principal difficulty arises from the fact that the characteristics of the turbulence, which will affect the outcome of the wave propagation analysis, is usually not known *a priori*. The problem is therefore iterative in nature: from a crude model of the turbulence its effect on the probing signal may be computed and compared with the actually observed signal. From this comparison a refined turbulence model, closer to the factual distribution of turbulence, may in principle be constructed, etc.

But also major technical problems arise when implementation of the scheme in Figure 1.1 is attempted. As in terrestrial propagation experiments, the effect of turbulence on electromagnetic radiation frequently falls into one of the two limiting categories of weak or strong scattering. In the former case the fluctuations in signal strength are small in terms of the mean signal, whereas in strong scattering the root-mean-square fluctuations are comparable to the mean signal strength (saturated scintillations). While weak scattering theories were fully developed by the mid-sixties, only more recently have strong scattering theories, due to their greater mathematical complexity, been developed into explicit forms that allow confrontation with observations. In radio occultations two additional factors add to the complexity of this problem: (i) the actual inhomogeneous nature of the ambient atmosphere cannot be neglected, as is routinely done in propagation theories tailored to terrestrial conditions involving much shorter path lengths, and (ii) the fluctuations in angle of arrival of the wavefront, a key quantity for assessing the effect of turbulence on atmospheric profiles derived from Doppler measurements, requires also the precise spatial extent of the turbulence to be stipulated (local properties are not sufficient) and leads to a very complicated analysis. (For stellar occultations *only the former* of these complications applies.) We also note that, because of the non-linear relationship between the turbulent refractivity fluctuations and the amplitude and phase, the calculated profiles of temperature and pressure contain both a *systematic* and a *random* part. During weak scattering conditions the systematic effect will be of second order in small quantities, and hence much smaller than the leading first-order, random effect.

Having described and categorized above the full problem, we here restrict ourselves to giving a detailed treatment of certain, however important, aspects of the overall problem, essentially covering and expanding on the material developed in the quoted publications by this author (Haugstad 1978b,c,d,e, Haugstad 1979a, Eshleman and Haugstad 1977, Eshleman and Haugstad 1978, Eshleman and Haugstad 1979, Haugstad and Eshleman 1979, Haugstad 1980). Thus, giving an exposé of the basic theory of radio and stellar occultations in section 2, we proceed to develop in section 3 the theory of electromagnetic wave propagation in a non-turbulent atmosphere as the limiting form of a general wave-optical formulation. From this approach the error incurred by the routine neglect of wave-optical effects in the conventional occultation theories is readily assessed. In section 4 the *weak scattering* theory of radiation propagating through a turbulent planetary atmosphere is developed from a stationary phase method (Haugstad 1978c). After having established an atmospheric model, the resulting formulae are used to derive explicit results for the weak scattering scintillation index in both radio and stellar occultation experiments. We establish here also the form of the power spectra of the fluctuations in phase and intensity, and compare the predicted spectra with experimental data from the encounters of Mariner 5 and 10 with Venus. Section 4 concludes with a general discussion of the validity of the weak scattering approximation, which is a fundamental limitation of all the results derived in this work. In section 5 we investigate to what extent turbulence, again within the realm of weak scattering, affects the derived profiles of temperature and pressure. Answering this question turns out to be relatively simple for atmospheric

profiles derived from stellar or radio occultation intensity measurements. However, for atmospheric profiles derived from radio Doppler measurements the technical problems are formidable, as previously indicated. For this case a physical, semi-quantitative approach avoiding the core of the mathematical difficulties has been adopted. The section concludes with a discussion of the small systematic effects of turbulence on occultation profiles. In section 6 we devote attention to a relatively new topic in this field: the effect of turbulence in deep radio occultation measurements. The basic theory of deep radio occultations (Eshleman *et al* 1979a) is combined here with the scintillation theory developed in section 4 to yield results for the scintillation index and power spectrum close to a refractive focus (Haugstad 1981). The theory is applied to deep radio occultations of planetary atmospheres (the Voyager 1 Jupiter encounter), and to the suggested use of the gravitational lens of the sun for cavedropping and communication over interstellar distances (Eshleman 1979). We conclude the present work in section 7 by discussing a general procedure by which information on the strength and spatial distribution of turbulence may be extracted from occultation measurements, exploring both the potential feasibility and the inherent limitations of this scheme. Section 8 summarizes the results of the present work, and expands the perspective by recommending where future work in this field should be directed.

2 RADIO AND STELLAR OCCULTATIONS; FORMAL THEORY

2.1 Profiles of refractivity, temperature and pressure

The derivation of vertical profiles of temperature and pressure from occultation measurements proceeds in two stages. In the first a refractivity profile is determined from the atmospheric perturbations of either phase or intensity of the probing signal. In the second stage the refractivity profile is used together with possible knowledge about the chemical composition of the atmosphere to calculate profiles of temperature and pressure.

For the first of these steps, consider Figure 2.1 which illustrates a spacecraft partially occulted by a planetary atmosphere, the refractivity of which is assumed to be a

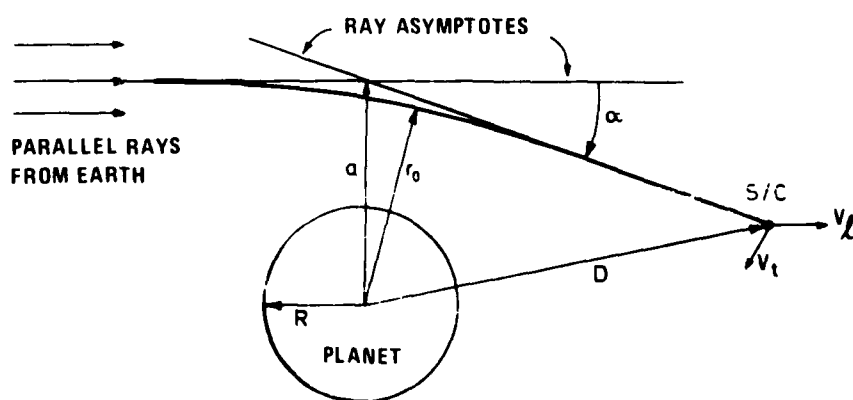


Figure 2.1 Ray path and simplified occultation geometry defining the ray bending angle α , the impact parameter a , the radial distance to the point of closest approach (periapsis) r_0 , and the planet to spacecraft distance D as measured from the planetary centre

The spacecraft velocity is resolved into a component v_{\parallel} parallel to the incoming ray asymptote, and a component v_{\perp} in the plane of the sky.

function of the radial coordinate only. (For stellar occultations the earth replaces the spacecraft and D is now the planet-to-earth distance.) It is assumed throughout that $r_0 > r_{0c}$, where r_{0c} is the level of superrefraction, below which the ray encircles the planet and fails to reach the spacecraft. (For a discussion of this interesting possibility, see Lipa and Croft (1975), who also calculate the refractive attenuation of the critical ray.)

Let the refractive index $n = 1 + \nu$, where ν is the atmospheric refractivity. The quantities n and α are related by an Abelian transform pair (e.g., Fjeldbo *et al* 1971, Phinney and Anderson 1968)

$$\alpha(a) = -2a \int_a^\infty \frac{dn}{d\xi} \frac{d\xi}{n(\xi^2 - a^2)^{1/2}} \quad (2.1a)$$

$$\pi \ln n(r_0) = - \int_a^\infty \frac{d\alpha(a')}{da'} \cosh^{-1} \left(\frac{a'}{a} \right) da' \quad (2.1b)$$

where $\xi \equiv nr$, and where r_0 and a are related by Bouguer's rule (Born and Wolf 1975) as in

$$a = n(r_0) r_0 \quad (2.2)$$

Let \mathbf{k} ($k \equiv |\mathbf{k}| = 2\pi/\lambda$) be the vector wavenumber of the radio wave after refraction. If the planet is assumed stationary with respect to the earth, the additional Doppler frequency f caused by atmospheric refraction through an angle α is

$$-\lambda f = \hat{\mathbf{k}} \cdot \mathbf{v} = v_t (\cos \alpha - 1) + v_t \cos \theta \sin \alpha \quad (2.3a)$$

where $\hat{\mathbf{k}} \equiv \mathbf{k}/k$, and where θ is the (positive) angle between v_t and the plane of refraction. If \mathbf{v} is lying entirely in the plane of propagation ($\theta=0$), the simpler first-order form of equation (2.3a) is

$$-\lambda f = v_t \alpha \quad (2.3b)$$

From extrapolation of radio tracking data during times when there is no atmospheric perturbations of the radio wave, the position and velocity of the spacecraft are known. According to equations (2.3a) or (2.3b), a measurement of the atmospheric Doppler f yields the bending angle α and hence the impact parameter a . From corresponding values of α and a , the differential $d\alpha/da$ may be formed and hence, upon performing the indicated integration in equation (2.1b), the refractive index corresponding to a given impact parameter is obtained. Application of the Bouguer-relation (2.2) finally yields the desired $n(r_0)$ -profile.

Calculation of a refractivity profile from stellar or radio occultation intensity measurements follows an essentially similar path. The fundamental equation is still (2.1b), but now $d\alpha/da$ is expressed in terms of the *intensity* of the probing signal. Indeed, for small bending angles and neglecting focusing of the wavefront around the curved limb ($\alpha D \ll R$), geometrical optics flux conservation yields for the intensity ϕ of the near-limb ray

$$1 - \phi^{-1} = D d\alpha/da \quad (2.4)$$

when ϕ is normalized to unity before refraction. Thus, since $a(t)$ is known, a measurement of ϕ versus time t establishes $d\alpha/da$, and via equations (2.1b) and (2.2) also the refractivity as a function of atmospheric depth.

For an isothermal atmosphere, where ν varies exponentially with height with a constant scale height H , equation (2.4) may be manipulated to yield

$$\frac{v_{\perp}}{H} = \left(\frac{1}{\phi} - 2\right) + \ln\left(\frac{1}{\phi} - 1\right) \quad (2.5)$$

Here v_{\perp} is the component of the spacecraft velocity in the plane of refraction that is perpendicular to the ray before refraction. The time t is taken to be zero when $\phi = 1/2$, *i.e.*, corresponding to the nominal *occultation level*. An essentially identical form of equation (2.5) was first derived by Baum and Code (1953) and has since been used extensively in the interpretation of stellar occultation measurements. Thus, for an isothermal atmosphere the intensity-time profile $\phi(t)$ yields the temperature T directly if the mean molecular mass m is known, since $T = mgH/K$, where g is the acceleration of gravity and K is Boltzman's constant.

Equations (2.4) and (2.5) strictly apply only to a point source. For stellar occultations the intensity ϕ should be convolved with the brightness distribution of the projected stellar image in the occulting atmosphere. As shown by P J Young (1977), however, the resulting corrections for the finite angular width of the star are normally altogether negligible

Once a refractivity profile has been obtained from either Doppler or intensity measurements, the hydrostatic equation may be integrated to yield the temperature profile $T(r_0)$, and by the perfect gas law also the pressure profile $p(r_0)$. In a well-mixed atmosphere of non-polar molecules we have (*e.g.*, Fjeldbo and Eshleman 1968)

$$T(r_0) = T(r_{01}) \frac{\nu(r_{01})}{\nu(r_0)} + \frac{m}{K \nu(r_0)} \int_{r_{01}}^{r_0} g(r'_0) \nu(r'_0) dr'_0 \quad (2.6)$$

$$p(r_0) = \frac{KT(r_0)}{v_m} \nu(r_0) \quad (2.7)$$

In these equations m is the (constant) mean molecular mass of the atmospheric constituents, v_m is the mean "refractivity volume" (*i.e.*, the refractivity at standard conditions divided by Loschmidt's number), and K is Boltzman's constant. Equation (2.6) assumes a boundary condition high in the atmosphere at $r_0 = r_{01}$.

Having reviewed the formal occultation theory it is appropriate to add a few comments relative to our objective, as stated in section 1.2. We note first that the procedure described above assumes the atmospheric refractivity to be spherically stratified. Turbulence, representing small inhomogeneities in ν over a continuum of scale sizes, clearly violates this provision. One might think that, since occultation experiments are sensitive to atmospheric properties over a distance $\ell \cong (RH)^{1/2}$ in the direction of the ray, the calculated refractivity profile when turbulence is present would contain an additional component equal to the *average* turbulent refractivity over the distance ℓ . This is not the case, however. As indicated in section 1.2, turbulent refractivity fluctuations in fact produce changes in signal strength that grow with distance and may eventually become comparable to the mean occulted intensity, even though the turbulent refractivity fluctuations are a small fraction only of the ambient refractivity. The intensity fluctuations also depend on the radiation wavelength λ , whereas the geometrical optics intensity formulae (2.4) and (2.5) by their nature are independent of λ . We thus conclude that turbulent refractivity fluctuations cause the derived refractivity profile to depart from the "true" profile of the ambient atmosphere in ways that may be largely independent of the generic fluctuations in refractivity at the ray periapsis. For these reasons, exploring the effects of turbulence on atmospheric profiles obtained from occultation measurements constitutes both a legitimate and important scientific endeavour.

2.2 Effects of boundary conditions and various measurement errors

For practical reasons the integration in equation (2.1b) has to be truncated at some upper limit $a' = a_1$, say. For an isothermal atmosphere the resulting *fractional* error in derived refractivity, δ_ν , is approximately (Wasserman and Veverka 1973)

$$\delta_\nu = 1 - \operatorname{erf}[\beta(r_{01} - r_0)] \quad (2.8)$$

where $\beta^{-1} = H$ is the scale height, $\operatorname{erf}(\cdot)$ is the error function, and r_{01} is related to a_1 via Bouguer's rule. The form of equation (2.8) implies that the refractivity error decreases rapidly with increasing penetration of the ray; for $r_{01} - r_0 = 2H$, $\delta_\nu \approx 5\%$, while three scale heights below the starting point of the integration $\delta_\nu \approx 1.5\%$. From equations (2.6) and (2.7) it is found that also the associated temperature and pressure errors decrease rapidly below the first few scale heights of these profiles.

An additional error in T or p arises from the essentially unknown boundary condition in temperature. From equations (2.6) and (2.7) it is seen that an error $\Delta T(r_{01})$ in the boundary temperature yields errors

$$\Delta T(r_0) = \Delta T(r_{01}) \frac{\nu(r_{01})}{\nu(r_0)} \quad (2.9)$$

and

$$\Delta p(r_0) = \frac{K\nu(r_{01})}{v_m} \Delta T(r_{01}) \quad (2.10)$$

in temperature and pressure, respectively, at depth r_0 . While the temperature error decreases rapidly with depth (*e.g.*, exponentially for an isothermal atmosphere), the absolute pressure error is constant with depth. The *fractional* error in pressure decreases rapidly with atmospheric depth, however.

The effect of different types of measurement errors on the determination of p and T has been considered by Eshleman (1975), and in part also by Hubbard *et al* (1975). Following Eshleman (1975), the temperature scale height of an assumed isothermal atmosphere may be expressed in terms of spacecraft trajectory data, the radio Doppler f , and its time derivative df/dt as in

$$\frac{\lambda f D}{v_1 H} \left(\frac{v_1^2}{\lambda D |df/dt|} - 1 \right) = 1 \quad (2.11)$$

Alternatively this relation may be written as

$$M(S - 1) = 1 \quad (2.12)$$

where the dimensionless magnitude factor M and the sensitivity factor S are defined by comparison. Since M for planetary occultations may reach a hundred or more, S only slightly exceeds unity over most of the atmospheric region probed. As pointed out by Eshleman (1975), S is identically unity for bending around a fixed limb ($H=0$), as in classical knife-edge diffraction. All information about atmospheric structure is therefore contained in the small excess of S over unity.

Referring to equations (2.11) and (2.12), absolute errors ΔS in S and $\Delta(\alpha D) = \Delta(\lambda f/v_1)$ in the deflection of the ray produce a fractional error in H given by

$$\frac{\Delta H}{H} = M\Delta S + \frac{\Delta(\alpha D)}{\alpha D} \quad (2.13)$$

Thus fractional errors in any of the quantities v_1^2 , D , λ or $|df/dt|$ comprising S are magnified by the potentially large factor $M = \alpha D/H$, while a fractional error in α (*i.e.*,

in f) produces only a comparable error in H . If $|df/dt|$, D or λ equals $(1-\Delta)$ times its true value, or if the derived v_1^2 is $(1+\Delta)$ times its true value, then to first order in Δ and for large M (Eshleman 1975)

$$\frac{T_f}{T_t} = 1 + M\Delta \quad (2.14a)$$

$$\frac{p_f}{p_t} = \left(\frac{T_f}{T_t} \right)^{3/2} \quad (2.14b)$$

where T_f and T_t denote the false and true temperature profiles, respectively, and with a similar notation for p .

Despite the potentially large error in derived profiles induced by small errors in S , temperature/pressure profiles derived from Doppler measurements are still more accurate than corresponding profiles derived from radio or stellar occultation intensity measurements, provided that the radio Doppler can be measured at least M times more accurately than the intensity, which is normally the case. From equation (2.5) it is indeed found that errors in either v_1 or ϕ yield comparable errors in the scale height determination, and hence in T . This is also the reason why stellar occultations are routinely terminated when the residual light flux is comparable to the expected error in baseline determination, which is typically a few per cent.

Digitization and subsequent data processing also introduce errors in the final T - p profiles. Such errors are highly dependent on signal to noise ratio during data transmission, and on the specifics of the data processing algorithms used, as discussed in detail by Lipa and Tyler (1979).

The previous analysis apparently allows the following arguments to be made concerning the effect of turbulence on occultation profiles. Turbulence causes the actually observed bending angle α to deviate slightly from the "true" value of the quiescent, non-turbulent atmosphere. According to equation (2.13), a change in α produces a comparable (*i.e.* small) error in H and hence in T if these quantities are obtained from radio Doppler measurements. Atmospheric profiles derived from intensity measurements, on the other hand, contain errors that are comparable to those in intensity according to equation (2.5). Since intensity scintillations due to turbulence may become comparable to ϕ itself, it follows that the resulting temperature error may also be appreciable, unless some "smoothing" procedure is applied that suppresses the scintillations. We shall see from the more stringent analysis in section 5 that these contentions are indeed true.

3 ELECTROMAGNETIC WAVE PROPAGATION IN A NON-TURBULENT PLANETARY ATMOSPHERE

3.1 General formulation

Standard formulations of electromagnetic wave propagation in a spherically symmetric, non-turbulent atmosphere are based on geometrical optics. The rationale for this is the fact that the radius of the first Fresnel zone is smaller than the atmospheric scale height by typically a factor on the order of 10, cf Table 3.1. We depart here from the common geometrical optics approach by formulating the propagation problem in a wave-optical context, from which the proper approximations leading to the standard geometrical optics results will appear in a natural way. The small wave-optical corrections to these results are also readily obtained from this approach, which also provides the notational framework for the generalization in section 4 of

OCCULTATION	H	D	$a_{F,0}$	$a_{S,0}$
MARINER 10/VENUS	10	$1.5 \cdot 10^4$	1.4	—
MARINER 4/MARS	9	$2.6 \cdot 10^4$	1.8	—
PIONEER 10/JUPITER	30	$2.2 \cdot 10^5$	5.3	—
VOYAGER 1/JUPITER	30	$5.6 \cdot 10^5$	7.3	—
β ScoA/JUPITER	30	$6.5 \cdot 10^8$	0.57	0.55
BD17°4388/NEPTUNE	60	$4.5 \cdot 10^9$	1.5	5

Table 3.1 Representative values for various radio and stellar occultations

The table gives representative values for the scale height H , approximate planet-to-spacecraft (or earth) distance D , radius of the free-space Fresnel zone $a_{F,0}$, and projected linear radius $a_{S,0}$ of two occulted stars. All lengths are in kilometers. The two stars are observed at $\lambda = 0.5 \mu\text{m}$, while $\lambda = 0.13 \text{ m}$ (S-band) has been assumed in the calculation of $a_{F,0}$ for the radio occultations.

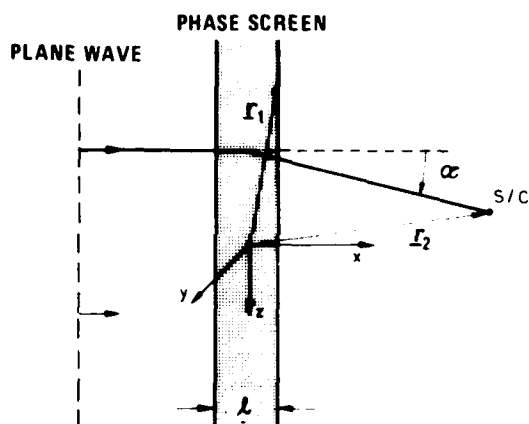


Figure 3.1 A phase-changing screen of thickness $l \ll D$ represents the inhomogeneous ambient atmosphere

Position vectors \mathbf{r}_1 and \mathbf{r}_2 refer to the exit face of the screen and an arbitrary field point a distance $|\mathbf{r}_2| \approx D \gg l$ from the screen, respectively

$$E(\mathbf{r}_2) = \frac{k}{2\pi i} \iint_{-\infty}^{\infty} E(\mathbf{r}_1) \frac{\exp[ik|\mathbf{r}_2 - \mathbf{r}_1|]}{|\mathbf{r}_2 - \mathbf{r}_1|} \cos(\hat{\mathbf{n}}, \hat{\mathbf{e}}) d\mathbf{r}_{1\perp} \quad (3.1)$$

where $d\mathbf{r}_{1\perp} = dy_1 dz_1$ is a differential area on the exit plane $x = l/2$ of the screen. The obliquity factor, $\cos(\hat{\mathbf{n}}, \hat{\mathbf{e}})$, accounts for the angle between the normal $\hat{\mathbf{n}}$ to the phase screen and the direction $\hat{\mathbf{e}} = (\mathbf{r}_2 - \mathbf{r}_1)/|\mathbf{r}_2 - \mathbf{r}_1|$ to the observer. If the spatial extent of the refracting medium perpendicular to the raypath is small compared to D , the angle $\angle \hat{\mathbf{n}}, \hat{\mathbf{e}} \approx 0$ and $\cos(\hat{\mathbf{n}}, \hat{\mathbf{e}}) \approx 1$, while $|\mathbf{r}_2 - \mathbf{r}_1| \approx D$. This paraxial approximation is assumed throughout. Consistent with the thin screen approximation, an incident plane wave of unit amplitude has an electric field at exit given by $E(\mathbf{r}_1) = \exp(ikS_0)$, where S_0 is the change in phase path through the screen. We shall see in section 3.2 that, consistent with the thin screen approximation, the phase change may be calculated by integrating ν_0 along a straight line path through the screen, instead of following the

the weak scattering scintillation theory to include the inhomogeneous ambient atmosphere.

We shall assume throughout that the effect of the actual atmosphere on electromagnetic waves may be represented by a thin slab of thickness $l \ll D$ and refractivity ν_0 , the effect of which is to change the phase of the wave but leaving its amplitude unchanged, see Figure 3.1. We shall find that this thin screen approximation is always valid for ray bending angles $\alpha \ll (H/R)^{1/2}$, where H is a typical scale of variation of the spherically stratified atmosphere.

Let $E(\mathbf{r}_1)$ be the complex electric field of the wave in the plane $x = l/2$ upon exit from the phase screen. In position \mathbf{r}_2 behind the screen the field is (e.g., Goodman 1968)

actual curved raypath. Thus $S_0 = \int \nu_0(x, y_0, z_0) dx$, where (y_0, z_0) are the lateral coordinates of the ray upon entering the screen. If $\ell = (2\pi RH)^{1/2}$, it also follows that $S_0 = \nu_0 \ell$, where ν_0 is now referred to the ray periapsis of the actual exponential atmosphere of scale height H .

With these provisions equation (3.1) may be expressed in the form

$$E(\mathbf{r}_2) = \frac{k}{2\pi i D} \iint_{-\infty}^{\infty} e^{i \frac{k}{2D} \psi} d\mathbf{r}_{1L} \quad (3.2a)$$

where

$$\psi \equiv 2D(D + S_0) + (y_2 - y_1)^2 + (z_2 - z_1)^2 \quad (3.2b)$$

Following Haugstad (1978c) (see also, Hubbard and Jokipii 1977b), we expand ψ around the point of stationary phase (y_0, z_0) of the integrand, i.e.

$$\psi = \sum_{i,j=0}^{\infty} c_{ij} (y_1 - y_0)^i (z_1 - z_0)^j \quad (3.3a)$$

where

$$c_{ij} = \frac{1}{i! j!} \left. \frac{\partial^{i+j} \psi}{\partial y^i \partial z^j} \right|_{\substack{y_1=y_0 \\ z_1=z_0}} \quad (3.3b)$$

The stationary phase point is defined by the conditions $c_{01}(y_1=y_0, z_1=z_0) = c_{10}(y_1=y_0, z_1=z_0) = 0$, yielding

$$y_0 = y_2 - D\beta, \quad z_0 = z_2 - D\alpha$$

where α and β are the ray bending angles in the xz - and xy -plane, respectively, as given by $\alpha = \int \nu_{0,z}(x, y_0, z_0) dx$ and $\beta = \int \nu_{0,y}(x, y_0, z_0) dx$. (Subscripts y, z, yy, yz , etc denote partial differentiation in the usual way.) Successive determination of the remaining coefficients c_{ij} yields, through second order

$$\begin{aligned} c_{00} &= 2D^2 \left[1 + \frac{1}{2} (\alpha^2 + \beta^2) \right] + 2DS_0 \\ c_{01} &= c_{10} = 0 \\ c_{02} &= 1 + M, \quad c_{11} = 0, \quad c_{20} = 1 + N \end{aligned} \quad (3.4)$$

The two quantities M and N play a central role in the subsequent analysis; they are defined by

$$M = \int \nu_{0,zz}(x, y_0, z_0) dx, \quad N = \int \nu_{0,yy}(x, y_0, z_0) dx \quad (3.5)$$

where the integration is again understood to be through the screen from $x = -\ell/2$ to $x = \ell/2$.

Equations (3.2)–(3.5) constitute the basic mathematical framework for the subsequent analysis in this and also in the next main section.

3.2 Geometrical optics

We shall assume, tentatively, that the stationary phase expansion (3.3) can be truncated after the second-order terms, i.e., we define $c_{ij}(i+j > 2) = 0$. In this case equation (3.2a) becomes

$$E(r_2) = \frac{ke^{i\frac{c_{00}}{2D}}}{2\pi i D} \iint_{-\infty}^{\infty} e^{i\frac{k}{2D} [\phi_y^{-1}(y_1 - y_0)^2 + \phi_z^{-1}(z_1 - z_0)^2]} dr_{1\perp} \quad (3.6)$$

where we have defined

$$c_{20} \equiv \phi_y^{-1} = 1 + N, \quad c_{02} \equiv \phi_z^{-1} = 1 + M \quad (3.7)$$

The integrals in equation (3.6) are of the Fresnel type when evaluated between the limits $\pm \infty$ as indicated. Apart from possible contributions from the neglected terms in the stationary phase expansion, the very presence of the planet itself requires that a circular region of radius R , centered at $z_1 = r_0$, be excluded from the integration. However, due to the rapidly decreasing contribution to the integral from wavelets originating from positions $|z_1 - z_0| > (\lambda D)^{1/2} \phi_z^{1/2}$ and $|y_1 - y_0| > (\lambda D)^{1/2} \phi_y^{1/2}$ from the stationary phase point, the presence of the planet can be ignored. Evaluating equation (3.6) for the intensity $\phi = |E|^2$ thus yields

$$\phi = \phi_y \phi_z \quad (3.8)$$

This result, independent of k , is the geometrical optics intensity formula for a spherically symmetric refractivity field. It can be derived from a flux conservation argument directly, or from a geometrical optics formulation based on the Eikonal equation (Haugstad 1978e). Truncation of the stationary phase expansion after the second-order terms therefore restricts the validity of the resulting intensity formula to the realm of geometrical optics. We calculate in the next section the lowest-order, k -dependent correction to equation (3.8), and thereby also establish the region of validity of this result.

Equation (3.6) provides an interesting wave-optical interpretation of ray bending in an inhomogeneous medium. Indeed, the phase-factor

$$\psi = \frac{k}{2D} [\phi_y^{-1}(y_1 - y_0)^2 + \phi_z^{-1}(z_1 - z_0)^2]$$

has the constant value π on the circumference of an ellipse centered at (y_0, z_0) with semi-axes

$$a_{F,h} \equiv \phi_y^{1/2} (\lambda D)^{1/2}, \quad a_{F,v} \equiv \phi_z^{1/2} (\lambda D)^{1/2} \quad (3.9)$$

in the y - and z -directions, respectively. Refraction thus distorts the originally circular shape of the free-space Fresnel zone of radius $a_{F,0} = (\lambda D)^{1/2}$ into an ellipse with semi-axes given by equation (3.9). The property that the intensity is proportional to the square of the area of the first Fresnel zone is preserved, however, since $(\pi a_{F,h} a_{F,v} / \pi a_{F,0}^2)^2 = \phi_y \phi_z$, in agreement with equation (3.8). We note also that diffraction effects, through the inclusion of higher-order terms in the stationary phase expansion and in ψ above, will cause the atmospheric Fresnel zone to deviate slightly from its strictly elliptical shape in the geometrical optics limit.

For a spherically symmetric and exponential atmosphere the definitions (3.5) may be used to show that

$$M = \alpha D / H, \quad N = -\alpha D / R \quad (3.10)$$

in this case. The corresponding result for the intensity is

$$\phi^{-1} = (1 + \frac{\alpha D}{H}) (1 - \frac{\alpha D}{R}) \quad (3.11)$$

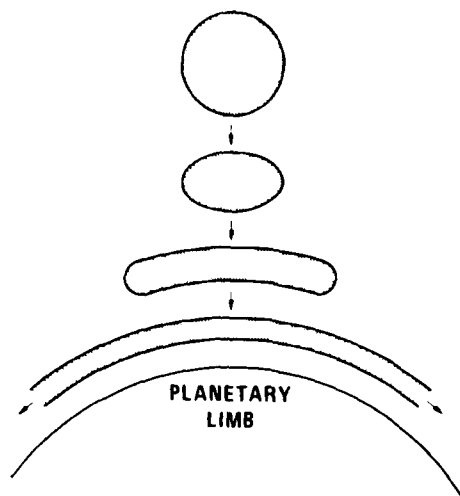


Figure 3.2 Schematic illustration of the changing shape of the atmospheric Fresnel zone as the observer approaches the focal line in the plane of the sky

which reduces to equation (2.4) when focusing is negligible ($\alpha D \ll R$). In the present case refraction expands the free-space Fresnel zone by a factor $(1 - \alpha D/R)^{-1/2} \geq 1$ parallel to the limb, while at the same time compressing the vertical scale by the factor $(1 + \alpha D/H)^{-1/2} \leq 1$, see Figure 3.2. As $\alpha D \rightarrow R$, the spacecraft approaches the center of the planet, as viewed in the plane of the sky, and equation (3.11) predicts $\phi \rightarrow \infty$. Diffraction effects limit, however, the intensity to a finite value whose magnitude is readily obtained from the physical picture developed above (cf. Eshleman *et al* 1979a).

The phase in the geometrical optics approximation is obtained from equation (3.6) by writing the electric field as $E = A \exp[i(kS - \omega t)]$, where A is the amplitude and kS is the phase. Performing the integration over the screen it is found that

$$kS = k[D + S_0(y_0, z_0) + \frac{1}{2}D(\alpha^2 + \beta^2)] \quad (3.12)$$

The sum $kD[1 + 1/2(\alpha^2 + \beta^2)]$ is simply the increase in phase by following the geometrical, refracted path to the receiver, while kS_0 is the additional atmospheric phase perturbation inside the refractive medium.

The previous developments are all based on the thin screen approximation, as defined in section 3.1. Equation (3.8), or more conveniently equation (3.11), may now be used to explore the validity of this approximation. For this approximation to be valid it is sufficient that the change in intensity ϕ through the medium be small. Thus, putting $D = \ell \cong (RH)^{1/2}$ in equation (3.11), we find that the thin screen approximation is satisfied if

$$\alpha \ll H/\ell \cong (H/R)^{1/2} \quad (3.13)$$

That is, the deflection of the ray inside the refractive medium should be a small fraction of a scale height only. The integration of ν_0 along the actual curved raypath to obtain the atmospheric phase perturbation can therefore be approximated by integration along a straight line path, as already assumed.

The seemingly restrictive condition (3.13) is found to have been satisfied for most past radio occultations. It is invariably satisfied in stellar occultations where the optical rays suffer much smaller bending. Using a direct flux conservation argument not restricted by the thin screen approximation, Eshleman *et al* (1979a) have derived a generalization of our equation (3.11) that reduces to this result when the condition (3.13) is satisfied.

3.3 Wave-optical effects

Since the free-space Fresnel zone is a small but finite fraction of atmospheric scales of variation, the true phase and intensity of the radio wave deviate slightly from the geometrical optics results of the previous section. Close to the focus, where $a_{F,h}$ increases without bound, wave-optical effects eventually become dominant for any finite value of the wavenumber k , as noted previously. We calculate below the magnitude of these diffraction effects in the two limits where, (i) $a_{F,h} \cong a_{F,0}$, but with no additional restriction on $a_{F,v}$, and (ii) when $a_{F,h} \rightarrow \infty$, i.e., when the intensity is critically controlled by focusing of the wave around the curved limb.

The former of these cases is most easily treated by expanding the phase factor ψ beyond the quadratic terms and retaining the lowest-order correction to the electric field E . Writing

$$\psi = [\phi_Y^{-1}(y_1 - y_0)^2 + \phi_Z^{-1}(z_1 - z_0)^2] = c_{03}(z_1 - z_0)^3 + c_{12}(z_1 - z_0)^2(y_1 - y_0) + \dots \quad (3.14)$$

it is found that the leading, finite wavelength correction to the electric field involves terms of the form $(z_1 - z_0)^4$ and $(z_1 - z_0)^6$. Putting $E = E_0(1 + \delta E)$, where the geometrical optics field $E_0 = \phi_Y^{-1/2} \phi_Z^{-1/2} \exp[i(kS - \omega t)]$ and δE is the lowest-order fractional correction to E , we find after considerable algebra that

$$\delta E = -\frac{i}{32} \phi_Z(1 - \phi_Z) \frac{\beta^2 D}{k} - \frac{35}{384} \phi_Z^2(1 - \phi_Z)^2 \frac{\beta^4 D^2}{k^2} \quad (3.15)$$

where we have defined $\beta \equiv 1/H$ as the reciprocal scale height. Thus there is a correction $k\delta S$ to the geometrical optics phase by an amount

$$k\delta S = -\frac{1}{32} \phi_Z(1 - \phi_Z) \frac{\beta^2 D}{k} \quad (3.16)$$

There is also a fractional intensity correction given by

$$\frac{\delta \phi}{\phi} = -\frac{35}{192} \phi_Z^2(1 - \phi_Z)^2 \frac{\beta^4 D^2}{k^2} \quad (3.17)$$

This latter result is functionally similar to a corresponding result by Hubbard (1979) for propagation in two dimensions.

Since the atmospheric phase perturbation $kS_0 = k\nu_0 \ell \cong kH\alpha$, it follows from equation (3.16) that the fractional change in phase due to diffraction is

$$\frac{k\delta S}{kS_0} \cong -\frac{1}{32} \phi_Z^2 \frac{\beta^4 D^2}{k^2} \quad (3.18)$$

That is, there are fractional corrections in phase and intensity that are both proportional to $\kappa \equiv \beta^4 D^2/k^2$ and that decrease rapidly with occultation depth. Since κ spans a range of order of magnitude 10^{-4} – 10^{-8} for past radio and stellar occultations, these corrections will normally be altogether negligible.

Sufficiently close to the focal line $\alpha D = R$, diffraction effects eventually become dominant for any finite value of k . Letting r_\perp denote the perpendicular distance of the spacecraft from the focal line, Hubbard (1977) has shown that for an exponential atmosphere the intensity close to the focus is given by

$$\phi = 4\pi^2 \frac{RH}{\lambda D} J_0^2 \left(\frac{2\pi r_\perp R}{\lambda D} \right) \quad (3.19)$$

where J_0 is a Bessel function of zero order. The focal intensity maximum is thus

$$\phi_{\max} = 4\pi^2 RH/\lambda D \quad (3.20)$$

with a characteristic width

$$w \cong \lambda D/R \quad (3.21)$$

For $w \ll r_{\perp} \ll R$, the average intensity reduces to the geometrical optics result (3.11) when allowance is made for a doubling of the intensity close to the focal line where the two limbs yield nearly identical contributions to the average intensity. Since w is typically a small fraction of a meter, the ray-optical intensity formula (3.11) is valid extremely close to the focal line. As shown by Eshleman *et al* (1979a), the results (3.20) and (3.21) may also be derived from simple physical arguments relating to the limiting distortion of the atmospheric Fresnel zone as the focal line is approached.

4 PROPAGATION IN A TURBULENT PLANETARY ATMOSPHERE

4.1 Phase and intensity in the weak scattering approximation

The development of the previous section provides a framework for calculating the effect of turbulence on electromagnetic wave propagation. In the thin phase screen approximation turbulence merely adds a component

$$S_1 = \int_{\ell/2}^{\ell/2} \nu_1(x, y_0, z_0) dx \quad (4.1)$$

to the total optical path length at the exit face of the screen. It is assumed throughout that the turbulent component of refractivity, ν_1 , has zero mean and satisfies $\langle \nu_1^2 \rangle^{1/2} \ll \nu_0$. Equation (3.1) takes the form

$$E(\mathbf{r}_2) = \frac{k}{2\pi i D} \iint_{-\infty}^{\infty} e^{i \frac{k}{2D} [2D^2 + (y_2 - y_1)^2 + (z_2 - z_1)^2 + 2D(S_0 + S_1)]} d\mathbf{r}_{1\perp} \quad (4.2)$$

In the weak scattering approximation $k|S_1| \ll 1$, and the integrand in equation (4.2) may be expanded around the point of stationary phase as before. Expanding the electric field $E = E_0 + E_1 + \dots$, where $E_0 = \mathcal{O}(1/\nu_0)$, $E_1 = \mathcal{O}(\nu_1)$, etc, we thus obtain

$$E_1(\mathbf{r}_2) = k\phi_y\phi_z e^{ik \frac{c_{00}}{2D} \ell/2} \int_{\ell/2}^{\ell/2} \nu_1(x, y_0, z_0) dx \iint_{-\infty}^{\infty} e^{i \frac{k}{2D} [\phi_y^{-1}(y_1 - y_0)^2 + \phi_z^{-1}(z_1 - z_0)^2]} d\mathbf{r}_{1\perp} \quad (4.3)$$

after retaining only the quadratic terms in the stationary phase expansion. Let

$$\nu_1(x_1, y_1, z_1) = \iiint_{-\infty}^{\infty} e^{i[u_x x_1 + u_y(y_1 - y_0) + u_z(z_1 - z_0)]} dZ(\mathbf{u}) \quad (4.4)$$

be the Fourier-Stieltjes representation of ν_1 , where $dZ(\mathbf{u}) = Z'(\mathbf{u})d\mathbf{u}$ ($d\mathbf{u} = du_x du_y du_z$), with u_x, u_y, u_z being the spatial wavenumber components in the x -, y -, and z -directions, respectively. The Fourier amplitude Z' of ν_1 has been referenced to the stationary phase point (y_0, z_0) . For a homogeneous and isotropic random field $\langle Z'(\mathbf{u}_1)Z'^*(\mathbf{u}_2) \rangle = \Phi(\mathbf{u}_1) \delta(\mathbf{u}_1 - \mathbf{u}_2)$, where Φ is the spatial power spectrum of ν_1 and $\delta(\cdot)$ is the Dirac delta-function. Combination of equations (4.3) and (4.4) yields after algebraic manipulations

$$E_1(\mathbf{r}_2) = k\phi_y\phi_z e^{ik \frac{c_{00}}{2D} \ell/2} \iiint_{-\infty}^{\infty} \text{sinc}\left(\frac{u_x \ell}{2\pi}\right) Z'(\mathbf{u}) \Omega(\mathbf{u}_\perp) d\mathbf{u} \quad (4.5)$$

Here $\text{sinc}(\cdot)$ is the sinc-function, $\mathbf{u}_\perp = (u_y, u_z)$ and we have defined

$$\Omega = \ell c^{-1} \frac{D}{2k} [\phi_y u_y^2 + \phi_z u_z^2] + i \frac{k}{2D} (\phi_y^{-1} y_0^2 + \phi_z^{-1} z_0^2) \iint_{-\infty}^{\infty} e^{-i \frac{k}{2D} [\phi_y^{-1} y_1'^2 + \phi_z^{-1} z_1'^2]} dy_1' dz_1' \quad (4.6)$$

The first-order perturbation in intensity normalized by the average intensity, $\hat{\phi}_1$, and the first-order perturbation in phase path, S_1 , are related to E_1 as in

$$\hat{\phi}_1 = 2 \text{Re}[E_0^{-1} E_1], \quad S_1 = k^{-1} \text{Im}[E_0^{-1} E_1]$$

respectively. Since $E_0 = \phi_y \phi_z \exp(ik c_{00}/2D)$, we obtain after integration over the phase screen in equation (4.6)

$$\hat{\phi}_1 = 2k\ell \iiint_{-\infty}^{\infty} \text{sinc}\left(\frac{\mathbf{u}_\perp \ell}{2\pi}\right) Z'(\mathbf{u}) \sin(P) d\mathbf{u} \quad (4.7)$$

$$S_1 = \ell \iiint_{-\infty}^{\infty} \text{sinc}\left(\frac{\mathbf{u}_\perp \ell}{2\pi}\right) Z'(\mathbf{u}) \cos(P) d\mathbf{u} \quad (4.8)$$

where we have defined

$$P = \frac{D}{2k} (\phi_y u_y^2 + \phi_z u_z^2) \quad (4.9)$$

For the mean square of these quantities we obtain, assuming $L_0 \ll \ell$ (L_0 is the outer scale of turbulence)

$$\langle \hat{\phi}_1^2 \rangle = 8\pi\ell k^2 \iint_{-\infty}^{\infty} \Phi(\mathbf{u}_\perp) \sin^2(P) d\mathbf{u}_\perp \quad (4.10)$$

$$\langle S_1^2 \rangle = 2\pi\ell \iint_{-\infty}^{\infty} \Phi(\mathbf{u}_\perp) \cos^2(P) d\mathbf{u}_\perp \quad (4.11)$$

The quantity $\langle \hat{\phi}_1^2 \rangle$ is called the scintillation index, the square root of which is often termed the modulation index.

Equations (4.10) and (4.11) are the appropriate generalizations of the weak scattering, mean square fluctuations in intensity and phase path to turbulence superimposed on an inhomogeneous background. (For stellar occultations the intensity should be convolved with the projected stellar brightness distribution in the occulting atmosphere, see section 4.3.) The effect of the ambient atmosphere is seen to appear only through the quantities ϕ_y and ϕ_z , whose interpretation in terms of the mean signal intensity was established in the previous section. A sufficient condition for neglecting coupling to the inhomogeneous background atmosphere is therefore that ϕ_y, ϕ_z both be essentially unity, or equivalently, that the change in intensity caused by the ambient atmosphere alone be negligible. This condition is not satisfied in either radio or stellar occultation experiments, however, implying that interpretation of weak scintillation data in such experiments should proceed from the generalized formulas derived here. Surveillance of the earth's upper atmosphere using a pair of satellites may also involve sufficient ray bending for weak scintillation data to be analyzed in terms of the results given here, especially if the raypath traverses regions of thermal inversion where the local value of $\partial^2 \nu_0 / \partial z^2$, contained in the definition of ϕ_z , may attain appreciable values. It may be noted that although the previous derivation has assumed ν_1 to be a strictly homogeneous and isotropic random variable, the results (4.10) and (4.11) are still valid if ν_1 is inhomogeneous, provided that the scales on which the inhomogeneities occur are large compared to any other scale of interest, i.e., to L_0 and the Fresnel scales $a_{F,h}, a_{F,v}$.

Having established the first-order, weak scattering results for phase and intensity appropriate to radio and stellar occultations, it is important to explore their validity. For the ambient atmosphere the thin screen approximation was found to require

$\alpha \ll (H/R)^{1/2}$. Since the first-order intensity and phase perturbations are both functions of ϕ_y, ϕ_z , the condition on the smallness of α also applies in this case. The thin phase screen approximation also requires that the scintillations in intensity be small inside the screen. This condition is automatically satisfied, however, since we shall prove in section 4.3 that $\langle \hat{\phi}_1^2 \rangle$ is small compared to unity at any distance from the screen when $k|S_1(\mathbf{r}_1)| \ll 1$, i.e., when the turbulent phase perturbation at exit from the screen is small. We observe, finally, that since $\ell \ll D$ the quantities ϕ_y and ϕ_z do not change appreciably through the screen and may hence be associated with a fixed spacecraft-limb distance $x = D$.

The stationary phase expansion also imposes certain restrictions on the validity of the previous results. These limitations are most easily appreciated by noting from the derivation of equation (4.5) that if $\Delta y \equiv y_1 - y_0$ and $\Delta z \equiv z_1 - z_0$, a Fourier component of wavenumber $\mathbf{u}_\perp = (u_y, u_z)$ gives a contribution proportional to

$$\iint e^{i \frac{k}{2D} [\phi_y^{-1} (\Delta y + \frac{D}{k} \phi_y u_y)^2 + \phi_z^{-1} (\Delta z + \frac{D}{k} \phi_z u_z)^2]} d\Delta y d\Delta z \quad (4.12)$$

to the perturbed electric field at the receiver. Defining $u_y = 2\pi/\ell_y$ and $u_z = 2\pi/\ell_z$, it is seen from this expression that an eddy of wavenumber components u_y, u_z gives a contribution to the perturbed electric field that originates from a position $(|\Delta y| = \phi_y \lambda D / \ell_y, |\Delta z| = \phi_z \lambda D / \ell_z)$ relative to the stationary phase point. Such elementary wave contributions are thus scattered through angles $\theta_y = \phi_y \lambda / \ell_y$ and $\theta_z = \phi_z \lambda / \ell_z$ in the xy - and xz planes, respectively. When $\phi_y = \phi_z = 1$, this is essentially the Bragg condition for diffraction by a sinusoidal spatial diffraction grating. Now, for Kolmogorov turbulence $\langle S_1^2 \rangle$ and $\langle \hat{\phi}_1^2 \rangle$ may be shown to derive their principal contributions from eddies of dimension $(\ell_y, \ell_z) \sim L_0$ and $(\ell_y, \ell_z) \sim (a_{F,h}, a_{F,v})$, respectively. The quadratic approximation of the stationary phase expansion should therefore be validated to distances $|\Delta y| \sim \phi_y \lambda D / L_0$, $|\Delta z| \sim \phi_z \lambda D / L_0$ and $|\Delta y| \sim a_{F,h}$, $|\Delta z| \sim a_{F,v}$ for these two quantities, respectively. Evaluation of the next-order terms in the stationary phase expansion indeed turn out to be small at these distances if $H \gg L_0 \gg a_{F,v}$, and provided also that $\phi_y \ll (L_0/a_{F,0}) (L_0 R/a_{F,0}^2)^{1/2}$ in the evaluation of $\langle S_1^2 \rangle$, and $\phi_y \ll (RH)^{1/2}/a_{F,0}$ in the evaluation of $\langle \hat{\phi}_1^2 \rangle$. In shallow occultations these constraints are always met, but very close to the focal line both conditions are violated and neither $\langle \hat{\phi}_1^2 \rangle$ nor $\langle S_1^2 \rangle$ will be given by simple formulas of the type (4.10) and (4.11).

We are now prepared to discuss another quantity of principal interest in radio occultation experiments: the ray bending angle. It is readily shown from the previous equations that a major component of the mean square perturbation in bending angle involves an integral of the form

$$\iint \Phi(u_\perp) u_\perp^2 \cos^2(P) du_\perp \quad (4.13)$$

For Kolmogorov turbulence this integral diverges as a function of the upper limit, and is thus controlled by the smallest eddies of dimension $\sim \ell_0$, the inner scale of the turbulence. By relation (4.12), eddies of this size yield scattered waves that originate from distances $d \sim \lambda D / \ell_0$ from the stationary phase point. With $\ell_0 \sim 1$ cm, d is commensurable with the dimensions of the planet. The implication is therefore that a calculation of the perturbation in ray bending angle requires the complete spatial extent of the scattering medium to be stipulated, and the stationary phase expansion cannot be truncated after the second-order terms. The problem is compounded by the fact that in going from equation (3.1) to (3.2), the exact kernel

$$\frac{\exp[ik|\mathbf{r}_2 - \mathbf{r}_1|]}{|\mathbf{r}_2 - \mathbf{r}_1|}$$

of equation (3.1) was approximated by the Fresnel kernel

$$\frac{1}{D} \exp[i \frac{k}{2D} \rho^2]$$

which requires that $\kappa \equiv k \rho^4 / D^3 \ll 1$, where $\rho \equiv [(y_2 - y_1)^2 + (z_2 - z_1)^2]^{1/2}$ is the lateral separation of the receiver and an arbitrary point on the exit face of the phase screen (Tatarskii 1971, pp 223). For the perturbations in intensity and phase this condition is strongly satisfied, since for these quantities $\rho \leq (\lambda D)^{1/2}$ and $\leq \lambda D / L_0$, respectively. However, the fluctuations in ray bending angle derive their principal contribution from waves scattered from distances ℓ from the stationary phase point, where ℓ is the effective lateral extent of the turbulent medium. For turbulence that varies exponentially with altitude on a scale H_t (cf section 4.2), the medium extends effectively to a distance $\rho = \ell \cong (RH_t)^{1/2}$ parallel to the limb. Assuming $H_t = H = 10$ km, we find that for X- and S-band occultations of US spacecraft typical values of κ are such that $\kappa \gg 1$. Hence a numerical approach is apparently required to obtain the mean square fluctuations in bending angle.

Most previous analyses of scintillation data from radio and stellar occultation experiments have ignored the coupling effect between the turbulence and the ambient background described and calculated here (Gurvich 1969, Golitsyn and Gurvich 1971, Woo and Ishimaru 1973, Woo *et al* 1974, Woo and Ishimaru 1974, Woo 1975a, Jokipii and Hubbard 1977). The first attempt to account for the coupling effect on the scintillation index was apparently made by Woo *et al* (1975). Later and independently the problem was treated by Haugstad (1977, 1978c,e), by Hubbard *et al* (1978) and recently also by Woo *et al* (1980). An interesting heuristic approach to the problem was taken by A Young (1976). The problem of calculating the mean square fluctuations in phase and bending angle does not appear to have been addressed by other authors.

4.2 An atmospheric model

Explicit evaluation of the intensity and phase scintillations requires a model to be stipulated for both ν_0 and ν_1 . The former quantity has already been assumed to correspond to a spherically symmetric and exponential atmosphere, for which

$$\nu_0(\mathbf{r}) = \nu_0(r_0) \exp[-\beta(r - r_0)] \quad (4.14)$$

where $\beta^{-1} = H$ is the scale height, and $r = |\mathbf{r}|$ is measured from the center of the planet. For the turbulence component we assume

$$\nu_1(\mathbf{r}) = \langle \nu_1^2(r) \rangle^{1/2} \nu_1^*(\mathbf{r}) \quad (4.15a)$$

$$\langle \nu_1^2(r) \rangle^{1/2} = \langle \nu_1^2(r_0) \rangle^{1/2} \exp[-\beta_t(r - r_0)] \quad (4.15b)$$

That is, ν_1 is the product of a spherically symmetric component that varies exponentially with height on a scale $\beta_t^{-1} = H_t$, and a strictly homogeneous and isotropic random component ν_1^* of zero mean and unit variance. The power spectrum Φ of ν_1 will be assumed to be of the Von Kármán type, i.e.

$$\Phi(u) = \langle \nu_1^2 \rangle \frac{\Gamma(p/2)}{\pi^{3/2} \Gamma(\frac{p}{2} - \frac{3}{2})} \frac{L_0^3 \exp(-\ell_0^2 u^2)}{[1 + L_0^2 u^2]^{p/2}} \quad (4.16)$$

Here $u \equiv (u_x^2 + u_y^2 + u_z^2)^{1/2}$ is the three-dimensional scalar wave number, L_0 and ℓ_0 are the outer and inner scale of the turbulence, respectively, and p is a parameter controlling the slope of Φ in the inertial subrange, where $L_0^{-1} \ll u \ll \ell_0^{-1}$. For Kolmogorov turbulence $p = 11/3$.

For purposes for numerical evaluation also the magnitude of $\langle \nu_1^2 \rangle$ should be stipulated. Turbulent fluctuations in refractivity may be related to those in temperature and pressure using the relation (e.g., Tatarskii 1971)

$$\nu = 7.9 \cdot 10^{-5} p/T \quad (4.17)$$

which assumes that the refractivity from any vapors present can be neglected. Small changes in refractivity, ν_1 , are thus related to similar changes p_1 in pressure and T_1 in temperature according to

$$\nu_1 = 7.9 \cdot 10^{-5} \left[\frac{p_1}{T} - \frac{p}{T^2} T_1 \right] \quad (4.18)$$

For the centimeter to kilometer eddy sizes of interest here the temperature relaxation is slow enough to suggest an adiabatic relationship between p_1 and T_1 (Lawrence and Strohbehn 1970), so that $p_1/p = \gamma/(\gamma-1) \cdot T_1/T$, where γ is the ratio of specific heats at constant pressure and volume. With this assumption equations (4.17) and (4.18) combine to give

$$\frac{\langle \nu_1^2 \rangle}{\nu_0^2} = (\gamma - 1)^{-2} \frac{\langle T_1^2 \rangle}{T_0^2} \quad (4.19)$$

For an isothermal ambient atmosphere the fractional mean square fluctuations in refractivity thus vary with altitude as the variance of the temperature fluctuations. An estimate of the latter quantity may be obtained from the temperature structure function

$$D_T(\Delta r) = C_T^2 |\Delta r|^{2/3} \quad (4.20)$$

valid for Kolmogorov turbulence and separations $\ell_0 \ll |\Delta r| \ll L_0$. An approximate value of $\langle T_1^2 \rangle$ is obtained from this relation by putting $\Delta r = L_0$ and noting from the definition of L_0 that $D_T(L_0) \cong 2 \langle T_1^2 \rangle$. Thus*

$$D_T(L_0) = C_T^2 L_0^{2/3} \cong 2 \langle T_1^2 \rangle$$

The fractional fluctuations in refractivity are thus approximately

$$\frac{\langle \nu_1^2 \rangle}{\nu_0^2} \cong \frac{1}{2} (\gamma - 1)^{-2} \frac{C_T^2 L_0^{2/3}}{T_0^2} \quad (4.21)$$

Values for the outer scale may be obtained by direct measurements, or its value may be inferred from the bulk flow properties. The temperature structure constant, C_T^2 , may be estimated from the mean flow characteristics for various types of turbulence (see, e.g., Tatarskii 1971, pp 72-74). Alternatively one might use the estimate $C_T^2 \cong 2 \cdot 10^{-3} \text{ K}^2 \text{ m}^{-2/3}$ corresponding to an altitude level of ~ 15 km in the earth's atmosphere (Bufton *et al* 1972). Assuming $L_0 = 10^3$ m and $T_0 = 200$ K we obtain

$$\frac{\langle \nu_1^2 \rangle}{\nu_0^2} \cong 10^{-5} \quad (4.22)$$

This estimate may be appropriate for Jupiter. For the atmosphere of Venus the higher ambient temperature (and perhaps also the smaller value of L_0) probably makes equation (4.22) an over-estimate of the turbulence strength in this case. As we shall see in section 7, the best way to estimate $\langle \nu_1^2 \rangle$ is probably by direct analysis of radio or stellar scintillation measurements. Lacking such direct information on the turbulence strength, we shall explore in a forthcoming section the implications of turbulence of the relative strength given by relation (4.22).

* For Kolmogorov turbulence the more correct relationship is given by $C_T^2 L_0^{2/3} = 1.91 \langle T_1^2 \rangle$.

4.3 Radio and stellar intensity scintillations

The turbulence model described in the previous section may now be combined with the scintillation formula (4.10) to yield an explicit result for the radio scintillation index. Evaluation of this equation by transforming to polar coordinates yields for $3 < p < 6$ (Haugstad 1978e)

$$\langle \hat{\phi}_1^2 \rangle = \frac{\pi^{1/2} (2\pi)^{3-p/2}}{\Gamma(\frac{p-3}{2})} \left| \sec \frac{\pi p}{4} \right| \left(\frac{L_0}{a_{F,0}} \right)^{3-p} \frac{LD^2}{a_{F,0}^3} W_R(\phi_Y, \phi_Z; p) \langle \nu_1^2 \rangle \quad (4.23a)$$

where

$$W_R(\phi_Y, \phi_Z; p) = \int_{-\pi}^{\pi} (\phi_Y \cos^2 \theta + \phi_Z \sin^2 \theta)^{\frac{p}{2}-1} d\theta \quad (4.23b)$$

In deriving this result we have assumed that $L_0 \gg a_{F,h} \geq a_{F,v}$, implying that the major contribution to the scintillations is from turbulent eddy sizes in the inertial subrange. In its present form this result is therefore not applicable to very deep occultations, where $a_{F,h}$ may exceed L_0 . We shall consider this case separately in section 6.

In equation (4.23) coupling between the turbulence and the inhomogeneous background appears through W_R only. For a strictly homogeneous background, or when the differential ray bending is sufficiently small that $\phi_Y \approx \phi_Z \approx 1$, $W_R = 2\pi$ for any value of the spectral slope parameter p . In this case, after manipulations involving the gamma function, equation (4.23a) may be shown to coincide with the classic Rytov result in the thin screen approximation.

If we now consider occultations for which the approximation $\phi_Y \approx 1$ can be made, but with no restriction on ϕ_Z , evaluation of equation (4.23b) gives

$$W_R(1, \phi_Z; p) = \begin{cases} 2\pi, & \phi_Z = 1 \\ \frac{\Gamma^2(\frac{p-1}{2})}{2^{p-1} \Gamma(\frac{p}{2})}, & \phi_Z \leq 1 \end{cases} \quad (4.24)$$

Since for $p = 11/3$ the lower value corresponding to $\phi_Z \leq 1$ is about 0.6 times the upper value, it follows that, (i) coupling to the inhomogeneous background reduces the scintillation index by less than a factor of two, and (ii) this reduction is essentially independent of $\phi \approx \phi_Z$ whenever defocusing reduces the average intensity by a few dB or more. This result disagrees with a prediction by A Young (1976), who concluded from a heuristic calculation that the scintillation index should *increase* by a factor $\phi^{-2/3}$ as deeper atmospheric regions were probed. Although neither the works of Hubbard *et al* (1978) or Woo *et al* (1980) gave explicit results for the coupling effect, their expressions for the scintillation index may be manipulated to yield a similar result to that derived here. We shall see in the next section that the rather small effect of the inhomogeneous background on the scintillation index does result, however, in substantial changes in the *shape* of the radio and stellar scintillation power spectra.

For stellar occultations the point source intensity correlation function should be convolved with the normalized stellar brightness distribution as projected above the limb of the planet. In the spectral domain this operation yields the general expression (c f, Hubbard *et al* 1978)

$$\iint \Phi_{\hat{\phi}_1}(\mathbf{u}_1) \psi(\mathbf{u}_1) d\mathbf{u}_1$$

for the scintillation index of a stellar source. In this expression $\Phi_{\hat{\phi}_1}(\mathbf{u}_1)$ is the spatial power spectrum of $\langle \hat{\phi}_1^2 \rangle$ (i.e., the integrand of equation (4.10)), and

$$\psi = \iint f(\mathbf{r}) e^{i\mathbf{r}_\perp \cdot \mathbf{u}_\perp} d\mathbf{r}_\perp$$

where $f(\mathbf{r})$ is the normalized brightness distribution of the projected stellar disk. For a uniformly illuminated stellar disk of projected radius a_s one obtains

$$|\psi(\mathbf{u}_\perp)|^2 = \left[\frac{2 J_1(a_s u_\perp)}{a_s u_\perp} \right]^2$$

where J_1 is a Bessel function of order one. Instead of the point source result (4.10) we thus obtain

$$\langle \hat{\phi}_1^2 \rangle = 8\pi \kappa^2 \iint \Phi(u_\perp) \sin^2(p) \left[\frac{2 J_1(a_s u_\perp)}{a_s u_\perp} \right]^2 du_\perp \quad (4.25)$$

The additional factor in the integrand is due to averaging over the stellar disk and acts to suppress contributions to the scintillation index from eddy sizes smaller than the projected stellar disk. A closely similar result to equation (4.25) has been obtained by Hubbard *et al* (1978).

If the double inequality $L_0 \gg a_s \gg a_{F,h}$ is satisfied, evaluation of equation (4.25) yields for $3 < p < 6$

$$\langle \hat{\phi}_1^2 \rangle = \frac{4}{\pi} \frac{\Gamma(\frac{6-p}{2})}{\Gamma(\frac{p-2}{2})} \left(\frac{L_0}{a_s} \right)^{3-p} \frac{\kappa D^2}{a_s^3} W_s(\phi_Y, \phi_Z; p) \langle v_1^2 \rangle \quad (4.26a)$$

where in this case

$$W_s(\phi_Y, \phi_Z; p) = \int_{-\pi}^{\pi} (\phi_Y \cos^2 \theta + \phi_Z \sin^2 \theta)^2 d\theta \quad (4.26b)$$

For intermediate and small values of the ratio $a_s/a_{F,h}$, numerical integration of equation (4.25) is required. For shallow occultations equation (4.26b) gives

$$W_s(1, \phi_Z; p) = \begin{cases} 2\pi, & \phi_Z \gg 1 \\ 2^5 \frac{\Gamma^2(5/2)}{\Gamma(5)}, & \phi_Z \ll 1 \end{cases} \quad (4.27)$$

Since the lower value for $\phi_Z \ll 1$ is ~ 1.76 , we conclude that coupling to the inhomogeneous background reduces the stellar scintillation index by at most a factor ≈ 3.6 under the previous assumptions. A Young's prediction for this case was an *increase* in the scintillation index by a factor $\phi_Z^{4/3}$, attending a compression of the stellar image by a factor ϕ_Z perpendicular to the planetary limb.

It is instructive to express the scintillation index as a function of occultation depth under the assumption that $\langle v_1^2 \rangle / \nu_0^2$ is constant. To this end we first note that

$$\langle v_1^2 \rangle = \frac{H^3 M^2}{2\pi R D^2} \frac{\langle v_1^2 \rangle}{\nu_0^2}$$

We have here used the fact that $\alpha = (2\pi R/H)^{1/2} \nu_0$ for bending angles $\alpha \ll (H/R)^{1/2}$ and $M = \alpha D/H$ as before. Eliminating $\langle v_1^2 \rangle$ between this relation and either of equations (4.23a) or (4.26a) yields for $\phi_Y \sim 1$

$$\langle \hat{\phi}_1^2 \rangle = [\kappa(p) \left(\frac{L_0}{a} \right)^{3-p} \left(\frac{H}{a} \right)^3 \frac{\kappa \langle v_1^2 \rangle}{R \nu_0^2}] \left(\frac{1}{\phi} \right)^2 W(1, \phi; p) \quad (4.28)$$

For radio occultations $W = W_R$ and $a = a_{F,0}$, while for stellar occultations $W = W_s$ and $a = a_s$. The numerical factor κ is the co-factor of equations (4.23a) and (4.26a), res-

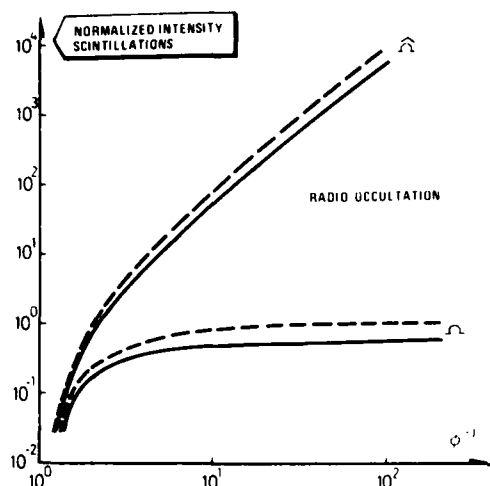


Figure 4.1 Variation with occultation depth ϕ^{-1} of the quantities Ω and $\hat{\Omega}$ for radio occultations

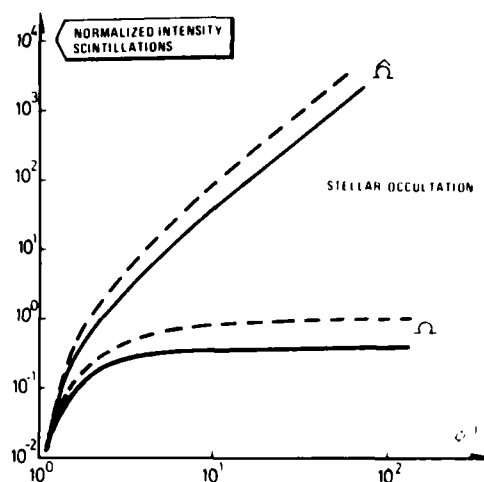


Figure 4.2 Variation with occultation depth ϕ^{-1} of the quantities Ω and $\hat{\Omega}$ for stellar occultations

The solid curves display $\hat{\Omega}$ and Ω when coupling to the inhomogeneous background is properly accounted for, while the broken curves are calculated for a model where this effect is not included. The curves are normalized such that $\hat{\Omega}$ in the latter case approaches unity as $\phi^{-1} \rightarrow \infty$.

pectively. If the spacecraft (or the earth for stellar occultations) is moving perpendicular to the incoming ray asymptote, D is approximately constant for small α , and all variation of $\langle \hat{\phi}_i^2 \rangle$ with depth is contained in the two last factors of equation (4.28). Figures 4.1 and 4.2 show the variation with occultation depth of the quantity

$$\hat{\Omega} \equiv \left(\frac{1-\phi}{\phi} \right)^2 \frac{W(1, \phi; 11/3)}{2\pi} \quad (4.29)$$

for both radio and stellar occultations, along with the result that would have been obtained if coupling to the inhomogeneous background were falsely neglected. Note that for constant D and H , M is proportional to atmospheric density or pressure at the ray periastris. Also shown in the figures is the corresponding variation of the absolute mean square fluctuations in intensity, which are proportional to $\Omega \equiv \phi^2 \hat{\Omega}$. In contrast to the scintillation index which increases rapidly with depth, the absolute intensity scintillations, $\langle \phi_i^2 \rangle = \phi^2 \langle \hat{\phi}_i^2 \rangle$, approaches a constant determined by the asymptotic value of W as $\phi \rightarrow 0$.

We conclude this section by proving that in the weak scattering regime $\langle \hat{\phi}_i^2 \rangle \ll 1$ also when coupling to the inhomogeneous background is accounted for. For turbulence superimposed on a homogeneous background this result has previously been proved by Salpeter (1967) and others. Consider the mean square fluctuations in optical path at exit from the phase screen. This quantity may be obtained from equation (4.11) by putting $P = 0$ and evaluating the double integral over the power spectrum, yielding

$$\langle S_1^2(\mathbf{r}_1) \rangle = \frac{4\pi^{1/2} \Gamma(P/2)}{\Gamma(\frac{P-3}{2}) (P-2)} \ell L_0 \langle \nu_i^2 \rangle \quad (4.30)$$

Eliminating $\langle \nu_i^2 \rangle$ between this result and equation (4.23a) gives

$$\langle \hat{\phi}_i^2 \rangle = \kappa(p) \left(\frac{a_{F,0}}{L_0} \right)^{p-2} \frac{W_R(\phi_Y, \phi_Z, p)}{2\pi} |k^2 \langle S_1^2(\mathbf{r}_1) \rangle| \quad (4.31)$$

where $\kappa(p) \equiv (2\pi)^{2-p/2} [\sec \pi p/4 / \Gamma(p/2)]$ is of order of magnitude unity for $p = 11/3$. Since $a_{T,0} \ll L_0$ per assumption, and we have shown that $W_R \leq 2\pi$, it follows that $\langle \hat{\phi}_1^2 \rangle \ll 1$ in the weak scattering approximation where $k \langle S_1^2(\mathbf{r}_1) \rangle^{1/2} \ll 1$. Even though the weak scattering condition has been used to derive the previous results, it is likely that only the weaker condition $\langle \hat{\phi}_1^2 \rangle \ll 1$ is necessary, however. For turbulence superimposed on a homogeneous background this has been proved by Tatarskii (1971, pp 256). One-dimensional, numerical computations of intensity scintillations superimposed on an inhomogeneous background indicate that $\langle \hat{\phi}_1^2 \rangle \ll 1$ is indeed the proper criterion also in this case (French *et al* 1980).

4.4 Temporal power spectra

4.4.1 Theoretical phase and intensity power spectra

The scintillation index provides only an averaged representation of the effect of the inhomogeneous background on radio and optical wave propagation in turbulent planetary atmospheres. More detailed information is contained in the temporal power spectrum, the shape of which will be shown here to depend critically on both occultation depth and geometry when coupling to the inhomogeneous background is accounted for.

The phase autocovariance function in the plane $x = D$ of the observer is given by

$$B = k^2 \langle S_1(D, y_2, z_2) S_1(D, y_2 + \Delta y_2, z_2 + \Delta z_2) \rangle \quad (4.32)$$

Geometrical optics energy conservation implies that separations $\Delta y_2, \Delta z_2$ at the receiver project into ray separations $\Delta y_1 = \phi_Y \Delta y_2$ and $\Delta z_1 = \phi_Z \Delta z_2$ at ray periapsis. Velocity components v_Y, v_Z of the spacecraft are therefore related to corresponding components v_Y^* and v_Z^* at the ray periapsis according to

$$v_Y^* = \phi_Y v_Y, v_Z^* = \phi_Z v_Z \quad (4.33)$$

It is customary to adopt the "frozen-field" hypothesis, whereby turbulent inhomogeneities are assumed to be convected across the line of sight at constant velocity, which for the present case equals the relative velocity between that of the ray at periapsis and the atmospheric bulk velocity, due to either planetary rotation or the presence of atmospheric winds, or both. We shall assume that the components of the latter are small compared to v_Y^*, v_Z^* . In this case ray separations $\Delta y_1, \Delta z_1$ at the periapsis are related to time separations τ according to $\Delta y_1 = v_Y^* \tau, \Delta z_1 = v_Z^* \tau$. Using relations (4.33) and drawing on the analysis of section 4.1, we find that

$$B = k^2 \iint \Phi_{S_1}(\mathbf{u}_\perp) \exp[i(u_Y \phi_Y v_Y + u_Z \phi_Z v_Z) \tau] d\mathbf{u}_\perp \quad (4.34a)$$

where

$$\Phi_{S_1}(\mathbf{u}_\perp) = 2\pi \langle \Phi(\mathbf{u}_\perp) \cos^2(P) \rangle \quad (4.34b)$$

is the spatial power spectrum of the scintillations in phase path, as given implicitly by equation (4.11). Fourier transformation over τ yields for the temporal power spectrum of the phase scintillations

$$W_1(\omega) = 2\pi k^2 \iint \Phi_{S_1}(\mathbf{u}_\perp) \delta[u_Y \phi_Y v_Y + u_Z \phi_Z v_Z - \omega] d\mathbf{u}_\perp \quad (4.35)$$

Using the turbulence power spectrum (4.16) this integral may be evaluated by transforming to polar coordinates and performing the integration over the angular variable.

After a suitable change of integration variable in the remaining integral we find that (Haugstad 1979a)

$$W_1(\omega) = \kappa_1 \omega \sum_{i=1}^2 \int_1^{\infty} \frac{x \cos^2 \left\{ \left(\frac{\omega x}{\omega_c} \right)^2 [\phi_Y \cos^2(\theta_1 + \delta) + \phi_Z \sin^2(\theta_1 + \delta)] \right\}}{\left[1 + \left(\frac{\omega x}{\omega_0} \right)^2 \right]^{p/2} (x^2 - 1)^{1/2}} dx \quad (4.36)$$

We have here defined $\theta_1 = \theta_2 = \cos^{-1}(1/x)$, $\omega_0 = v^*/l_0$, $\omega_c = 2\pi^{1/2} v^*/a_{F,0}$, $\delta = \tan^{-1}(v_Z^*/v_Y^*)$, and $\kappa_1 = [4\pi^{1/2} \Gamma(p/2)/\Gamma((p-3)/2)] \ell k^2 L_0^3 \langle v_1^2 \rangle / v^*$. We observe from this result that the shape of the phase power spectrum is controlled by the four parameters ω_0 , ω_c , ϕ_Y and ϕ_Z . In view of their definition, ω_0 and ω_c are the characteristic frequencies associated with the ray speed at periaapsis and the outer scale and the free space Fresnel zone, respectively.

Through entirely analogous procedures the radio and stellar intensity scintillation power spectra are obtained as

$$W_2(\omega) = \kappa_2 \omega \sum_{i=1}^2 \int_1^{\infty} \frac{x \sin^2 \left\{ \left(\frac{\omega x}{\omega_c} \right)^2 [\phi_Y \cos^2(\theta_1 + \delta) + \phi_Z \sin^2(\theta_1 + \delta)] \right\}}{\left[1 + \left(\frac{\omega x}{\omega_0} \right)^2 \right]^{p/2} (x^2 - 1)^{1/2}} dx \quad (4.37)$$

$$W_3(\omega) = \kappa_3 \omega^3 \sum_{i=1}^2 \int_1^{\infty} \frac{x^3 [\phi_Y \cos^2(\theta_1 + \delta) + \phi_Z \sin^2(\theta_1 + \delta)]^2}{\left[1 + \left(\frac{\omega x}{\omega_0} \right)^2 \right]^{p/2} (x^2 - 1)^{1/2}} J_1^2 \left(\frac{\omega x}{\omega_c} \right) dx \quad (4.38)$$

respectively. For the former result $\kappa_2 = (16\pi^2 \Gamma(p/2)/\Gamma((p-3)/2)) \ell k^2 L_0^3 \langle v_1^2 \rangle / v^*$; θ_1 , θ_2 and ω_0 , ω_c are defined as before. The stellar intensity scintillation power spectrum is subjected to the same limitations as the expression (4.26) for the scintillation index. In this case $\omega_c = v^*/a_S$, and $\kappa_3 = (16\pi^3 \Gamma(p/2)/\Gamma((p-3)/2)) D^2 L_0^3 \langle v_1^2 \rangle / (a_S v^{*3})$. We note that all of the power spectra calculated here are valid only for frequencies much larger than the characteristic frequency v^*/H associated with either of the scale heights H or H_T .

Figures 4.3 to 4.9 show the phase and intensity power spectra as a function of normalized angular frequency ω/ω_c or ω/ω_0 , for different values of $m = v_Y^*/v_Z^*$ and ϕ , assuming $\phi_Y = 1$. In all cases computed we have assumed $\omega_c/\omega_0 = 3$. For the phase spectra coupling to the inhomogeneous background is seen to reduce the fringes in the spectrum for $\omega > \omega_c$ in a central occultation ($m = 0$) as deeper atmospheric regions are probed. Figure 4.5 displays the change in spectral shape from a central to a more nearly grazing occultation, for a fixed value $\phi = 0.1$ of the mean signal intensity.

By contrast to this behavior, the intensity power spectra display a strong dependence on both occultation geometry (m) and depth (ϕ). According to Figure 4.6, the characteristic fringes in the power spectrum above the Fresnel frequency ω_c altogether disappear as deeper regions are probed in a central occultation. In a grazing occultation, however, these fringes become increasingly deeper and follow a characteristic decrease in scintillation power below ω_c as denser regions are probed. Figure 4.8 shows the progressive change in spectral shape from a central to a more nearly grazing occultation for a fixed occultation depth corresponding to $\phi = 0.1$. With only minor modifications the changes in spectral shape with m and ϕ for a point source are reproduced also for an extended source when the projected stellar radius substantially exceeds the free-space Fresnel zone. Figure 4.9 shows the change in spectral shape with occultation depth for a grazing occultation. If the projected stellar radius is small compared to the free-space Fresnel zone, averaging over the stellar disk

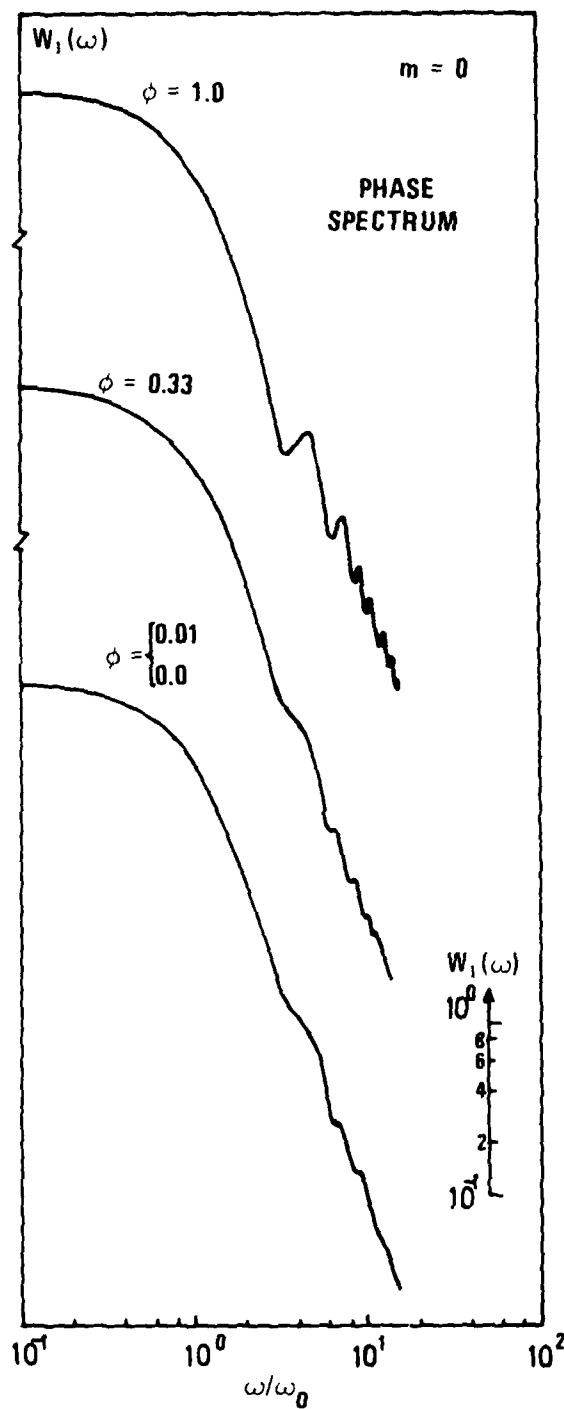


Figure 4.3 Phase scintillation power spectrum at various depths ϕ in a central occultation, assuming $\omega_c/\omega_0 = 3$

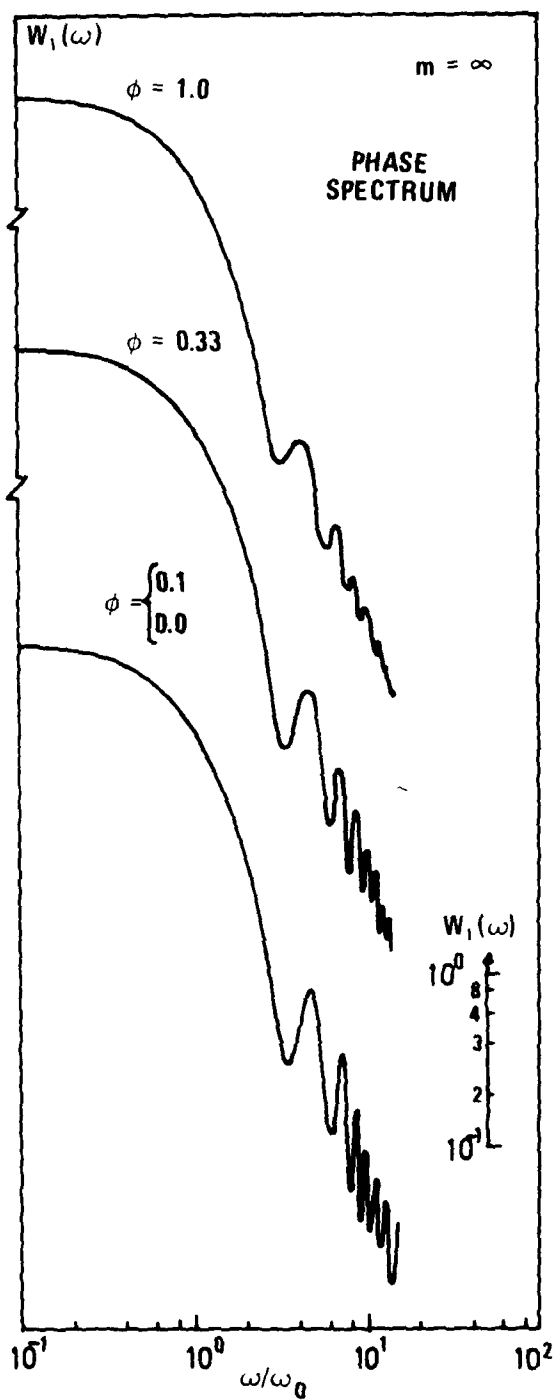


Figure 4.4 Phase scintillation power spectrum at various depths ϕ in a grazing occultation, assuming $\omega_c/\omega_0 = 3$

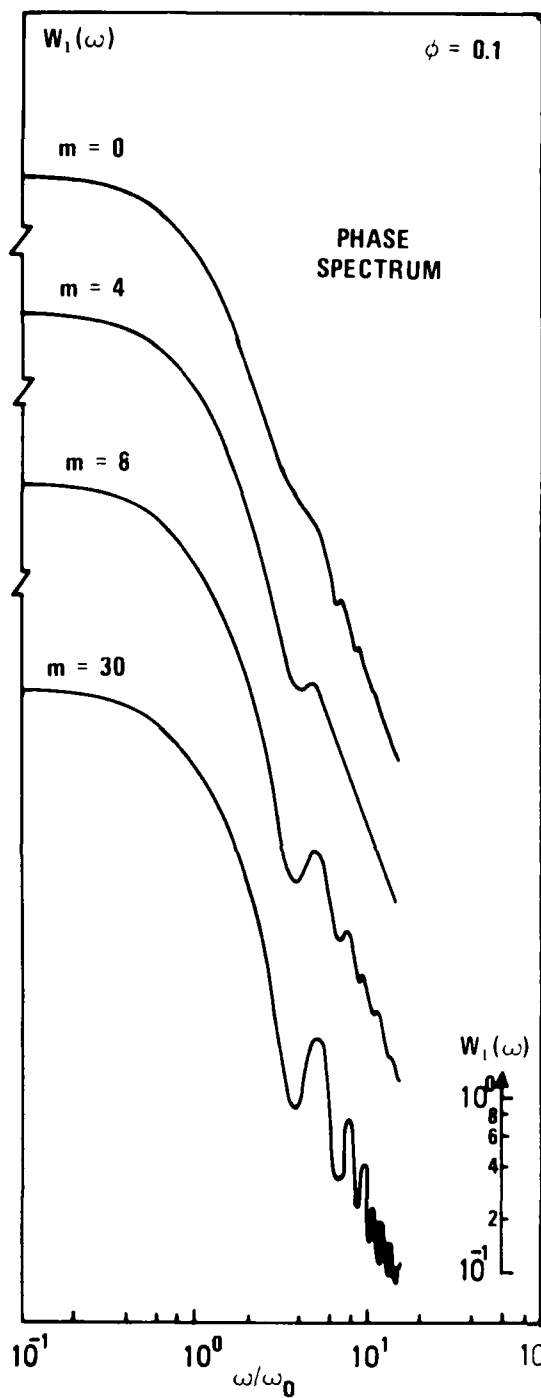


Figure 4.5 Phase scintillation power spectrum for different occultation geometries and a fixed depth $\phi = 0.1$, assuming $\omega_c/\omega_0 = 3$

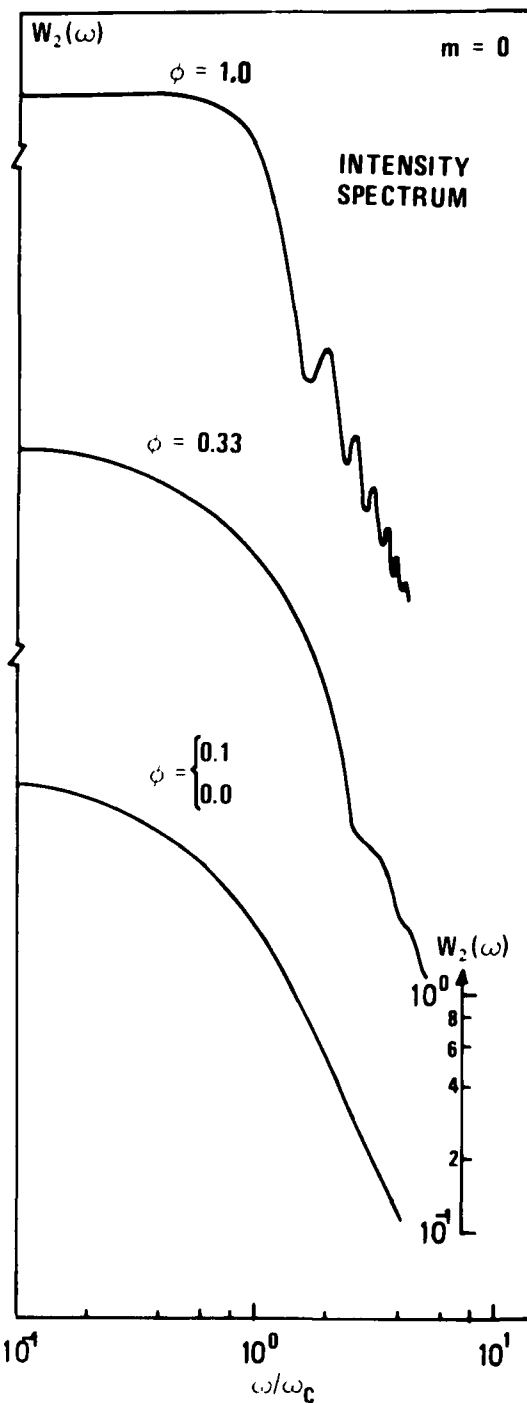


Figure 4.6 Point source intensity scintillation power spectrum at various depths ϕ in a central occultation, assuming $\omega_c/\omega_0 = 3$

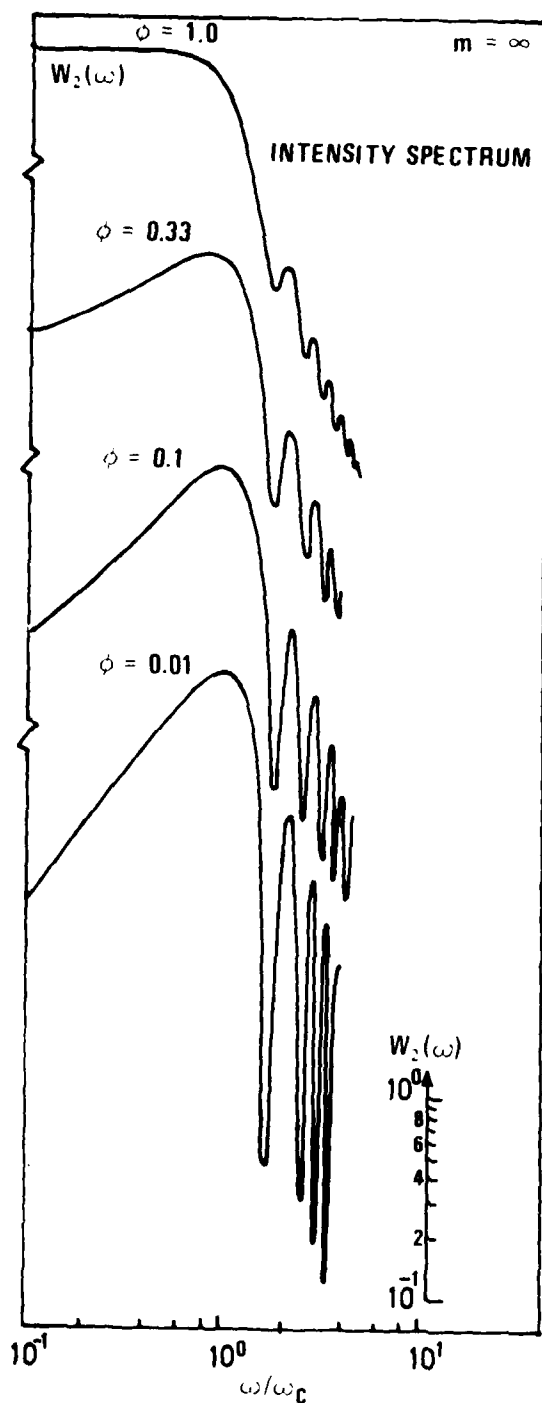


Figure 4.7 Point source intensity scintillation power spectrum at various depths ϕ in a grazing occultation, assuming $\omega_c/\omega_0 = 3$

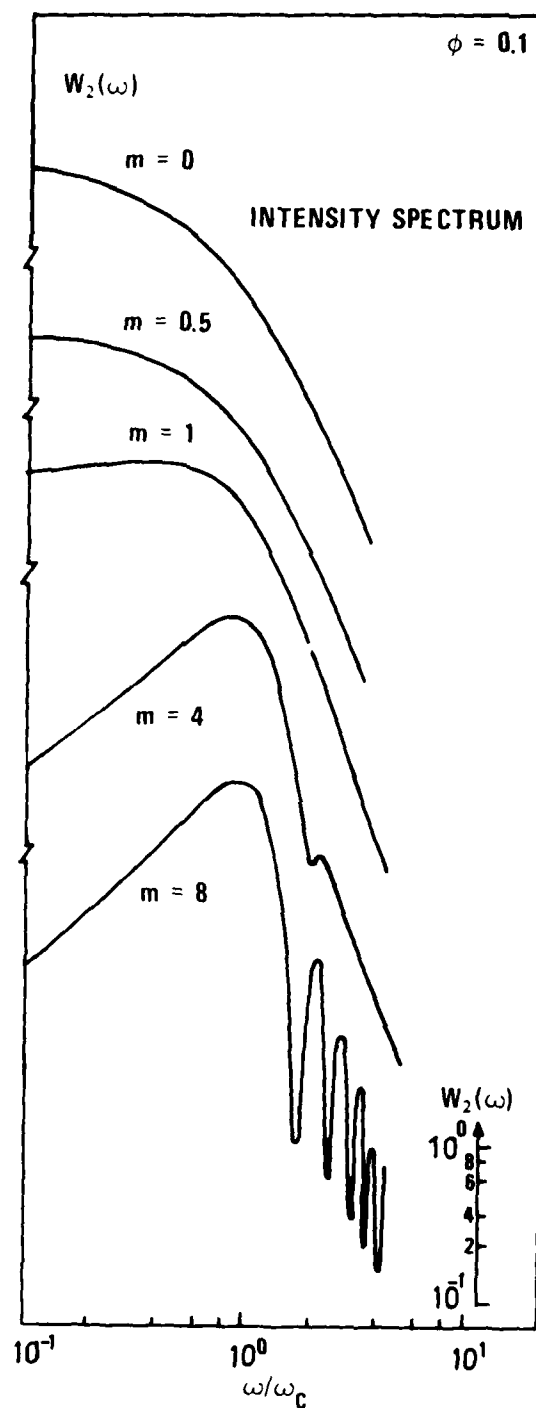


Figure 4.8 Point source intensity scintillation power spectrum for different occultation geometries and a fixed depth $\phi = 0.1$, assuming $\omega_c/\omega_0 = 3$

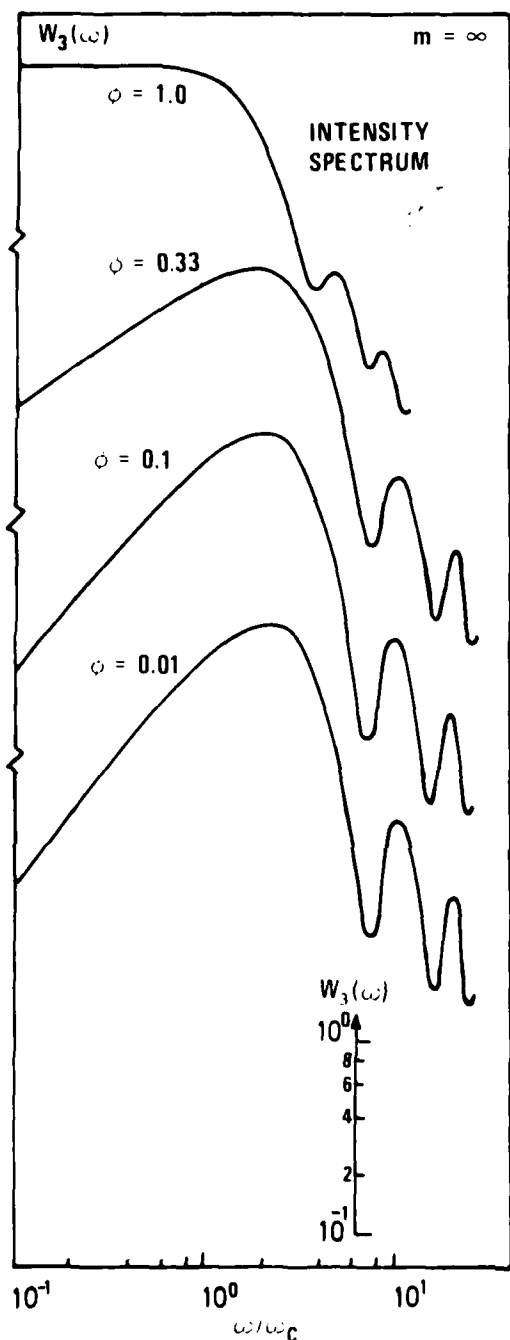


Figure 4.9 Stellar scintillation power spectrum for various occultation depths ϕ in a grazing occultation, assuming $\omega_c/\omega_0 = 3$ and $a_s/a_{F,0} \gg 1$

will yield no substantial effect on either the scintillation index or the power spectrum. In this case power spectra will correspond closely to the point source scintillation spectra of Figures 4.6–4.8.

The classical Rytov results for the phase and intensity power spectra calculated for turbulence superimposed on a homogeneous background correspond to the cases $\phi = 1.0$ in Figures 4.3, 4.6 and 4.9.

4.4.2 Observed power spectra

Power spectra calculated from the Mariner 5 and 10 Venus encounters (Woo *et al* 1974, Woo 1975a, Woo *et al* 1980) and from the Pioneer-Venus entry probes (Woo *et al* 1979) have been reported in the literature. For missions by other planetary spacecraft and for stellar occultations no corresponding results have been published.

Figures 4.10a–b, taken from Woo *et al* (1974), show the recorded part of the Mariner 5 S-band entrance and exit occultation as a function of universal time and altitude above the mean Venusian surface. Regions marked A to D were suspected of containing structures due to turbulence, and were selected for further analysis. After removal of a quadratic trend function from the exit data, Woo *et al* (1974) calculated the temporal power spectra and compared with predictions from a layered turbulence model fitted to standard weak scintillation formulas, assuming *a priori* that $L_0 \ll a_{F,0}$. In a later comparison Woo (1975a) claimed improved theoretical fit to the Mariner 5 spectra by instead assuming $L_0 \gg a_{F,0}$. Neither analyses accounted for coupling to the inhomogeneous background, however. As apparent from the previous analysis, accounting for this effect is instrumental in the present case where ϕ^{-1} may reach a hundred or more.

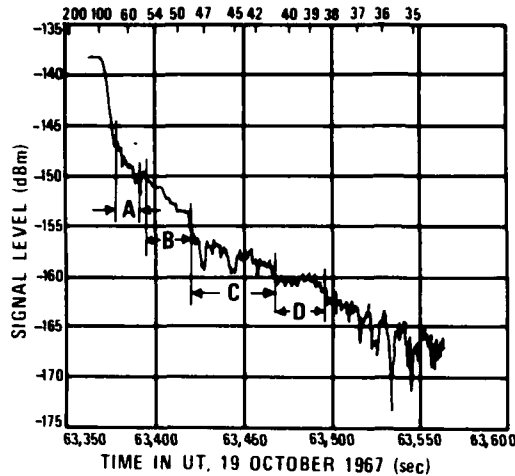


Figure 4.10a

Time history of signal intensity for the recorded part of the Mariner 5 Venus entrance occultation, as adapted from Woo et al (1974)

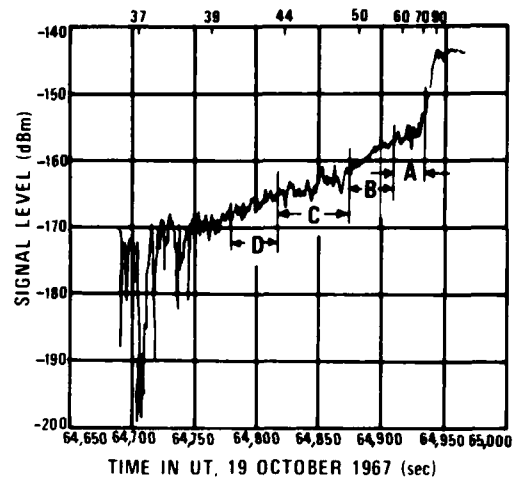


Figure 4.10b

Time history of signal intensity for the recorded part of the Mariner 5 Venus exit occultation, as adapted from Woo et al (1974)

The upper abscissa gives the altitude of the ray periapsis above the mean Venusian surface. Regions A to D were suspected for their turbulence content and selected for further examination.

In Figures 4.11 and 4.12 we have overlaid experimental spectra from regions A and C of the Mariner 5 exit occultation with theoretical spectra calculated from equation (4.37). (Experimental spectra from other atmospheric regions do not raise significantly above the noise level.) The relevant input parameters for this calculation were obtained from Fjeldbo et al (1971), yielding $a_{F,0} \cong 1.3 \cdot 10^3$ m, $v_z \cong 7.5 \cdot 10^3$ ms⁻¹ and $v_y \cong 3 \cdot 10^2$ ms⁻¹ for both regions A and C. Since $\phi_y \cong 1$, we have $v_y^* \cong v_y$ and $v_z^* \cong \phi v_z$, with ϕ estimated from Figure 4.10b as $\cong 0.05$ for region A and $\cong 0.01$ for region C. Weak scintillation theory is here appropriate since the computed scintillation index for both events is small compared to unity.

It is apparent from Figure 4.11 that the position of the "knee" in the theoretical and experimental power spectra agree quite well, a fact strongly favoring turbulence as the cause of the observed fluctuations in signal strength. For region A there is a clear discrepancy between the spectral shapes, however. While the theoretical spectrum appears to match the average high frequency slope of the Mariner 5 spectrum, the strong fringes in the experimental spectrum are not reproduced in the theoretical prediction. Even though both spectra display a decrease in scintillation power below the Fresnel frequency, they are clearly discrepant also in this region. The reason for this difference is presently not clear; a contributing factor may be a possible low quality of the experimental spectrum itself, however. Indeed, the remarkable uniformity of this spectrum, as compared to the other Mariner 5 spectrum in Figure 4.12 and when contrasted with the 90% confidence limits indicated in the figure, clearly cast doubts on the validity of the spectrum. It may be that the "zero-fill" operation applied to the original data in order to evaluate the Fourier transforms at closer-spaced intervals than would otherwise be possible (Woo et al 1974, pp 1700), has introduced substantial correlation between neighboring power estimates with a corresponding reduction in power variance. For a sharp spectral knee this correlation would leave essentially unchanged the position of the knee, but would tend to smooth any structures, e.g fringes, in the spectrum. This does not, however, explain the regular fringes that still persist in the experimental spectrum, nor its strong decay at sub-Fresnel frequencies.

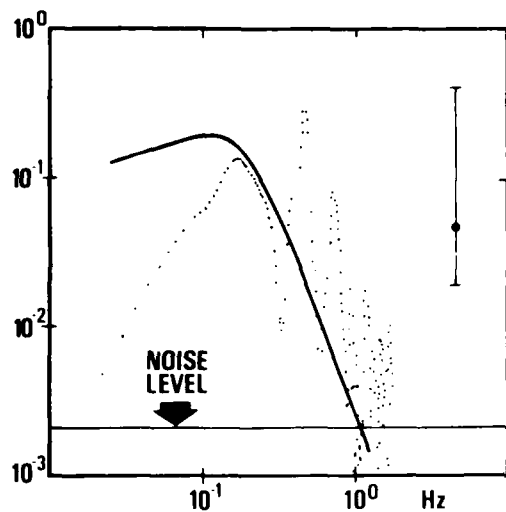


Figure 4.11 Log-amplitude power spectrum for region A of the Mariner 5 exit occultation (dotted curve), as adapted from Woo *et al* (1974)

Superimposed is the theoretical spectrum (solid curve) based on the actual occultation parameters, and displaced along the ordinate axis to yield maximum fit. The error bar represents a 90% confidence interval.

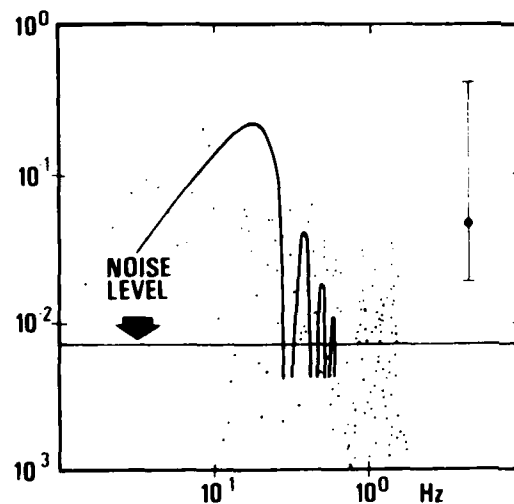


Figure 4.12 Log-amplitude power spectrum for region C of the Mariner 5 exit occultation (dotted curve), as adapted from Woo *et al* (1974)

Superimposed is the theoretical spectrum (solid curve) based on the actual occultation parameters, and displaced along the ordinate axis to yield maximum fit. The error bar represents a 90% confidence interval.

The experimental spectrum shown in Figure 4.12 displays scatter among individual spectral estimates that appears more consistent with the indicated 90% confidence limits. There is an indication that both the predicted position of the spectral knee and a decrease in power at lower frequencies is reproduced in this event.

Power spectra calculated by Woo (1975a) from the Mariner 10 Venus occultation lack the low-frequency part below ω_c , and also appear to be smoothed at higher frequencies to an extent that would make a comparison with the theoretical power spectra virtually impossible. Due to the much smaller turbulent medium-to-probe distances involved, the Pioneer Venus entry probes failed to detect any intensity scintillations, establishing essentially an upper bound on the refractivity fluctuations in this case (Woo *et al* 1979).

Figure 4.13 shows a power spectrum based on the Mariner 10 Venus occultation profile as calculated by Lipa and Tyler (1979). The spectrum corresponds in altitude approximately to the region labeled A by Woo *et al*. The figure shows both the experimental and theoretical power spectra, together with part of the exit occultation intensity time profile and the small segment subjected to spectral analysis. The experimental spectrum is calculated by first fitting a polynomial of varying degree to the intensity background, and then subtracting this trend function from the signal to obtain the fluctuating part. The residual variance of the signal relative to the polynomial trend is shown as a function of the degree N of the polynomial in Figure 4.14. Initially the residual variance is seen to decrease rapidly with N , but then becoming virtually insensitive to this parameter for $N > 5$. Thus a fifth degree polynomial was subtracted from the intensity-time profile, and the difference was normalized by the trend function and subjected to a power spectral analysis, the result of which is shown in Figure 4.13. The corresponding theoretical spectrum has been shifted along

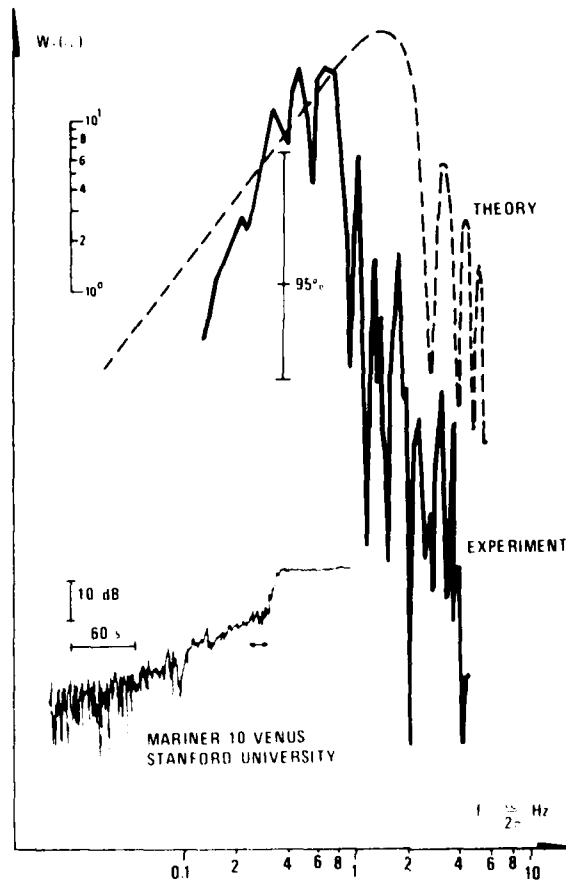


Figure 4.13 Experimental and theoretical power spectrum corresponding to the approximately 16 s portion of the Mariner 10 Venus exit occultation indicated in the lower left part of the figure

power spectra from different occultations, or through substantial *spatial* averaging in a single grazing occultation, where the ray moves many Fresnel scales at essentially constant altitude. Removal of the background intensity from the scintillations poses yet another fundamental problem. When the scintillation spectrum and the trend function have finite power in a common frequency range, which may normally be the case, complete separation of fluctuations and trend is not possible even in principle (Yaglom 1962). It is nevertheless imperative that a common and well-defined procedure be used when removal of the trend is attempted. The technique suggested here is both well-defined and statistically sound (Draper and Smith 1960, Chatterjee and Price 1977).

the ordinate axis to yield maximum fit. The low-frequency parts are seen to agree fairly well. Also the high frequency portions are not in obvious disagreement, the large scatter of the data points taken into account. The possible discrepancy between the position of the Fresnel knees may, at least in part, be attributed to the limited statistical significance of the experimental spectrum.

Preliminary analysis of other parts of the Mariner 10 occultation profile suspected of containing structures due to turbulence has not yielded a consistent result. Most of the fluctuations seen in the deeper parts of the occultation profile turn out to be noise, consistent with the findings of Woo and colleagues for the Mariner 5 occultation. At least in one other region does the power spectrum raise above the background noise, but yet does not match its theoretical prediction. It is possible that this region does not correspond to well-developed turbulence, or that the statistical significance is simply too low to provide a meaningful comparison with the statistical mean spectrum of the theoretical analysis.

Spectra of higher statistical significance, essential to an experimental assessment of the theory developed here, may in principle be obtained from the averaging of

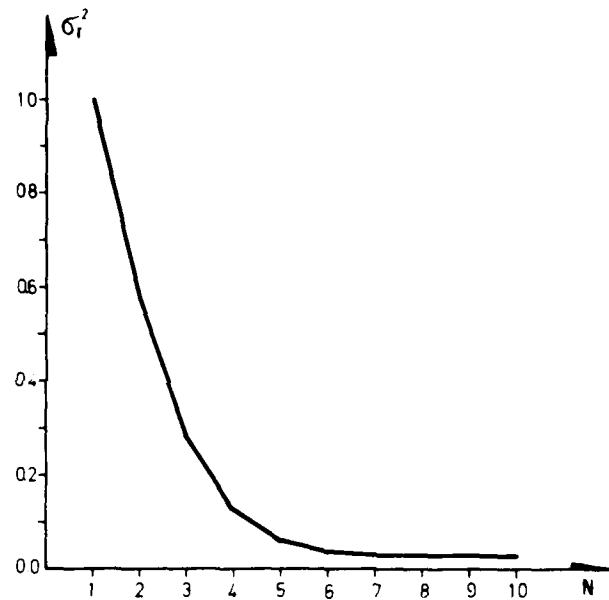


Figure 4.14 Rest variance, σ_r^2 , of intensity fluctuations around a polynomial trend, as a function of the degree N of the polynomial

The time series analyzed corresponds to the segment of the Pioneer 10 Venus occultation indicated in Figure 4.13.

4.5 The weak scintillation approximation in planetary occultations

Consistent with the contention made in section 4.3, we shall assume here that the theoretical results of the previous sections are valid if $\langle \hat{\phi}_1^2 \rangle \ll 1$, irrespective of the magnitude of the phase fluctuations at exit from the atmosphere. Below we explore to what extent this weak scintillation assumption may have been satisfied in past radio and stellar occultations, examining both theoretical and experimental evidence.

We define formally a critical occultation depth ϕ^* , such that

$$\langle \hat{\phi}_1^2(\phi^*) \rangle = 1$$

The theoretical results developed here are thus valid only for occultation depths such that $\phi \gg \phi^*$. In terms of ϕ^* , the scintillation index at an arbitrary depth ϕ is from equations (4.23) and (4.26)

$$\langle \hat{\phi}_1^2 \rangle = \frac{W(1, \phi; p)}{W(1, \phi^*; p)} \left(\frac{\phi^*}{\phi} \right)^2 \left(\frac{1 - \phi^*}{1 - \phi} \right)^2 \quad (4.39)$$

where W takes either of the forms given by equations (4.23b) and (4.26b) for radio and stellar occultations, respectively. In Table 4.1 we have calculated the critical depth ϕ^* for two past radio and stellar occultations. For all cases we have assumed $\langle \nu_1^2 \rangle / \nu_0^2 = 10^{-5}$ and $L_0 = H/3$, where H along with the free-space Fresnel zone and the stellar angular radius are given in Table 3.1. Since $\phi^* \ll 1$ for all four occultations, equation (4.39) simplifies to

$$\langle \hat{\phi}_1^2 \rangle \sim (\phi^* / \phi)^2 \quad (4.40)$$

when $\phi \ll 1$. It is apparent from Table 4.1 that the weak scintillation condition may have been violated in the deeper parts of these occultations if turbulence of the

	ϕ^*	ϕ_{\min}
M10/VENUS	$4 \cdot 10^{-2}$	$4 \cdot 10^{-3}$
P10/JUPITER	$3 \cdot 10^{-2}$	$1 \cdot 10^{-2}$
βSCO/JUPITER	$1 \cdot 10^{-1}$	$\cong 10^{-2}$
BD-17 4388/NEPTUNE	$6 \cdot 10^{-2}$	$\cong 10^{-2}$

Table 4.1 Approximate critical occultation depths ϕ^ and minimum occulted intensity ϕ_{\min} for two past radio and stellar occultations*

Data for the stellar occultations by Jupiter and Neptune are from Liller *et al* (1974) and Freeman and Lynga (1970), respectively.

tillation index in the ~ 60 km altitude region of pronounced turbulence identified in their analysis. In his analysis of turbulence in the Mariner 10 Venus occultation, Woo (1975a) found a value $\cong 0.1$ for the scintillation index in the same $\sim 55-70$ km altitude region previously probed by Mariner 5. While the radio occultation measurements, including that of Venera 9 (Timofeeva *et al* 1978), appear mutually consistent, estimates of the refractive index structure constant that would yield much higher values for the scintillation index have been derived from radio link analyses of the Venera 4-8 landers (Kolosov *et al* 1970, Yakovlev *et al* 1974). While this discrepancy has not yet been satisfactorily resolved, the recent Pioneer Venus entry probe measurements appear to support the radio occultation data (Woo *et al* 1979). The spacecraft measurements thus appear to predict a lower turbulence strength than would be predicted from extrapolation of measurements in the earth's troposphere.

No determination of a scintillation index for the Pioneer Jupiter missions, for the Voyager Jupiter and Saturn missions, or for any of the several past stellar occultations have been reported. The large excursions in intensity commonly observed in stellar occultations strongly indicate, however, that non-uniform atmospheric structures, possibly turbulence, would yield a formal value for the scintillation index comparable to or larger than unity. It is deemed important, after properly separating the scintillations from the main structure of the event, to calculate the scintillation index also in such cases. Since numerical simulations indicate that the scintillation index saturates to unity also when an inhomogeneous atmospheric background is accounted for (French *et al* 1980)*, values of $\langle \phi_1^2 \rangle$ that were larger than unity, for example, would immediately rule out turbulence as the sole cause of these intensity variations. Additional clues as to the nature of the underlying atmospheric structure might then be obtained from an examination of the scintillation power spectrum, as discussed more fully in section 7.

strength found at the ~ 15 km level of the earth's troposphere is also present at the higher altitudes probed on Venus, Jupiter and Neptune.

Data from the Mariner 5 Venus occultation have been analyzed by Gurvich (1969), Golitsyn and Gurvich (1971) and by Woo *et al* (1974) for the variance of the log-amplitude fluctuations. Accounting for a factor of 4 between this quantity and the scintillation index, Golitsyn and Gurvich (1971) estimated the scintillation index to be about $2 \cdot 10^{-2}$ for both the night side immersion and day side emersion. This value is an average over altitude corresponding to an approximate pressure range of 1-5 bar. Woo *et al* (1974) obtain a similar figure ($\sim 4 \cdot 10^{-2}$) for the scin-

* Recent results by this author, based on a slight generalization of the stationary phase technique developed in section 3, shows that the scintillation index indeed saturates to unity also in the presence of an inhomogeneous background.

5 PROFILE ERRORS DUE TO TURBULENCE

As previously stated, the inversion procedure to obtain profiles of refractivity, temperature and pressure from occultation measurements assumes the atmospheric refractivity to have a spherical distribution. Turbulence violates this condition, and since the perturbations in signal intensity and Doppler frequency due to turbulence are non-linear functionals of the generic refractivity fluctuations, such profiles will contain both random (zero mean) and systematic (finite mean) errors. We estimate in this section the magnitude of these errors, and shall find that the random and systematic errors are both small in the limit of weak scintillations, consistent with the simple argument given in section 2.2.

5.1 Random errors in atmospheric profiles from radio or stellar intensity measurements

Let $n_{\star} = 1 + \nu_{\star}$ be the refractive index calculated from the formal inversion given by equation (2.1b). Let $a' = a + p$, where $p/a \sim p/R \ll 1$. To lowest order in ν_{\star} this equation becomes

$$\nu_{\star}(r_0) = \frac{1}{\pi D} \left(\frac{2}{R}\right)^{1/2} \int_0^{\infty} M(a+p) p^{1/2} dp \quad (5.1)$$

We have here used the approximation $\cosh^{-1}(a'/a) \sim (2p/R)^{1/2}$, and the argument $a+p$ of $M = \alpha D/H$ signifies that α is the bending angle of a ray with impact parameter $a+p$. Since $\alpha = (2\pi R/H)^{1/2} \nu_0$ for small bending angles in a spherically symmetric and isothermal atmosphere, direct substitution in equation (5.1) yields $\nu_{\star} = \nu_0$, as required in this case.

When turbulence is present, the signal intensity may be expanded in powers of ν_1 as in

$$\phi \equiv \phi_Z + \phi_1 + \dots = \phi_Z (1 + \hat{\phi}_1 + \dots) = (1 + M)^{-1} \quad (5.2)$$

The last equality assumes that the signal intensity is still related to the ray bending angle as if no turbulence were present in a shallow occultation. Combination of the two previous equations yields for the lowest order error $\nu_{\star 1}$ relative to the "true" refractivity ν_0 of the ambient atmosphere

$$\nu_{\star 1} = \frac{1}{\pi D} \left(\frac{2}{R}\right)^{1/2} \int_0^{\infty} \frac{\hat{\phi}_1(a+p)}{\phi_Z(a+p)} p^{1/2} dp \quad (5.3)$$

The argument $a+p$ of $\hat{\phi}_1$ and ϕ_Z signifies again that these quantities are calculated with respect to a ray of impact parameter $a+p$. Clearly, as $\langle \hat{\phi}_1^2 \rangle \rightarrow 0$ the refractivity error vanishes and $\nu_{\star} \rightarrow \nu_0$.

Since $\nu_{\star 1}$ is a stochastic quantity, only its mean and variance (and possibly also higher statistical moments) are of interest. The mean value is zero, since clearly $\langle \hat{\phi}_1 \rangle = 0$. The fractional variance of this quantity is, from equation (5.3)

$$\frac{\langle \nu_{\star 1}^2 \rangle}{\nu_0^2} = \frac{2}{\pi^2} \frac{\langle \hat{\phi}_1^2 \rangle}{RD^2 \nu_0^2} \iint_0^{\infty} (1 + M e^{-\beta p_1})(1 + M e^{-\beta p_2}) e^{-\beta t(p_1 + p_2)} \cdot p_1^{1/2} p_2^{1/2} \rho(p_2 - p_1) dp_1 dp_2 \quad (5.4)$$

All atmospheric variables where an argument has not been assigned are referenced to the ray impact parameter $a' = a$. In establishing this equation we have used the fact that $\langle \hat{\phi}_1(a+p_1) \hat{\phi}_1(a+p_2) \rangle = \langle \hat{\phi}_1^2(a) \rangle \exp(-\beta t(p_1 + p_2)) \rho(p_2 - p_1)$, where ρ is the (normalized) autocorrelation function of the (normalized) intensity scintillations at the receiver; $\beta^{-1} = H$ and $\beta_t^{-1} = H_t$ as before. In the following we shall not distinguish

between H and H_1 . Let

$$I \equiv \int_0^\infty \rho(\Delta p) d(\Delta p) \quad (5.5)$$

be the correlation length of the intensity scintillations, and let $F(p_1, p_2)$ be a function that changes slowly on a length scale $\sim I$, so that

$$\iint_{00}^\infty F(p_1, p_2) \rho(p_2 - p_1) dp_1 dp_2 \cong I \int_0^\infty F(p_1, p_1) dp_1 \quad (5.6)$$

It may be shown using the definition (5.5) together with equation (4.7) that I is typically on the order of $a_{F,0}$ in a shallow occultation. Therefore, in the range $0 \leq (p_1, p_2) \leq H$ where equation (5.4) derives its principal contribution, the co-factor of ρ in the integrand of this equation satisfies the condition for using relation (5.6). For the $\phi \sim 1$ region of principal interest we thus obtain

$$\frac{\langle p_{*1}^2 \rangle}{p_0^2} \sim \frac{1}{H} \langle \hat{\phi}_1^2 \rangle \quad (5.7)$$

From equations (2.6) and (2.7) it may be shown that the corresponding fractional errors in temperature and pressure are approximately

$$\left(\frac{\langle T_{*1}^2 \rangle}{T_0^2}, \frac{\langle p_{*1}^2 \rangle}{p_0^2} \right) \cong \frac{1}{H} \langle \hat{\phi}_1^2 \rangle \quad (5.8)$$

where T_{*1} and p_{*1} are the lowest-order errors in temperature and pressure, respectively, relative to the "true" ambient values T_0 and p_0 . Thus the fractional mean square errors in derived refractivity, temperature and pressure are all small in the limit of weak scintillations. For stellar occultations the same result applies, except that the correlation length I may be different from $\cong a_{F,0}$ in this case. If the projected stellar radius a_s significantly exceeds $a_{F,0}$, $I \cong a_s$, and relations (5.7) and (5.8) are still valid if also $a_s \ll H$.

It is interesting to note that if the Baum and Code equation (2.5) were used to estimate the scale height and hence the temperature, the corresponding mean square fractional error in temperature would be approximately $\langle \hat{\phi}_1^2 \rangle$ for $\phi \ll 1$. Thus the integral inversion technique is less sensitive to intensity scintillations than curve-fitting to the Baum and Code equation by a factor $1/H \ll 1$.

5.2 Random errors in atmospheric profiles from Doppler measurements

For a spherically stratified refractivity field the atmospheric Doppler frequency f is related to the small bending angle α approximately as in

$$-\lambda f = v_z \alpha \quad (5.9)$$

where v_z is the component of the spacecraft velocity in the plane of refraction that is perpendicular to the incoming ray asymptote. When turbulence is present, the Doppler frequency may be expanded as $f = f_0 + f_1 + \dots$, where $f_0 = \mathcal{O}(\nu_0)$, $f_1 = \mathcal{O}(\nu_1)$ etc. Since equation (5.9) is still used to infer the bending angle also when turbulence is present, the estimated angle, $\alpha = \alpha_*$, may be similarly expanded in powers of ν_1 according to $\alpha_* = \alpha_{*0} + \alpha_{*1} + \dots$. From equation (2.1b), and using a similar expansion of $\cosh^{-1}(a'/a)$ as in equation (5.1), we find that the estimated refractivity ν_* is

$$\nu_{*0} = \frac{1}{\pi} \left(\frac{2}{R} \right)^{1/2} \int_0^\infty \frac{d\alpha_0(a+p)}{dp} p^{1/2} dp \quad (5.10)$$

$$\nu_{*1} = \frac{\lambda}{\pi v_z} \left(\frac{2}{R} \right)^{1/2} \int_0^\infty \frac{df_1(a+p)}{dp} p^{1/2} dp \quad (5.11)$$

where, clearly, $\nu_{*0} = \mathcal{O}(\nu_0)$, $\nu_{*1} = \mathcal{O}(\nu_1)$, etc. Using the standard, small angle expression for α , equation (5.10) is readily shown to yield $\nu_{*0} = \nu_0$. The lowest-order error to this "true" refractivity profile is thus represented by equation (5.11). In terms of the covariance function (assuming local homogeneity)

$$B(p_1, p_2) \equiv \left\langle \frac{df_1(a+p_2)}{dp_2} \frac{df_1(a+p_1)}{dp_1} \right\rangle = \left\langle \left(\frac{df_1(a)}{da} \right)^2 \right\rangle \rho(p_2 - p_1)$$

the mean square fractional error in refractivity is in this case

$$\left\langle \frac{\nu_{*1}^2}{\nu_0^2} \right\rangle = \frac{2}{\pi^2} \frac{\lambda^2}{R v_z^2} \left\langle \left(\frac{df_1}{da} \right)^2 \right\rangle \int_0^\infty \int_0^\infty e^{-\beta_1(p_1+p_2)} \rho(p_2 - p_1) p_1^{1/2} p_2^{1/2} dp_1 dp_2 \quad (5.12)$$

The first-order Doppler perturbation is related to the corresponding perturbations in bending angle as in

$$-\lambda f_1 = v_y \beta_1 + v_z \alpha_1$$

where β_1 and α_1 are the first-order perturbations in ray bending angle in the xy - and xz plane, respectively.

Proceeding from this stage to evaluate $\langle (df_1/da)^2 \rangle$ and ρ via the statistical properties of β_1 and α_1 turns out to be extremely difficult, essentially for the reasons given at the end of section 4.1. As an alternative approach to a direct theoretical evaluation, one might estimate the right hand side of equation (5.12) from occultation data. In so doing, care should be taken to properly subtract from the total atmospheric Doppler the lowest-order component, f_0 , due to the ambient atmosphere, as explained in section 4.4.2. From a record of f_1 versus impact parameter a , df_1/da along with its mean square and correlation function ρ may be estimated, yielding eventually, through the operations indicated in equation (5.12), an estimate of the mean square fractional error in refractivity.

We have shown previously that in the evaluation of the mean square fluctuations in bending angle, the exact kernel in the field integral (3.1) cannot be approximated by the quadratic Fresnel kernel. Also the complete spatial extent of the turbulent medium will have to be considered in such a calculation, as explained in section 4.1. Instead of attempting a rigorous calculation, we shall make the following heuristic arguments, which will hopefully yield the proper functional form and order of magnitude of the right hand side of equation (5.12). It may be argued on general grounds that $\langle \alpha_1^2 \rangle \ll \langle \beta_1^2 \rangle$ when $\phi_z \ll 1$. We thus approximate $-f_1 \approx (v_y/\lambda) \beta_1$, while also assuming $v_y = \mathcal{O}(v_z)$. Due to the assumed exponential variation of the rms turbulent refractivity fluctuations, the *effective* width of the turbulent medium parallel to the limb is $\ell \sim (RH_1)^{1/2}$. Perpendicular to the limb the effective width may be shown to be at most on the order of H when $\phi < 1$. The smallest eddy sizes capable of scattering elementary waves within an aperture of these dimensions is therefore $\ell_y \sim \lambda D/\ell$ and $\ell_z \sim \lambda D/H$ in the y - and z -directions, respectively. The correlation length of $d\beta_1/da$ can therefore be no smaller than the least of these dimensions, i.e., ℓ_y . Also, when the turbulent phase perturbation of the wave is one radian, the rms turbulent bending angle can be at most on the order of $\beta_1 \sim \lambda/\ell_y$. Omitting numerical factors, we thus find that an approximate upper bound on the right hand side of equation (5.12) is such that

$$\left\langle \frac{\nu_{*1}^2}{\nu_0^2} \right\rangle \leq \left(\frac{H_{t,0}}{a_{F,0}} \right)^2 \left(\frac{\ell}{D} \right)^2 \frac{\ell}{R} \quad (5.13)$$

Adopting numerical values appropriate for the Mariner 10 Venus and Pioneer 10 Jupiter occultations, we find that the right hand side of relation (5.13) is approximately $6 \cdot 10^{-3}$ and $3 \cdot 10^{-5}$, respectively. Thus the refractivity error is small even when

the turbulent phase perturbation approaches the strong scattering regime. We also observe from relation (5.13) that the refractivity error *decreases* with increasing planet-spacecraft distance, all other quantities remaining constant. The refractivity error incurred from the inversion of radio intensity measurements yielded an increase in this error (proportional to $D^{7/3}$ for $\phi \ll 1$; cf equations (4.23) and (5.7)) with propagation distance, and is probably much larger than that calculated here for Doppler measurements at any occultation depth.

From equations (2.6) and (2.7), and consistent with the crudeness of the analysis presented here, we finally conclude that also the fractional temperature and pressure errors are small, being approximately

$$\left(\frac{\langle T_{*1} \rangle}{T_0^2}, \frac{\langle p_{*1}^2 \rangle}{p_0^2} \right) \lesssim \left(\frac{H_t \ell}{a_{F,0} D} \right)^2 \frac{\ell}{R} \quad (5.14)$$

where, as before, T_{*1} and p_{*1} are the lowest-order errors in temperature and pressure relative to the ambient values T_0 and p_0 .

5.3 Systematic profile errors

The possibility that atmospheric profiles obtained from occultation measurements were inflicted by *systematic* errors in addition to the random errors discussed here, was first raised by Hubbard and Jokipii (1975). As a result of additional contributions and subsequent critical responses by other authors, certain aspects of the theory of these higher-order effects, e.g. their wavelength dependence, are still under debate (cf discussion and references quoted in section 1.1). However, both parties apparently agree that the systematic effects are too small to be of much practical concern, and a discussion of this topic here may therefore seem unwarranted. From a theoretical point of view these effects command substantial interest, however, and they indeed appear to have passed virtually unnoticed in previous analyses of electromagnetic wave propagation in randomly inhomogeneous media*. We shall therefore provide here a brief discussion of these effects, developing first a geometrical optics result for the systematic phase error and proceed by generalizing to wave optics. From this result, the form and approximate magnitude of the systematic errors in intensity and bending angle will be established along with the resulting errors in the calculated refractivity profile.

5.3.1 The second-order phase bias

Following the treatment of Eshleman and Haugstad (1977) and Haugstad (1978b), consider a thin phase-changing screen representing homogeneous and isotropic turbulence superimposed on a homogeneous background, see Figure 5.1.

A plane wave impinging on the screen as indicated is refracted through small angles α_1 and β_1 in the xz - and xy -planes of propagation, respectively. The total phase change of the wave by propagating through the screen to the receiver at $x = \ell/2 + D \cong D$ is kS , where in geometrical optics the optical path S is simply

$$S = \int_0^D n(x, y(x), z(x)) ds \quad (5.15)$$

* Tatarskii (1971; pp 256) calculates the second-order, systematic phase change due to turbulence, but he uses the result to merely establish the conditions for convergence of the method of smooth perturbations. Keller (1962) has calculated the systematic, second-order phase shift for geometrical optics, but his result differs from that obtained here. Keller (1977) has later corrected for an error in his calculation, which brings his result into exact agreement with that given by equation (5.22) here.

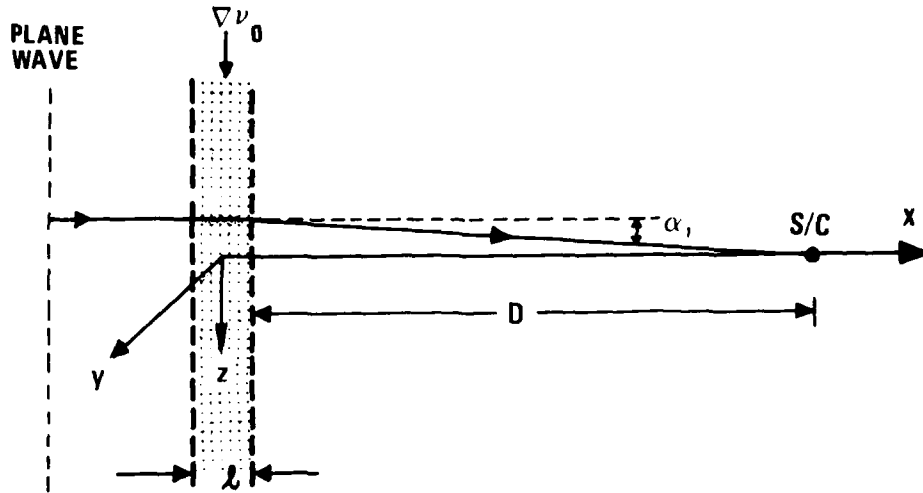


Figure 5.1 Radio wave propagation through homogeneous and isotropic turbulence superimposed on a homogeneous background

The spacecraft is located on the x-axis a distance $D \gg l$ from the exit face of the screen.

Here $n = 1 + \nu \equiv 1 + \nu_0 + \nu_1$ is the refractive index, and

$$ds = [1 + (\frac{dy}{dx})^2 + (\frac{dz}{dx})^2]^{1/2} dx \quad (5.16)$$

is a differential along the raypath represented by the space curve $y(x), z(x)$.

The zero-order raypath is clearly $y_0(x) = z_0(x) = 0$, since ν_0 is homogeneous. Denoting by $y_1(x), z_1(x)$ the first-order perturbations in the raypath induced by the turbulence, we find through second order in small quantities by expanding ν_1 and ds relative to the zero-order raypath

$$S = \int_0^D (1 + \nu_0 + \nu_1 + \nu_{1,y} y_1 + \nu_{1,z} z_1) (1 + \frac{1}{2} \beta_1^2 + \frac{1}{2} \alpha_1^2) dx \quad (5.17)$$

All quantities are here evaluated on the zero-order raypath, i.e., $\nu_1 = \nu_1(x, 0, 0)$, $\nu_{1,y} = \nu_{1,y}(x, 0, 0)$ etc, and subscript y or z on ν_1 denotes differentiation with respect to that argument. In deriving this result we have also used the fact that $\beta_1 = dy_1/dx$ and $\alpha_1 = dz_1/dx$ for small bending angles α_1 and β_1 .

The integral in equation (5.17) should be evaluated subject to the boundary conditions

$$\begin{aligned} \nu_1 = \nu_{1,y} = \nu_{1,z} = 0 \quad \text{at} \quad x = 0 \\ y_1 = z_1 = 0 \quad \text{at} \quad x = D \end{aligned} \quad (5.18)$$

Expanding formally $S = S_0 + S_1 + S_2$, where $S_1 = \mathcal{O}(\nu_1)$, $S_2 = \mathcal{O}(\nu_1^2)$, we then obtain

$$S_0 = \int_0^D (1 + \nu_0) dx \quad (5.19a)$$

$$S_1 = \int_0^D \nu_1 dx \quad (5.19b)$$

$$S_2 = \left\{ \int_0^D \nu_{1,y} y_1 dx + \int_0^D \nu_{1,z} z_1 dx \right\} + \frac{1}{2} D(\alpha_1^2 + \beta_1^2) \quad (5.19c)$$

In the last result we have used the fact that $\int \alpha_1^2 dx \cong D\alpha_1^2$ and $\int \beta_1^2 dx \cong D\beta_1^2$, where α_1 and β_1 are now the final, first-order bending angles in the xz- and xy plane, respectively. The ensemble averaged optical path length is now, since $\langle \nu_1 \rangle = 0$

$$\langle S \rangle = S_0 + \langle S_2 \rangle \equiv S_0 + \ell_1 + \ell_2 \quad (5.20)$$

where we have defined, in view of equation (5.19c)

$$\begin{aligned} \ell_1 &= \frac{1}{2} D (\langle \alpha_1^2 \rangle + \langle \beta_1^2 \rangle) \\ \ell_2 &= \int_0^D \langle \nu_{1,y} y_1 \rangle dx + \int_0^D \langle \nu_{1,z} z_1 \rangle dx \end{aligned} \quad (5.21)$$

Integrating by parts the last expression and applying the boundary conditions (5.18) yields

$$\ell_2 = -D(\langle \alpha_1^2 \rangle + \langle \beta_1^2 \rangle)$$

Thus there is a net *reduction* in average optical path by an amount

$$\langle S \rangle - S_0 = -\frac{1}{2} D (\langle \alpha_1^2 \rangle + \langle \beta_1^2 \rangle) \quad (5.22)$$

relative to a non-turbulent atmosphere of refractivity ν_0 . An alternative statement of this result is that the average phase velocity is *increased* in the presence of turbulence (Haugstad 1976, Eshleman and Haugstad 1977, Haugstad 1978b). The appropriate generalization of this result to an inhomogeneous background is (Haugstad 1978b)

$$\langle S_2 \rangle = -\frac{1}{2} D (\phi_y \langle \beta_1^2 \rangle + \phi_z \langle \alpha_1^2 \rangle) \quad (5.23)$$

where α_1 and β_1 are the bending angles produced by turbulence on a *homogeneous* background.

The above derivation of $\langle S_2 \rangle$ apparently allows the following interpretation to be made. The total change in phase path has two contributions, ℓ_1 and ℓ_2 . The former component represents the increase in phase path associated with the longer geometrical path to the receiver. This increase is more than offset, however, by the ℓ_2 -component, which represents a twice as large *decrease* in phase path associated with the rays "success" in traversing the refractive medium in such a way as to encounter, on the average, a lower than average refractivity. We observe from equation (5.22) that the bias in phase path increases with propagation distance in vacuum between the turbulent medium and the receiver.

A wave-optical calculation shows that the general weak scattering result for the bias in phase path is (Haugstad 1978c)

$$\langle S_2 \rangle = -\langle \chi_1 S_1 \rangle \quad (5.24)$$

where χ_1 and S_1 are the first-order, wave optical expressions for log-amplitude and phase path. Employing equations (4.7) and (4.8) and noting that $2\chi_1 = \phi_1$, we find that

$$\langle S_2 \rangle = -\pi k \ell \iint_{-\infty}^{\infty} \Phi(u_\perp) \sin(P) du_\perp \quad (5.25)$$

with P given as before. A comparison of this result with the geometrical optics expression (5.23) shows that the two results are indeed identical in the limit $k \rightarrow \infty$. A further comparison of the two results also reveals that diffraction strongly suppresses contributions to $\langle S_2 \rangle$ from turbulent eddy sizes smaller than the atmospheric

Fresnel zone. We also find that for Kolmogorov turbulence the bias in phase path scales with radiation wavelength as $\lambda^{-1/6}$, implying that an initially non-dispersive medium becomes slightly dispersive by the addition of turbulence (Haugstad 1978c,d, Haugstad and Eshleman 1979). A result similar to equation (5.25) has also been obtained by Lee (1976) from an evaluation of the second-order scattering produced by simple diffraction grating.

5.3.2 Systematic errors in atmospheric profiles from Doppler or intensity measurements

If the bias in optical path changes spatially, as a result of a spatial variation in either ν_0 or $\langle \nu_1^2 \rangle$, a finite bias in both bending angle (and hence in Doppler frequency) and intensity may result, as illustrated in Figure 5.2. The turbulence strength is here assumed to increase with atmospheric depth so that the average phase advance is greater in the denser region of the atmosphere (cf equations (5.22) or (5.25)). It is seen from the figure that a linear spatial variation of $\langle \nu_1^2 \rangle$ gives rise to a bias in ray bending angle, whereas a non-vanishing second derivative of this quantity yields a net focusing or defocusing of the rays and hence a bias in signal intensity.

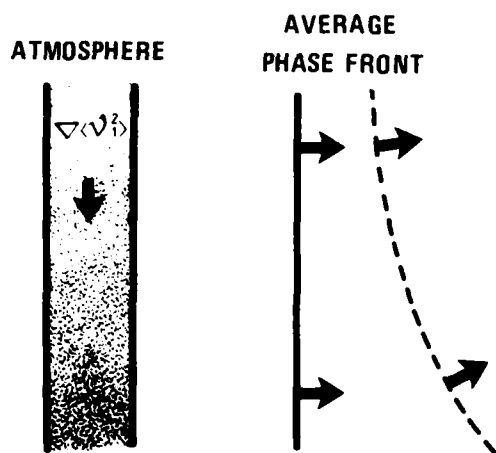


Figure 5.2 Illustration of the average effect of turbulence on phase path, bending angle and intensity

The solid curve shows the position of the phase front behind a homogeneous ambient atmosphere void of turbulence. The broken curve shows the curved phase front when turbulence of increasing strength in the z -direction is superimposed.

Haugstad 1978a, Eshleman and Haugstad 1979, Hubbard 1979). However, for shallow occultations several lines of reasoning indicate that the intensity bias must be of the form

$$\langle \phi_2 \rangle \sim \phi_z \int_0^D \frac{\partial \langle \alpha_2 \rangle}{\partial z} dz \quad (5.27)$$

in both geometrical optics and wave optics, since, for reasons of energy conservation, a finite value of $\langle \phi_2 \rangle$ is conditional on a systematic spatial variation of the angular bias*. As the arguments over the precise form of both the angular bias and the intensity bias, along with the question of their wavelength dependence, have become extremely technical in nature, we shall make no attempt here to provide a balanced exposé of these issues. Rather, since the resulting effect of these biases on derived profiles is agreed by both parties to be very small, we shall instead use simple order of magnitude arguments to merely establish the approximate magnitude of these errors.

* Relation (5.27) also assumes that $\langle \beta_2 \rangle \equiv 0$. This will always be true if both ν_0 and $\langle \nu_1^2 \rangle$ have strictly spherical symmetry, which will be assumed here.

Mathematically the bias in bending angle is related to that in phase path as in

$$\langle \alpha_2 \rangle = \frac{\partial \langle S_2 \rangle}{\partial y}, \quad \langle \beta_2 \rangle = \frac{\partial \langle S_2 \rangle}{\partial z} \quad (5.26)$$

where α_2 and β_2 are the second-order components of the ray bending angle in the xz - and xy planes of propagation, respectively. The exact relation between the intensity bias and that in phase path is still a matter of controversy, even for the geometrical optics case (Eshleman and Haugstad 1978,

Considering the nominal occultation level ($\phi_z = 1/2$) and disregarding numerical factors, relations (5.26) and (5.27) yield

$$\begin{aligned}\langle \alpha_2 \rangle &\sim \langle S_2 \rangle / H \\ \langle \hat{\phi}_2 \rangle &\sim \langle S_2 \rangle / H^2\end{aligned}\quad (5.28)$$

where $\hat{\phi}_2 \equiv \phi_2 / \phi_z$ is the fractional bias in intensity, and H is a typical vertical scale of variation of either $\langle \nu_1^2 \rangle^{1/2}$ or ν_0 . By virtue of the assumed spherical symmetry of these quantities, $\langle \beta_2 \rangle = 0$. In equation (5.26) the z -derivative at the receiver is related to a similar derivative in the atmosphere according to $\partial/\partial z(\text{receiver}) = \phi_z \partial/\partial z(\text{atmosphere})$, so that relations (5.28), being representative of $\phi_z \sim 1/2$, actually overestimates the biases in deeper atmospheric regions.

Refractivity profiles obtained from radio Doppler or intensity measurements will contain a bias, $\langle \nu_{*2} \rangle$, that is related to the biases (5.28) and to other second-order effects. This refractivity bias may be obtained from equation (2.1b) by formal expansion of ν_* in powers of ν_1 and collecting all terms of second order, yielding

$$\langle \nu_{*2} \rangle_{\text{Doppler}} = \frac{1}{2} \langle \nu_{*1}^2 \rangle + \left(\frac{2}{R} \right)^{1/2} \int_0^\infty \frac{d\langle \alpha_2 \rangle}{dp} p^{1/2} dp \quad (5.29a)$$

$$\langle \nu_{*2} \rangle_{\text{Intensity}} = \frac{1}{2} \langle \nu_{*1}^2 \rangle + D^{-1} \left(\frac{2}{R} \right)^{1/2} \int_0^\infty \phi_z^{-1} [\langle \hat{\phi}_2 \rangle - \frac{1}{2} (1 + \phi_z) \langle \hat{\phi}_1^2 \rangle] p^{1/2} dp \quad (5.30a)$$

A closer examination of equation (5.29a), using the previously derived approximate upper bound on $\langle \nu_{*1}^2 \rangle / \nu_0^2$, reveals that the refractivity bias is probably dominated by the second term in this case, *i.e.* by the angular bias. By contrast, the right hand side of equation (5.30a) is dominated by the second term in the integrand, yielding approximately for the two cases

$$\langle \nu_{*2} \rangle_{\text{Doppler}} \cong \left(\frac{2}{R} \right)^{1/2} \int_0^\infty \frac{d\langle \alpha_2 \rangle}{dp} p^{1/2} dp \quad (5.29b)$$

$$\langle \nu_{*2} \rangle_{\text{Intensity}} \cong - \left(\frac{1}{2RD^2} \right)^{1/2} \int_0^\infty \frac{1 + \phi_z}{\phi_z} \langle \hat{\phi}_1^2 \rangle p^{1/2} dp \quad (5.30b)$$

Explicit evaluation of these relations, using the first of relations (5.28) along with an explicit expression for $\langle S_2 \rangle$ obtained from equation (5.25), yields the following approximate results for the fractional, absolute bias in calculated refractivity

$$\left(\frac{\langle \nu_{*2} \rangle}{\nu_0} \right)_{\text{Doppler}} \sim \frac{H \mathcal{L} L_0^3}{R a_{F,0}^4} \left(\frac{a_{F,0}}{L_0} \right)^2 \frac{\langle \nu_1^2 \rangle}{\nu_0^2} \quad (5.30)$$

$$\left(\frac{\langle \nu_{*2} \rangle}{\nu_0} \right)_{\text{Intensity}} \sim \langle \hat{\phi}_1^2 \rangle \quad (5.31)$$

Although approximate only, these results are significant in several respects. The former result shows that the fractional refractivity bias is always small in the weak scattering limit. For the Mariner 10 Venus and the Pioneer 10 Jupiter occultations, for example, we estimate typical values $\sim 10^{-6} - 10^{-5}$ if $\langle \nu_1^2 \rangle / \nu_0^2 = 10^{-5}$ is a representative turbulence strength. We also observe that the refractivity bias decreases slightly with propagation distance (as $D^{-1/6}$ for Kolmogorov turbulence) and scales with radio wavelength in the same way as the bias in phase path, *i.e.* as $\lambda^{-1/6}$ for Kolmogorov turbulence. By contrast, the fractional systematic error in refractivity profiles derived from intensity measurements is controlled by the entirely different quantity $\langle \hat{\phi}_1^2 \rangle$, which may approach unity in the present theory. However, as long as the scintillations are weak also the fractional refractivity bias will be small, although being much larger than the corresponding error in profiles derived from Doppler measurements. Thus the fundamentally different character and magnitude found for the random refractivity error for the two cases also carry over to the refractivity bias, giving the radio Doppler technique a further advantage over the less accurate intensity measurements as a tool for remote probing of planetary atmospheres.

6 TURBULENCE IN DEEP RADIO OCCULTATIONS

6.1 General considerations

Most previous spacecraft occultations by planets have involved fairly shallow penetration of the probing radio waves into their atmospheres. Increased sensitivity of the radio links of current (Voyager 1 and 2) and future spacecraft will allow deeper atmospheric regions to be probed by the radio occultation method. Following Eshleman *et al* (1979a), we shall reserve the term "deep occultation" to denote situations where atmospheric refraction deflects the ray by about a tenth of a planetary radius or more, as viewed in the plane of the sky. Under such circumstances the probing wave may experience significant focusing due to the curved planetary limb. As explained in sections 3.2 and 3.3, in the central regions behind the planet the focusing may become comparable to and eventually substantially exceed the initial defocusing caused by differential refraction in the plane of propagation. Corresponding optical enhancements have been observed at earth during the central occultation of ϵ -Geminorum by Mars (Elliot *et al* 1977b).

For a general refractivity field the focus, or more properly the caustic surface, is the locus of intersection of infinitesimally close normals (rays) to the equirefractivity contours. If these contours are everywhere parallel to the planetary limb, this locus is also the evolute of the planetary limb. This circumstance has given rise to the term "evolute flash" (Eshleman *et al* 1979a), which refers to the brief but very strong signal enhancement associated with a crossing of the evolute. For an oblate planet characterized by two orthogonal radii of curvature, the locus resembles a four-cusp cylinder, extending along a line through the planetary center from a certain minimum distance behind the planet to infinity. For a strictly spherical refractivity field the evolute degenerates into a single line.

The basic theory of such evolute flashes has been worked out in two recent publications. These papers have either emphasized the potential information about gravitational moments, planetary rotation and zonal winds that can be obtained from observation of the evolute flash (Eshleman *et al* 1979a), or the possibility of using the gravitational focus of the sun for eavesdropping and communication over interstellar distances (Eshleman 1979). The theoretical predictions of these papers were based, however, on the assumption of a spherical or near-spherical distribution of refractivity. Any departure from such a degree of symmetry, as caused for example by a more complex global distribution of refractivity or by smaller-scale turbulence, will in principle affect the predictions from this theory. The extent to which this occurs is investigated here by evaluating the general results developed in section 4 for the scintillation index and intensity power spectrum close to the focal line, following essentially the development of Haugstad (1981). The general results of this analysis will then be applied to the actual conditions of the recent Voyager 1 Jupiter focal evolute crossing, and also to examine the effect of solar corona plasma irregularities on the performance of the gravitational lens of the sun.

For the reasons given at the end of section 4.1, no attempt will be made to evaluate the fluctuations in Doppler frequency near the focus.

6.2 Scintillation index and power spectrum close to the focus

The weak scattering scintillation index associated with the near-limb ray is, from equations (4.10) and (4.25)

$$\langle \hat{\phi}_i^2 \rangle = 8\pi k^2 \int \int \Phi(u_\perp) \sin^2(P) \left\{ \frac{1}{2J_1(a_s u_\perp)^2} \right\} du_\perp \quad (6.1)$$

where the upper form is for a coherent (radio) source, and the lower form for an extended (stellar) source of projected angular radius a_s above the planetary limb. For the far-limb ray, the quantities ϕ_y and ϕ_z contained in the definition of P remain of the same form, except that $\phi_y \rightarrow |\phi_y|$, since ϕ_y is negative ($\alpha D > R$) for the ray over the far limb.

Partly because of the ray-optical nature of ϕ_y and ϕ_z , and in part because of approximations made in the derivation of equation (6.1) itself, this result is only valid beyond a certain minimum distance from the focus. The former constraint coincides with the distance $w \cong \lambda D/R$ given in relation (3.21) as the width of the focal maximum. The more constraining condition associated with the neglected terms in the stationary phase expansion was established in section 4.1 as $\phi_y = (R/r_\perp) \ll (RH)^{1/2}/a_{F,0}$, where r_\perp is the distance from the spacecraft to the focal line in the plane of the sky. Thus equation (6.1) should not be used close to or within a distance $r_\perp = a_{F,0}(R/H)^{1/2}$ from the focal line.

Considering in the sequel the coherent source form of equation (6.1), the form of the scintillation index in the focal region is found to depend strongly on which of the two inequalities

$$a_{F,h} \geq L_0$$

that are satisfied. When $a_{F,0} \leq a_{F,h} \leq L_0$, the appropriate form of equation (6.1) is given by equations (4.23a,b). Evaluation of these equations yields for $\phi_z \ll 1$

$$\langle \hat{\phi}_1^2 \rangle \cong K_1 \left(\frac{a_{F,0}}{L_0} \right)^{p-3} \frac{\ell D^2}{a_{F,0}^3} \left(\frac{R}{r_\perp} \right)^{\frac{p}{2}-1} \langle \nu_1^2 \rangle \quad (6.2)$$

where $K_1 = [\pi^{1/2} (2\pi)^{3-p/2} (\sec \pi p / 4) 2^{p-1} \Gamma^2((p-1)/2)] / [\Gamma((p-3)/2) \Gamma(p-1)]$. This result is valid for $3 < p < 6$, and for depths of occultation such that $\phi_z/\phi_y \cong Hr_\perp/(R-r_\perp)R \ll 1$, while simultaneously $a_{F,0}(R/r_\perp)^{1/2} \leq L_0$. Thus focusing around the curved limb causes the scintillation index to increase as $r_\perp^{-5/6}$ (assuming $p = 11/3$) as the focus is approached.

When the occultation has proceeded to the level where $a_{F,h} > L_0$, equation (6.1) may be evaluated subject to the stronger condition $a_{F,h} \gg L_0$, to yield asymptotically

$$\langle \hat{\phi}_1^2 \rangle \cong K_2 \frac{L_0 \ell}{\lambda^2} \langle \nu_1^2 \rangle \quad (6.3)$$

where $K_2 = 16\pi^3 \Gamma(p/2) / [(p-2)\Gamma(3/2)\Gamma((p-3)/2)]$. According to this result there is no explicit r_\perp -dependence of the scintillation index in this regime, the only possible change in $\langle \hat{\phi}_1^2 \rangle$ being due to the very slow change in $\langle \nu_1^2 \rangle$ towards the focus. But close to the focus, where $a_{F,h} \gg L_0$ and $\phi_z \cong H/R$, the change in altitude of the ray periapsis as $r_\perp \rightarrow 0$ is a small fraction of a scale height only. Thus $\langle \nu_1^2 \rangle$, and hence also $\langle \hat{\phi}_1^2 \rangle$, is very nearly constant in this region. This situation is depicted schematically in Figure 6.1.

The immediate reason for the plateau in Figure 6.1 is the assumption imbedded in the turbulence power spectrum, equation (4.16), that Φ is itself constant for $u \ll L_0^{-1}$. A constant power spectrum in this region is merely a convenient way of imposing a finite variance on the fluctuations in refractivity, however, since Φ cannot increase as u^p all the way towards $u = 0$ if $p > 1$ and $\langle \nu_1^2 \rangle$ is finite. In actual practice no well-defined outer scale exists, and any structure in Φ in the range $u < L_0^{-1}$ will, of necessity, also affect $\langle \hat{\phi}_1^2 \rangle$ close to the focus.

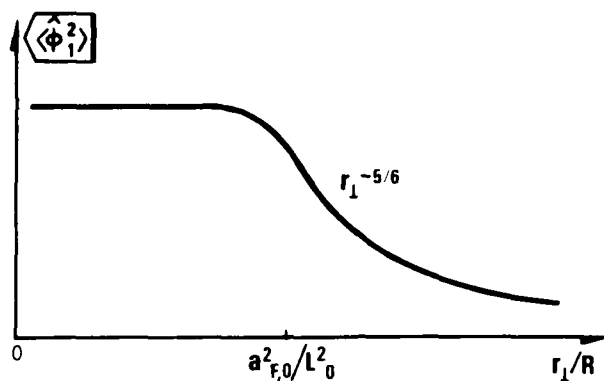


Figure 6.1 Illustration of the qualitative variation in scintillation index with fractional occultation depth, r_\perp/R , for a fixed planet to spacecraft distance

R is the planetary radius, and r_\perp is the distance from the spacecraft to the focal line in the plane of the sky.

The point source intensity scintillation power spectrum is, from equation (4.37)

$$W(\omega) = \kappa_2 \omega \sum_{i=1}^2 \int_1^\infty \frac{x \sin^2 \left\{ \left(\frac{\omega x}{\omega_c} \right)^2 [\phi_y \cos^2(\theta_i + \delta) + \phi_z \sin^2(\theta_i + \delta)] \right\}}{\left[1 + \left(\frac{\omega x}{\omega_0} \right)^2 \right]^{p/2} (x^2 - 1)^{1/2}} dx \quad (6.4)$$

As before, $\omega_c = 2\pi^{1/2} v^*/a_{F,0}$ is the Fresnel frequency, $\omega_0 = v^*/L_0$, and $\delta = \tan^{-1}(v_z^*/v_y^*)$, where $v_y^* = \phi_y v_y$, $v_z^* = \phi_z v_z$ are the ray velocity components at the ray periapsis corresponding to the velocity components v_y and v_z of the spacecraft in directions parallel and perpendicular to the limb, respectively. For the current conditions it is possible to derive an approximate analytical form of equation (6.4). To this end we first observe that normally $v_z^*/v_y^* < (v_z/v_y) \cdot (10Hr_1/R^2) \ll 1$ in deep occultations, so that $\delta \approx 0$, characteristic of a grazing occultation. Defining $\omega'_c = \omega_c \phi_y^{1/2}$, and noting from the definition of ω_c that $\omega'_c \propto \phi_y^{1/2}$ in deep occultations, we find that

$$W(\omega) \propto \omega \sin^2 \left(\frac{\omega^2}{\omega_c'^2} \right) \cdot \int_1^\infty \frac{x dx}{\left[1 + \left(\frac{\omega x}{\omega_0} \right)^2 \right]^{p/2} (x^2 - 1)^{1/2}} \quad (6.5)$$

Examination of the integral shows that

$$W(\omega) \propto \begin{cases} \sin^2 \left(\frac{\omega^2}{\omega_c'^2} \right) & \text{for } \omega \ll \omega_0 \\ \omega^{1-p} \sin^2 \left(\frac{\omega^2}{\omega_c'^2} \right) & \text{for } \omega \gg \omega_0 \end{cases} \quad (6.6)$$

Note that, while initially $\omega_0/\omega'_c \sim (a_{F,0}/L_0) \ll 1$ per assumption, in very deep occultations this ratio is reversed, since there $\omega_0/\omega'_c \sim (a_{F,0}/L_0) \cdot (R/r_\perp)^{1/2} \gg 1$.

The relations (6.6) imply that in very deep occultations the scintillation power spectrum has the form depicted qualitatively in Figure 6.2, with the bulk scintillation power confined within a band $\omega'_c \lesssim \omega \lesssim \omega_0$. As the focus is approached, both ω'_c and ω_0 increase. The bandwidth also increases, however, since $\omega'_c \propto (R/r_\perp)^{1/2}$ while $\omega_0 \propto R/r_\perp$ and therefore increases faster than ω'_c by the factor $(R/r_\perp)^{1/2}$. The increase in ω_0 towards the focus by the factor R/r_\perp is caused alone by the similar increase in ray speed at the periapsis. The slower increase of ω'_c is due, however, to the competing expansion of the horizontal Fresnel scale by a factor $(R/r_\perp)^{1/2}$, which, if acting alone would reduce ω'_c by a similar amount, and the increased ray speed which is proportional to R/r_\perp .

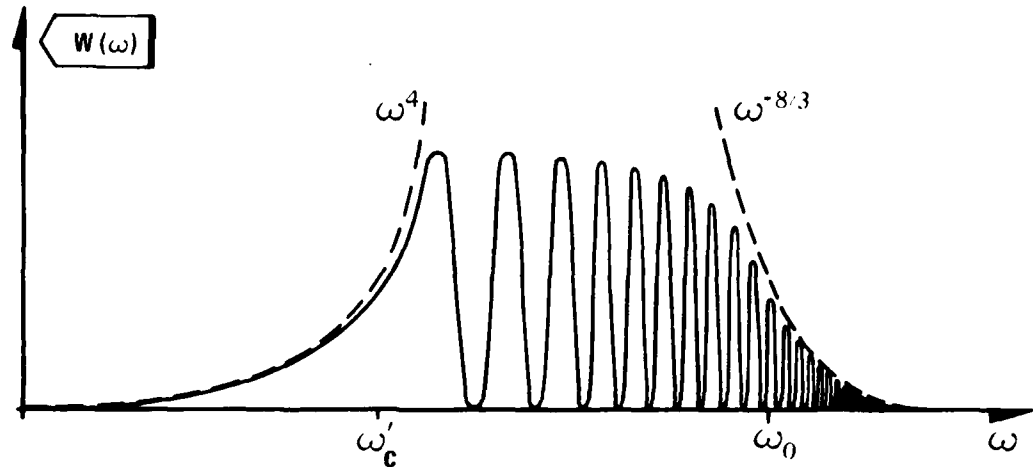


Figure 6.2 Qualitative sketch of the point source intensity scintillation power spectrum in very deep occultations

The characteristic frequencies ω'_c and ω_0 are defined in the text.

In the temporal domain, the bandlimited power spectrum described above corresponds to typical scintillation time scales less than, or at most equal to, that associated with the low frequency boundary of the pass-band, that is $\sim \omega'_c{}^{-1}$. Thus ω'_c is also a characteristic temporal frequency in very deep radio occultations.

By way of illustration, it is readily proved using the previous relations that one scale height from the focus, where the background intensity has risen to the unocculted level ($\phi = 1$) according to equation (3.11), the lower boundary of the scintillation pass band is at about 100 Hz, if $v_v = 1 \text{ km s}^{-1}$, $a_{F,0} = 1 \text{ km}$ and $R = 10^4 \text{ km}$ are representative values. Such rapid scintillations may severely impair the ability to track the radio signal through an evolute flash, in particular if the scintillations are also strong ($\langle \hat{\phi}_i^2 \rangle \geq 1$).

6.3 Applications

6.3.1 The Voyager 1 Jupiter encounter

The first positive identification of the refractive focus of a planetary atmosphere is due to Elliot *et al* (1977b), who observed the "central flash" of ϵ Geminorum as it was occulted by Mars on 8 April 1976. By contrast, the first attempted radio transmission from the focus occurred by the recent passage of Voyager 1 through the focal evolute of Jupiter. According to Martin *et al* (1980), the radio signal displayed several peaks in intensity near the expected position of the evolute crossing, but none could be identified as the evolute flash. The absence of a detectable evolute flash led Martin and colleagues to establish a lower bound on the microwave absorption, most likely caused by NH_3 , near the $\approx 4.3 \text{ bar}$ level of the ray periapsis when crossing of the evolute occurred. We estimate below the weak scattering scintillation index during this evolute crossing, and argue that its high value may have contributed to the unsuccessful attempt to identify the flash in this case.

A formal calculation of the scintillation index near focus requires an estimate of $\langle \hat{p}_i^2 \rangle$. We will assume that

$$\langle \hat{p}_i^2 \rangle / p_0^2 \sim 10^{-5} \quad (6.7)$$

where ν_0 is the ambient refractivity at the ray periapsis during the evolute crossing. The value in relation (6.7) corresponds roughly to turbulence of the strength found immediately above the earth's boundary layer (Bufton *et al* 1972), if also the outer scale and the ambient temperature at the ray periapsis are equated to 1 km and 200 K, respectively. The ambient refractivity is related to its value at standard temperature and pressure (STP) by

$$\frac{\nu_0}{\nu_{0,STP}} = \frac{p}{p_0} \frac{T_0}{T}$$

where (p_0, T_0) refer to the standard condition (STP). Using $\nu_{0,STP} = 0.000136$ as for a pure H_2 -atmosphere, we find that $\nu_0 \approx 8 \cdot 10^{-4}$, which yields the value $\approx 6 \cdot 10^{-12}$ for $\langle \nu_1^2 \rangle$. Putting $\ell = (RH)^{1/2}$ and $H = 30$ km, we obtain for the S-band ($\lambda = 0.13$ m) occultation using equation (6.3) and the previous estimates

$$\langle \hat{\phi}_1^2 \rangle \approx 6 \cdot 10^1 \quad (6.8)$$

This high value of the weak scattering scintillation index suggests that the scintillations have saturated to unity well before the focus is reached. If real, such strong scintillations would significantly change the maximum intensity relative to the ideal prediction for an oblate planet (*cf* equation 15 of Eshleman *et al* 1979a). Furthermore, the matched filter technique employed by Martin *et al* (1980) to detect the flash, requires signal coherence over a certain minimum time. In view of the discussion in section 6.2 it is clear, however, that this provision cannot be met close to the focus where the scintillation time scale approaches zero. Thus scintillations may have impaired the mere detection of the evolute flash, above and beyond the fundamental difficulty imposed by the very strong NH_3 absorption of the S-band radio signal along the atmospheric portion of the raypath.

6.3.2 The gravitational lens of the sun

Eshleman (1979) gives the maximum focused intensity for this case as

$$\phi_{\max} = 2\pi k r_g \quad (6.9)$$

where r_g is the gravitational radius of the sun ($r_g = 2955$ m). This result is derived for a plane, coherent wave of wavenumber k deflected through an angle $\alpha = 2r_g/a$ (a is the impact parameter) by the solar gravitational field. Any solar oblateness is too small to significantly degrade the maximum intensification given by equation (6.9). Such degradation may be caused, however, by the solar corona plasma, which imposes additional bending on the wave away from the focus by an amount depending on the local plasma gradient and the radio wavelength.

Inference from the continuum of scale sizes found in the solar wind plasma (*e.g.* Jokipii 1973), suggests that also the solar corona is inhomogeneous on a continuum of scale sizes ranging from the Debye length to those associated with the global dimensions of the corona.

The approximate effect of large-scale coronal plasma structures on ϕ_{\max} may be appreciated by finding the condition under which the additional phase shift imposed by the plasma is less than $\lambda/2$. This is the condition that the Fresnel zone be coherent and the signal intensity being essentially unaffected by the plasma. For larger phase shifts the Fresnel zone breaks up into two or more non-connected parts, with a corresponding drop in maximum intensity below the value given by equation (6.9). We thus require

$$k^2 \langle S_1^2 \rangle \ll 1 \quad (6.10)$$

where $\langle S_1^2 \rangle$ is the mean square change in phase path of the radio wave imposed by

the coronal plasma. An additional constraint to ensure the validity of equation (6.9) is that $\langle \hat{\phi}_1^2 \rangle \ll 1$. In very deep occultations, where $a_{F,h} \gg L_0$, this condition is, from equation (6.3)

$$\langle \hat{\phi}_1^2 \rangle \approx K_2 \frac{L_0 \ell}{\lambda^2} \langle \nu_1^2 \rangle \ll 1 \quad (6.11)$$

It is important to observe that as long as $a_{F,h} \gg L_0$, the two previous conditions are essentially identical regardless of the magnitude of L_0 . Indeed, from an explicit evaluation of $\langle S_1^2 \rangle$ it follows that in this case

$$\langle \hat{\phi}_1^2 \rangle = 2 k^2 \langle S_1^2 \rangle \quad (6.12)$$

It is thus immaterial which of conditions (6.10) or (6.11) that are imposed to ensure the validity of equation (6.9). A result similar to equation (6.12) has been obtained by Salpeter (1967) for a one-dimensional turbulence model. Equation (6.12) extends this result to three-dimensional turbulence on an inhomogeneous background when the leading dimension of the atmospheric Fresnel zone substantially exceeds the outer scale of turbulence.

Assuming $L_0 \sim R$ (R is the solar radius), so that the rms phase change is comparable to that imposed by the average corona, we calculate below the coronal change in phase path corresponding to the modified Baumbach-Allen plasma model proposed by Tyler *et al* (1977), which accounts for latitudinal variations and the effect of the solar wind plasma. Denoting by ρ and θ the heliocentric distance (in units of the solar radius) and solar latitude, respectively, this model asserts that

$$N_c = \left[\left(\frac{2.99}{\rho^{16}} + \frac{1.55}{\rho^6} \right) 10^{14} + \frac{3.44}{\rho^2} 10^{11} \right] (\cos^2 \theta + \frac{1}{64} \sin^2 \theta)^{1/2} \quad (6.13)$$

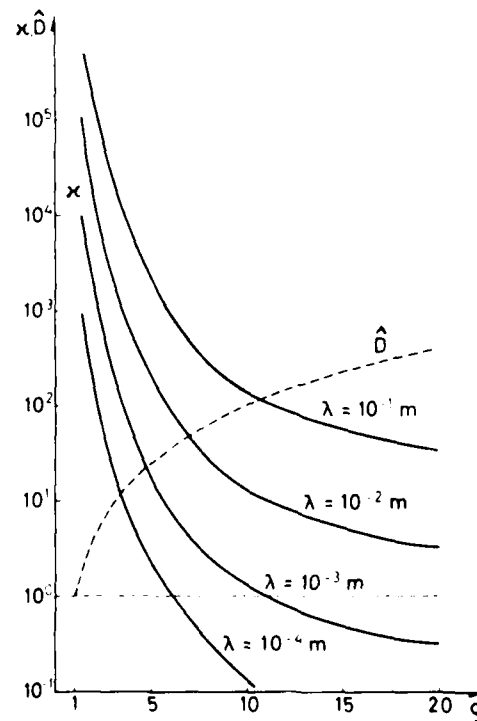


Figure 6.3 Values of the phase shift κ induced by the solar corona plasma, for various fractional heliocentric distances ρ and wavelengths λ .

The corresponding fractional distance $\hat{D} \equiv D/D_{\min}$ to the focus is also indicated.

where N_e is the density of electrons per m^3 . The associated refractivity is

$$\nu_p = -4.48 \cdot 10^{-16} \lambda^2 N_e \quad (6.14)$$

with λ in units of meters. Using equation (6.14) and the previous equations we have calculated in Figure 6.3 the ratio $\kappa \equiv \langle S_1^2 \rangle^{1/2} / \lambda$ for different values of ρ and λ . The very large values attained by κ for even large heliocentric distances ($\rho \approx 10$) and small wavelengths ($\lambda \approx 1$ mm), strongly suggest that coronal plasma irregularities both reduce the coherent size of the Fresnel zone (and thus ϕ_{\max}) and cause severe signal fading as the focus is approached.

According to Figure 6.3, near-optimum conditions can be restored either by moving the ray periapsis to larger heliocentric distances, or by reducing the wavelength below about 10^{-4} m. The former alternative is not particularly attractive, since the distance to the focus behind the sun increases as ρ^2 , and is already $100 D_{\min}$ at $\rho = 10$ ($D_{\min} = 550$ AU is the distance to the nearest focus corresponding to $\rho = 1$). The apparent solution is therefore to use very short wavelengths, provided present technological difficulties of sub-millimeter communication can be overcome.

7 DIAGNOSTICS OF SMALL-SCALE ATMOSPHERIC STRUCTURES

7.1 General considerations

Turbulence in the free atmosphere owes its existence to, (i) thermal instabilities, (ii) wind shear, or (iii) the breaking of large-scale, vertically propagating waves, such as internal gravity waves. These are physically distinct processes that may lead to different spatial distributions and characteristics of the turbulence. For example, a convective instability may be more likely to occur near the equatorial plane on the day side where the solar heating rate is a maximum. On the other hand, wind shear and the associated turbulence may be sharply confined in altitude, but may not be otherwise restricted to particular planetographic locations. A common feature of well-developed turbulence, regardless of the characteristics of the source, is the universal form of the turbulence power spectrum in the inertial subrange where $L_0^{-1} \ll u \ll \ell_0^{-1}$. The magnitude of the outer scale, being a characteristic dimension of the input region, depends directly on the specifics of the source, however.

In the turbulence model (4.16), the two quantities $\langle \nu_1^2 \rangle$ and L_0 are of principal interest. One might also want to estimate the slope parameter p from the occultation data, as has been done by Woo *et al* (1976, 1977). It should be emphasized, however, that a statistically significant departure of p from the universal value $p = 11/3$ in the inertial subrange, would imply the existence of turbulence that is not well-developed. That is, it is of an intermittent and nonstationary nature. The positive identification of such intermittent sources of turbulence would in itself be important, but the particular spectral shape recorded would be directly linked to the specific event and would not bear any universal significance. The quantities $\langle \nu_1^2 \rangle$ and L_0 in well-developed turbulence would be of much greater interest, since the atmospheric processes generating the turbulence will be of a more stationary character in this case. The specifics of such processes, such as the turbulence strength and characteristic dimensions of the source, may provide important observational constraints on theoretical circulation models of planetary atmospheres, as suggested initially by Woo *et al* (1974).

In order to estimate $\langle \nu_1^2 \rangle$ and L_0 from occultation data, one should in principle consider quantities that exhibit the strongest possible dependence on the magnitude of these parameters. For the former, the scintillation index and the associated power spec-

trum is such a quantity, while for the outer scale the phase scintillations is the natural quantity to examine. Also other signal characteristics may be used, but will not be considered here.*

We discuss below specifically how the characteristics of small-scale atmospheric structures can be obtained from occultation measurements. It is deemed important to explore both the limitations and capabilities of the occultation technique in this regard, since once this potential is realized, such experiments may be planned to take fullest possible advantage of their intrinsic capabilities. Parts of the discussion here closely parallel that of Haugstad (1979a).

7.2 Estimation of the turbulence strength

Before any "wiggly" occultation curve is analyzed for its expected turbulence content, it should be ascertained that the recorded small-scale structures are in fact due to turbulence and not to other atmospheric structures (e.g., "layers"), or to numerical artifacts introduced during the data recording or the subsequent analysis. The best way to make such a check, would probably be by examining the intensity power spectrum and the scintillation index. Assuming that the intensity background has been properly removed, the weak scintillation power spectrum should conform, within proper limits of statistical significance, with one of the characteristic shapes displayed in Figures 4.3 to 4.9, for various geometries and depths of occultation. As an alternative, one might identify the Fresnel "knee" at ω_c in the intensity power spectrum, and determine if it scales with wavelength as $\lambda^{1/2}$ for radio occultations. Within wide bounds on the spectral slope parameter p ($2 < p < 6$), this scaling is independent of p . In stellar occultation power spectra, the position and shape of the corresponding "knee" depend on the relative size of the projected stellar radius and the free-space Fresnel zone. If $a_s \approx a_{F,0}$, the "knee" is determined by a_s and is therefore essentially independent of wavelength. For $a_s \approx a_{F,0}$, stellar scintillation power spectra would in all respects resemble closely those of a coherent source.

A final check on the expected authenticity of the turbulence is provided by the scintillation index, which scales with wavelength as $\lambda^{-7/6}$ for values small compared to unity.

Once well-developed turbulence has been reliably identified, its strength and spatial variation may in principle be obtained from the observations via the theoretical relationships developed in section 4.3. Thus, for shallow radio occultations and $\phi_z \ll 1$, equation (4.23a) yields

$$\langle \nu_1^2 \rangle = \xi L_0^{3/3} H_t^{-1/2} R^{-1/2} D^{-5/6} \lambda^{-7/6} \langle \phi_1^2 \rangle \quad (7.1)$$

where ξ is a numerical constant. If an estimate of L_0 has been obtained, as discussed in the next section, equation (7.1) provides an estimate of $\langle \nu_1^2 \rangle$ in terms of the scintillation index if also H_t is known. A natural first choice of H_t , consistent with the atmospheric model adopted here, would be $H_t = H$. A more realistic estimate can be obtained from the spatial variation of $\langle \phi_1^2 \rangle$ itself if this quantity has been computed over a few turbulence scale heights or more. Indeed, if good quality scintillation data are available over a range in altitude, the actual variation of the scintillation index may be used to improve the exponential turbulence model suggested here, and thereby yield a more accurate estimate also of $\langle \nu_1^2 \rangle$.

* Woo *et al* (1977) have suggested using the mutual coherence function and also the quantity $\langle \chi_1 S_1 \rangle$ (Woo 1975b), which is proportional to $\langle S_2 \rangle$. The latter quantity does not appear to offer any advantage over the scintillation index. In the weak scattering regime, incorporation of the inhomogeneous background, not considered by Woo *et al* (1977), shows that the mutual coherence function is essentially identical to the phase scintillations in terms of its potential usefulness for determining $\langle \nu_1^2 \rangle$ or L_0 .

For stellar occultations the analogous relationship to equation (7.1) may be obtained from equation (4.25). As previously noted, however, the explicit form of this relationship depends critically on the ratio $a_s/a_{F,0}$. No general relationship of the form (7.1) can therefore be given in this case, except when the ratio is either very small or very large compared to unity. In the former case equation (7.1) clearly applies, while in the latter case the appropriate relationship is obtained from equation (4.26a) as

$$\langle \nu_1^2 \rangle = \eta L_0^2 a^{-7/3} H_1^{-1/2} R^{-1/2} D^{-2} \langle \hat{\phi}_1^2 \rangle \quad (7.2)$$

where η is a numerical constant. Again knowledge of L_0 and H_1 yields $\langle \nu_1^2 \rangle$ in terms of the scintillation index for the high altitude regions probed in stellar occultation experiments.

Instead of $\langle \nu_1^2 \rangle$ one might want to estimate the refractive index structure constant, C_n^2 . Since

$$D_n(\Delta r) = C_n^2 |\Delta r|^{2/3}, \quad \ell_0 \ll \Delta r \ll L_0$$

where D_n is the refractive index structure function, it follows from the definitions of D_n and L_0 that

$$\langle \nu_1^2 \rangle \cong \frac{1}{2} C_n^2 L_0^{2/3} \quad (7.3)$$

From the previous results it therefore follows that

$$C_n^2 \cong \left(\frac{\kappa_R H_1^{-1/2} R^{-1/2} D^{-5/6} \lambda^{7/6}}{\kappa_S a_s^{-7/3} H_1^{-1/2} R^{-1/2} D^{-2}} \right) \langle \hat{\phi}_1^2 \rangle \quad (7.4)$$

The upper form with $\kappa_R \cong 2\xi$ is for radio occultations, and the lower form with $\kappa_S \cong 2\eta$ for stellar occultations. The unknown value of L_0 is here absorbed into the structure constant. The temperature structure constant corresponding to C_n^2 for assumed adiabatic conditions is given by equation (4.21). For radio occultations we find that

$$C_T^2 \sim 2\xi(\gamma - 1)^2 L_0^2 H_1^{-1/2} R^{-1/2} D^{-5/6} \lambda^{7/6} \frac{\langle \hat{\phi}_1^2 \rangle}{\nu_0^2} \quad (7.5)$$

and with a corresponding result for stellar occultations when the conditions leading to equation (7.2) are satisfied.

Thus equations (7.1) and (7.2) yield the variance of the refractive index fluctuations in terms of the scintillation index once L_0 and H_1 have been stipulated. From the relationships (7.4) and (7.5), rough estimates of the appropriate structure constants may also be obtained from a measurement of the scintillation index, using prior knowledge of H_1 only.

From the analysis of section 6 it may be shown that formal relationships closely similar to those developed here also hold for deep occultations.

7.3 Estimation of the outer scale

As we have seen, an approximate measure of L_0 is a prerequisite for estimating $\langle \nu_l^2 \rangle$ from the scintillation data. However, by virtue of its character as a typical dimension of the macroscopic flow generating the turbulence, knowledge of the magnitude of L_0 is also important in its own right.

The natural quantity to examine in this case is the phase scintillation power spectrum, as given in analytic form and computed for different occultation geometries and depths in section 4.4. The relevant feature of the spectra is the "knee" at $\omega \cong \omega_0 = v^*/L_0$. Since v^* is known, the position of the "knee" is directly related to the magnitude of L_0 . It is moreover significant that the position of the "knee" is independent of both occultation depth and geometry for shallow occultations. In actual practice the turbulence power spectrum will not have the idealized form assumed here, with constant power for $\omega \lesssim L_0^{-1}$. A significant *departure*, one way or the other, from the average high frequency slope of the phase spectrum is probably the feature that in practice signifies the wavenumber location of the input region.

In deep occultations the estimation of L_0 is less easy. The situation is simplest for moderately deep occultations, where $a_{F,0} < a_{F,h} \ll L_0$. In this case the spectral shape corresponds closely to that of Figure 4.4, with the transition to small fringes at $\omega = \omega_c$ approaching ω_0 as $a_{F,h}$ increases towards L_0 . At still greater depths of penetration of the ray, where $a_{F,h} \gg L_0$, the phase power spectrum assumes the asymptotic form

$$W(\omega) \propto \begin{cases} \cos^2\left(\frac{\omega^2}{\omega_c'^2}\right), & \omega \ll \omega_0 \\ \omega^{-8.3} \cos^2\left(\frac{\omega^2}{\omega_c'^2}\right), & \omega \gg \omega_0 \end{cases} \quad (7.6)$$

The power spectrum thus has the form displayed qualitatively in Figure 7.1. Identification of L_0 is seen to depend on the possibility of detecting the onset of the $\omega^{-8.3}$ decrease in scintillation power above $\cong \omega_0$. The large fringes in the power spectrum in this region may hamper this identification, a problem likely to be compounded by the expected rapid increase of ω_0 itself near the focus. On the other hand, if the transition in spectral shape at $\omega \sim \omega_0$ has been identified, determination of L_0 is readily accomplished by the usual relationship $\omega_0 = v^*/L_0$.

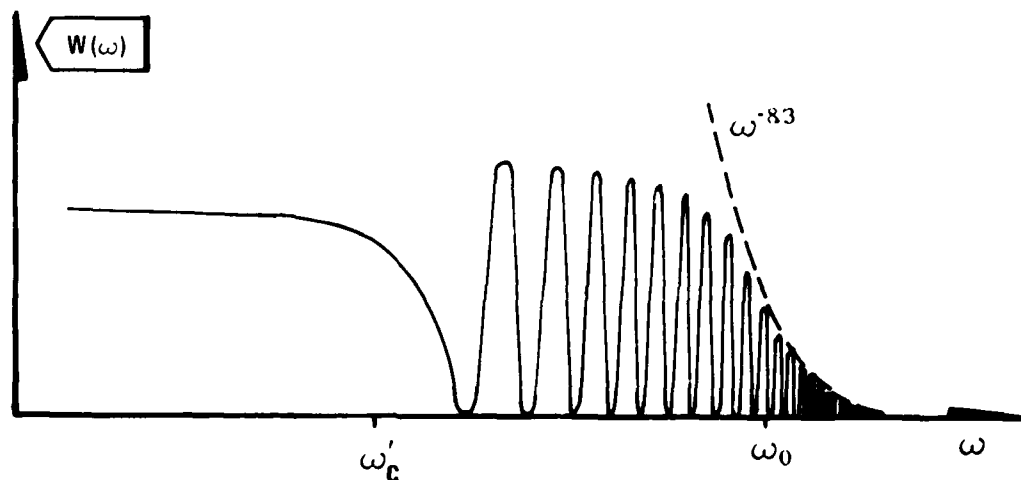


Figure 7.1 Qualitative sketch of the phase scintillation power spectrum in very deep occultations

The characteristic frequencies ω_c' and ω_0 are defined in the text.

7.4 Planetary rotation and atmospheric winds

We discuss here the possibility of extracting from the scintillation measurements information about planetary rotation and atmospheric winds. In the earth's atmosphere this technique has been used extensively, having in fact reached the level of sophistication where a horizontal wind *profile* has been obtained (Lee 1974). Scintillation measurements have also been used to derive bulk flow velocities of the solar corona and solar wind (e.g. Woo 1978).

The theoretical feasibility of such measurements rests in all cases on the identification of characteristic features in the scintillation power spectrum whose location or shape depends on the atmospheric velocity across the line of sight. Considering the fixed-axes coordinate system of Figure 2.1, the ray velocity components at periapsis relative to the atmospheric motion are

$$v_Y^* = \phi_Y v_Y^s - v_Y^d, \quad v_Z^* = \phi_Z v_Z^s - v_Z^d \quad (7.7)$$

where a superscript *s* has now been added to the spacecraft velocity components to distinguish from the corresponding components of atmospheric motion, v_Y^d and v_Z^d . The latter may be dominated by atmospheric rotation or by winds, depending on planetary rotation rate and occultation geometry.

While in the previous sections we have assumed both v_Y^d and v_Z^d to be negligible, we here ask for effects that can be attributed to the finite values of these quantities. For a spherically symmetric atmosphere the rotational part of v_Z^d is zero. Since vertical wind velocities are normally very small compared to their horizontal counterparts, we shall assume in the sequel that $v_Z^d = 0$. In this case

$$v^* = [(\phi_Y v_Y^s - v_Y^d)^2 + \phi_Z^2 v_Z^s]^2 \quad (7.8a)$$

$$m = \frac{v_Y^*}{v_Z^*} = \frac{\phi_Y v_Y^s - v_Y^d}{\phi_Z v_Z^s} \quad (7.8b)$$

where the relative ray speed v^* and obliquity factor *m* determine the location and shape, respectively, of the intensity power spectrum, as depicted in Figures 4.6 - 4.9 for shallow occultations. These spectra are also valid in deep occultations, provided $a_{F,h} \ll L_0$, as explained in section 6.2. In very deep occultations, where $a_{F,h} \gg L_0$, the form of the intensity power spectrum must in general be established from the general result (4.37). If v_Y^d is such that $|m| \gg 1$, the power spectrum has the characteristic shape displayed in Figure 6.2, with the low frequency boundary related to the characteristic frequency $\omega'_c = 2\pi^{1/2} v^* / a_{F,h}$, and hence to v^* and v_Y^d .

It is clear from equations (7.8a) and (7.8b) that in order to relate v_Y^d to the location of the spectral "knee" at $\omega = \omega_c$ (ω'_c for deep occultations), or to the spectral shape, it is necessary that $|v_Y^d|$ be at least comparable to the component $\phi_Y v_Y^s$ due to the spacecraft alone. This fact accentuates in the present context the importance of near-central (*i.e.*, *deep*) occultations. Indeed, if over some range of the occultation $\phi_Y |v_Y^s| \lesssim |v_Y^d|$, then both v^* and *m* depend crucially on v_Y^d whenever $\phi_Z |v_Z^s| \lesssim |v_Y^d|$, which is likely to occur at some stage of the occultation. In this regime, both the shape and location of the power spectrum yield indirect information on the magnitude of v_Y^d . In some cases the magnitude of v_Y^d may be such as to dominate v^* and *m* even for shallow occultations. For Jupiter, for example, the rotational component alone is about 13 km s^{-1} for a meridional occultation over the equator. For an occultation over the polar regions, the rotational component is very small and v_Y^d may here be dominated by the wind component.

It is apparent from the sketchy discussion above that information on wind speeds and atmospheric rotation rates are indeed within the capability of the occultation technique. However, since such measurements depend critically on details of the occultation geometry, it is important to fully examine these capabilities in the planning stage of any spacecraft mission.

7.5 Practical considerations

In the discussion of the previous sections we have only briefly alluded to the several practical problems involved in the estimation of turbulence parameters and atmospheric motion from occultation measurements.

The major practical obstacle in the estimation of $\langle \nu_1^2 \rangle$ appears to be the limited statistical significance of the scintillation index. This problem is most acute for a central or near-central occultation, since a meaningful evaluation of $\langle \hat{\phi}_1^2 \rangle$ must employ scintillation data covering a range in altitude of less than a turbulence scale height. In a near-central occultation, the number of independent "ripples" in the intensity-time record is at most $N_0 \sim H_1/a_{F,0}$, since $a_{F,0}$ is an approximate lower bound on the correlation length of the intensity fluctuations in this case. Since N_0 is typically on the order of 10, it is clear that the statistical significance of $\langle \hat{\phi}_1^2 \rangle$, and hence of $\langle \nu_1^2 \rangle$, may indeed be very poor in this case. The problem of low statistical significance is compounded by the principal difficulty of subtracting the intensity background from the fluctuation part of the signal, as discussed more fully in section 4.4.2. Because also $H/a_{F,0} = \mathcal{O}(10)$, the intensity trend function may have significant power at spatial frequencies $\sim a_{F,0}^{-1}$, implying that irremovable contamination of the scintillation index and power spectrum from the ambient background may be the normal situation in near-central occultations. Despite this fundamental difficulty, it is important that an efficient and common procedure be used to separate the intensity background from the fluctuation part in order to minimize this problem, as previously argued.

The situation is entirely different for shallow occultations. In this case the ray has only a very slow vertical motion, but covers a large horizontal distance at essentially constant altitude. Indeed, in the central portion of the occultation the ray moves a horizontal distance $\sim \ell \cong (RH_1)^{1/2}$ before the altitude of the ray periapsis is changed by one turbulence scale height. In this case $N_1 \sim \ell/a_{F,0} \gg N_0$, so that considerable spatial averaging and corresponding high statistical significance of $\langle \hat{\phi}_1^2 \rangle$ and $\langle \nu_1^2 \rangle$ is possible.

The practical estimation of L_0 is probably most hampered by the inherent lack of a well-defined value of this quantity. Indeed, the transition from spatial scales in the inertial subrange to the input-range will for all practical cases be gradual, and any quantity or explicit result that depend on the precise value of L_0 should therefore be handled with corresponding caution. Apart from this inherent imprecision of L_0 itself, the statistical argument presented above apply for similar reasons also to the estimation of this quantity.

The estimation of atmospheric bulk flow and turbulence parameters in deep occultations is affected by statistical limitations in the same way as described above for shallow occultations. Extremely close to the focus, where both ω_0 and ω'_c change rapidly due to the rapid change in ϕ_y , the effective length of the scintillation time series, over which $\hat{\phi}_1$ may be considered stationary, depends critically on the various parameters involved and must be assessed for each particular case.

We have described above some important constraints of statistical nature that are likely to affect the practical estimation of turbulence parameters and atmospheric motions from occultation measurements. Neither the potential nor the statistical limitations of this technique appear to have been fully appreciated in the past. It is

deemed important that both aspects be addressed at an earliest possible stage in the planning of planetary fly-by missions, so as to realize in each case the maximum potential of the occultation technique.

8. DISCUSSION AND FURTHER PERSPECTIVES

It is a notable fact that while effects of turbulence on radio and optical wave propagation in the earth's atmosphere and ionosphere have attracted considerable attention over the past decades, only very recently has this issue been pursued systematically in occultation measurements of planetary atmospheres. This lack of interest is naturally explained for radio occultations by the short history of this kind of measurements, and also by the fact that the first analyses of such observations (*i.e.*, the Mariner missions to Mars and Venus) produced atmospheric profiles that were largely acceptable. The low interest is less explicable for stellar occultations, the much longer history of which is marred by "spiky" luminosity profiles indicative of turbulence or other small scale atmospheric structures.

The present analysis attempts to categorize and analyze the various aspects of the overall problem posed by turbulence in planetary atmospheres subjected to radio or stellar occultation measurements. Thus the primary task has been to extend existing theory of electromagnetic wave propagation in a random medium to account for the inhomogeneous ambient atmosphere upon which the turbulence is superimposed. While negligible in terrestrial propagation experiments involving short raypaths, in radio and stellar occultation experiments over much longer paths such coupling to the ambient atmosphere becomes very important. The theoretical results derived here for the scintillation index agree with similar results obtained simultaneously (Hubbard *et al.* 1978) or later (Woo *et al.* 1980) by other authors. In the form expressed here the total effect of the coupling on the scintillation index is readily assessed. We have found that in shallow occultations coupling to the ambient background reduces the scintillations by at most a factor of two for a point source, while for an extended stellar source the reduction varies between this limit when the projected stellar radius is small compared to the radius of the free space Fresnel zone, to a maximum reduction of approximately a factor of 3.6 when this ratio is large. These fairly moderate changes are contrasted by very substantial changes in the shape of the intensity power spectrum, which is now a strong function of both occultation depth and geometry. These conclusions, as further detailed in the appropriate sections, express a major theoretical result of the present work.

The analysis also shows that the generalized scintillation formulas derived here should replace their analogs in the standard Rytov approach whenever differential refraction changes the average intensity by a significant amount. Analysis of radio and optical scintillations during occultation observations should therefore always proceed from the generalized formulas derived here. But also other, terrestrial applications may be found for these results. Satellite-to-satellite communication, where the communication path is intercepted by the earth's atmosphere or ionosphere, may involve sufficient differential refraction. Propagation *within* the earth's atmosphere, where the ray traverses regions of thermal inversion may also yield substantial values of $M^2 \propto d^2/H$, even though the effective distance D between the medium and the transmitter or receiver is small in this case. It is possible, finally, that a version of the present scintillation theory may find application in acoustic (or elastic) wave propagation in the earth's atmosphere, in the ocean or in the earth's interior, whenever sufficient refractive coefficients due to anomalies in either temperature or density are present.

The identification and evaluation of the second order, systematic propagation effects also constitute a principal result, though of mainly theoretical interest. Contrary to the initial result of Hubbard and Jokipii (1975), who concluded that the average

phase was retarded by turbulence relative to a non-turbulent medium with similar average refractivity, we have found from a simple geometrical optics analysis that the average phase is in fact *advanced* in the presence of zero-mean turbulence. Extension of this result to wave-optics has furthermore demonstrated a weak wavelength dependence of the bias in phase path (or phase speed), yielding the important result that an initially non-dispersive medium becomes slightly dispersive by the addition of turbulence. When a systematic spatial variation in turbulence strength or in the ambient refractivity is present, a bias in ray bending angle and intensity may also result.

While these second-order propagation effects were found to yield only insignificant errors in occultation experiments, in other, more controlled experiments requiring extreme accuracy, such effects may have to be accounted for. A potential candidate may be relativistic time-delay experiments, in which the raypath is intercepted by a turbulent neutral or ionized medium.

It is a principal conclusion from the present work that the propagation effects discussed above produce only very marginal errors in profiles of temperature and pressure derived from occultation measurements, provided that the weak scintillation assumption fundamental to these calculations is not violated. In view of the large errors in the Pioneer 10 and 11 Jupiter profiles, as caused by the magnification effect discussed in section 2.2, this conclusion is in no way obvious. The result is however, fully consistent with radio occultation experiments, where individual T-p profiles from the same atmosphere both exhibit substantial mutual agreement, and are also broadly consistent with other observations where comparisons can be made. Stellar occultation profiles are typified by a much higher intensity fluctuation level, probably violating the weak scintillation assumption, but are also more susceptible to instrumental errors. It is clear that errors of this type played a major role in the several independent recordings of the β Scorpii occultations by Jupiter, which displayed substantial disagreement (see, Hunten and Veverka 1976). Thus stellar occultation profiles, though clearly containing sizable errors, do not necessarily contradict the conclusion that the part of these errors that can be attributed to turbulence is small whenever the weak scintillation assumption is satisfied.

The natural and important extension of the theory developed in this work will be to incorporate strong scattering effects. This extension should also include an evaluation, by theoretical or numerical analysis, of the mean square fluctuations in bending angle, essential to a more rigorous assessment of turbulence effects in radio Doppler measurements during both weak and strong scattering conditions. These tasks, probably being of a numerical nature, indeed constitute the principal remaining problems in the theory of turbulence effects in radio and stellar occultation experiments. The rapid increase of the scintillation index with atmospheric depth in radio occultations, along with the commonly observed "spike structure" of stellar occultation light curves, make it desirable to pursue these goals vigorously. Of the two tasks, a numerical calculation of the mean square fluctuations in bending angle is probably the simplest. For a one-dimensional scattering model, evaluation of a double integral is required, while for a more realistic two-dimensional model a four-tuple integral is involved. By contrast, the scintillation index involves a four-tuple integral even in the one-dimensional case, while in two dimensions evaluation of an eight-tuple integral is called for. A simpler approach involving less computation, will be to calculate a spatial realization involving a four-tuple integral in a two-dimensional model of the intensity corresponding to a spatial realization of the turbulence, and then form the mean square of the intensity from an ensemble of such calculations.

Though even this latter approach may lead to prohibitive computation times, a direct analytical calculation may be no easier. Indeed, even ordinary strong scintillation theory has only recently been developed to a stage where certain limiting expressions for the scintillation index are available (see, e.g. Lunte 1975, Lee and Jokipii 1975a,b). Judging from the substantial added complexity by introducing the inhomogeneous ambient atmosphere in the weak scattering case, a similar approach in the

strong scintillation regime may be beyond feasibility. It is possible, however, that a more heuristic approach, *e.g.* of the sort suggested by Salpeter (1967) for turbulence on a homogeneous background, can be used to treat strong scintillations with the ambient background included. Together with selected numerical computations, first in a one-dimensional model, a combined approach of this sort may be the only realizable path towards a better understanding of the various aspects of strong scattering effects in occultation experiments*.

An extension of the present theory to strong scattering should also encompass the systematic effects. In strong scattering they are likely to involve all powers of ν_1 , and should therefore exhibit entirely different characteristics in this regime. Remarkably, the intensity bias *may* be the easiest quantity to generalize to strong scattering. This contention rests on the result of a preliminary analysis (Haugstad 1979b) which indicates that the mutual coherence function, which reduces to the average intensity when the two field points of its argument coalesce, may be extended in analytical form to strong scattering and an inhomogeneous background. No similar indications have been found for the phase and bending angle. These latter quantities are more easily obtained from numerical calculations, since they both involve only double integrals for even a two-dimensional propagation model. While a numerical evaluation may not be satisfactory for assessing the qualitative aspects of the systematic effects in strong scattering, this approach is fully acceptable for assessing their approximate quantitative impact on occultation experiments.

The fundamental problem and question motivating the present analysis has been to what extent turbulence in planetary atmospheres limit the accuracy of profiles of refractivity, temperature and pressure obtained from occultation measurements. We have contended, either explicitly from rigorous analysis, or from approximate or heuristic reasoning, that in the limit of weak scattering this influence is very small. An answer to the basic question should be pursued also for strong scattering conditions, and we have indicated how this might be done. The fact that turbulence effects are in all probability small, at least in weak scattering, implies an added potential of the occultation technique to also yield information on small-scale atmospheric structures. Thus, even though the effects of turbulence on derived profiles are small, its various imprints on the occultation data may be extracted and subjected to a separate analysis. Subject to the practical limitations discussed in section 7.5, this analysis would yield estimates of the turbulence strength and the outer scale in both shallow and deep occultations. In very deep occultations, where atmospheric rotation or velocities intrinsic to the atmosphere dominate over the ray speed, information also on the two former quantities are within the capabilities of the occultation technique. Since the formal, weak scattering scintillation index is typically very high in such experiments, as exemplified by the estimate for the Voyager 1 Jupiter evolute crossing, an extension to strong scattering conditions of the theory developed here is a prerequisite for measurements of this kind. If this has been successfully done, and if other sources of error can be controlled and kept on a low level, careful planning and interpretation of occultation observations may provide a very important source of information also on atmospheric circulation and dynamics.

* Recent results by this author, based on a slight generalization of the stationary phase technique developed in section 3, does show, however, that some analytical, strong scattering results for a homogeneous background (*e.g.* the mutual coherence function and the asymptotic scintillation index and power spectrum) may be simply modified to accommodate the effect of an inhomogeneous background.

Acknowledgements

The work reported here was initiated, and for the most part also completed, while the author was a visiting scientist at Center for Radar Astronomy (SCRA), Stanford University, USA. The author is deeply indebted to colleagues and friends at Stanford, who all contributed to making this place such a competent and stimulating environment for scientific endeavour. The author has particularly appreciated the close professional and personal contact with Professor Von R Eshleman, whose competent advice and encouragement have been of great help throughout the preparation of this work. The author is also indebted to Professor George L Tyler for numerous stimulating exchanges, and for permission to use the Mariner 10 Venus occultation data. Special thanks go to Dr Richard Simpson for encouragement and help, to Mr Lon Raley for his able handling of practical matters, to Mrs Harriet Smith for secretarial help and to Mrs Michal Plume for her expert typing of the various publication manuscripts. Professional contacts with Professor Allan T Waterman jr, and Dr Robert Lee are appreciated. Numerous discussions with my friend and colleague, Dr Eng-Chong Ha have also contributed to my intellectual growth while at Stanford.

The sabbatical period at Stanford was supported jointly by the Norwegian Defence Research Establishment (NDRE), by the Royal Norwegian Council for Scientific and Industrial Research through a fellowship program, and by Stanford University through a grant from the US National Aeronautics and Space Administration. The author is grateful to Director Finn Lied of the NDRE for granting the extended leave of absence, and to his Superintendent and Head of Department, Dr philos Per Thoresen, for moral and practical support during the completion of this work.

Mrs Kari Skovli and Mrs Rannveig Løken have very skilfully handled the typing and preparations for printing of this report. Mr Svein Moen is responsible for the high technical quality of all illustrations.

References

- | | |
|-------------------------------------------------------------------------|------------------------------------------------------------------------------------------------------------------------------------------------------------------------------------------|
| <p>Avduevsky, V S
M Ya Marov
M K Rozhdestvensky</p> | <p>Model of the atmosphere of the planet Venus based on results of measurements made by the Soviet automatic interplanetary station Venera 4. <i>J Atmosph Sci</i> 25, 537-45 (1968)</p> |
| <p>Baum, W A
A D Code</p> | <p>A photometric observation of the occultation of α-Arietis by Jupiter. <i>Astron J</i> 58, 108-12 (1953)</p> |
| <p>Berge, G L
S Gulkis</p> | <p>Earth-based radio observations of Jupiter: millimeter to meter wavelengths. In: <i>Jupiter</i> (Ed T Gehrels), Univ Arizona Press, Tucson, Ariz (1976)</p> |
| <p>Born, M
E Wolf</p> | <p><i>Principles of optics</i>, 5 ed, Pergamon (1975)</p> |
| <p>Bufton, J L
P O Minott
M W Fitzmaurice
P J Titterton</p> | <p>Measurements of turbulence profiles in the troposphere. <i>J Opt Soc Amer</i> 62, 1068-70 (1972)</p> |
| <p>Chatterjee, S
B Price</p> | <p><i>Regression analysis by example</i>. Wiley (1977)</p> |

- de Vaucouleurs, G
D H Menzel
- Results of the occultation of Regulus by Venus, July 7, 1959, *Nature* **188**, 28-33 (1960)
- Draper, N R
H Smith
- *Applied regression analysis*, Wiley (1966)
- Elliot, J L
D Dunham
D Mink
- The rings of Uranus, *Nature*, **267** 328-30 (1977a)
- Elliot, J L
R G French
E Dunham
P J Gierasch
J Veverka
C Church
C Sagan
- Occultation of ϵ Geminorum by Mars. II. The structure and extension of the Martian upper atmosphere. *Astrophys J* **217**, 601-9 (1977b)
- Eshleman, V R
- Radar astronomy of solar system plasmas, Scientific report 4, SU SEL-64-105, Stanford University, Calif (1964)
- Eshleman, V R
- Atmospheres of Mars and Venus. A review of Mariner 4 and 5 and Venera 4 experiments. *Radio Sci* **5**, 2, 325-32 (1970)
- Eshleman, V R
- Jupiter's atmosphere: Problems and potential of radio occultation, *Science* **189**, 876-8 (1975)
- Eshleman, V R
- Gravitational lens of the sun: its potential for observations and communication over interstellar distances, *Science* **205**, 1133-5 (1979)
- Eshleman, V R
G Ejeldbo
J D Anderson
A J Kliore
R B Dyce
- Venus: Lower atmosphere not measured, *Science* **162**, 661-2 (1968)
- Eshleman, V R
B S Haugstad
- Lowest-order average effect of turbulence on atmospheric profiles derived from radio occultation, *Astrophys J* **214**, 928-33 (1977)
- Eshleman, V R
B S Haugstad
- Effects of turbulence on average refraction angles in occultations by planetary atmospheres, *Icarus* **34**, 396-405 (1978)
- Eshleman, V R
B S Haugstad
- Comments on the W B Hubbard paper "On the atmosphere with exponential turbulence", *Icarus* **39**, 479-85 (1979)
- Eshleman, V R
G L Tyler
W T Freeman
- Deep radio occultations and "evolute flashes": Their characteristics and utility for planetary studies, *Icarus* **37**, 612-26 (1979a)

- Eshleman, V R
G L Tyler
G E Wood
G F Lindal
J D Anderson
G S Levy
T A Croft
- Fabry, C
- Fante, R L
- Fjeldbo, G
- Fjeldbo, G
W C Fjeldbo
V R Eshleman
- Fjeldbo, G
W C Fjeldbo
V R Eshleman
- Fjeldbo, G
V R Eshleman
- Fjeldbo, G
V R Eshleman
- Fjeldbo, G
A J Kliore
V R Eshleman
- Fjeldbo, G
B Seidel
D Sweetnam
T Howard
- Fjeldbo, G
A J Kliore
B Seidel
D Sweetnam
D Cain
- Freeman, K C
G Lynga
- French, R G
J L Elliot
P J Gierasch
- Radio Science with Voyager 1 at Jupiter: Preliminary profiles of the atmosphere and ionosphere, *Science* **204**, 976-8 (1979b)
- Le rôle des atmosphères dans les occultations par les planètes, *J Obs* **12**, 1-10 (1929)
- Electromagnetic beam propagation in turbulent media, *Proc IEEE* **63**, 12, 1669-92 (1975)
- Bistatic radar methods for studying planetary ionospheres and surfaces, Final Report SU-SEL-64-015, Stanford University, Calif (1964)
- Models for the atmosphere of Mars based on the Mariner 4 occultation experiment, *J Geophys Res* **71**, 9, 2307-16 (1966a)
- Atmosphere of Mars: Mariner IV models compared, *Science* **153**, 3743, 1518-23 (1966b)
- The atmosphere of Mars analyzed by integral inversion of the Mariner IV occultation data, *Planet Space Sci* **16**, 1035-59 (1968)
- Atmosphere of Venus as studied with the Mariner 5 dual radio-frequency occultation experiment, *Radio Sci* **4**, 10, 879-97 (1969)
- The neutral atmosphere of Venus studied with the Mariner V radio occultation experiments, *Astron J* **76**, 2, 123-40 (1971)
- The Mariner 10 radio occultation measurements of the ionosphere of Venus, *J Atmos Sci* **32**, 6, 1232-6 (1975)
- The Pioneer 10 radio occultation measurements of the ionosphere of Jupiter, *Astrophys J* **39**, 91-6 (1975)
- Data for Neptune from occultation observations, *Astrophys J* **160**, 767-80 (1970)
- Analysis of stellar occultation data. Effects of photon noise and initial conditions, *Icarus* **33**, 186-202 (1978)

- French, R G
J I Elliot
R V E Lovelace
- Turbulence models and the atmosphere of Uranus, *Proc 1980 Annual Meeting American Astronomical Society (DPS)*, Tucson Arizona
- Golitsyn, G S
A S Gurvich
- An estimate of refractive index fluctuations in the Venus atmosphere from Mariner 5 data, *J Atmosph Sci* 28, 138-40 (1971)
- Goodman, J W
- *Introduction to Fourier optics*, McGraw-Hill, San Francisco (1968)
- Gurvich, A S
- An estimate of the parameters of small-scale turbulence in the atmosphere of Venus obtained from fluctuations of radio signals from "Venus-4" and "Mariner-5", *Izv Atmosph Oceanic Phys* 5, 11, 1172-8 (1969)
- Haugstad, B S
- Effects of turbulence on atmospheric profiles deduced from radio occultation, *Proc 1976 Annual Meeting American Astronomical Society (DPS)*, Austin, Texas
- Haugstad, B S
- Radio occultations by turbulent planetary atmospheres: Power spectra of intensity scintillations, *Proc 1977 Annual Meeting American Astronomical Society (DPS)*, Honolulu, Hawaii
- Haugstad, B S
- Systematic turbulence errors in radio or stellar occultation intensity measurements, *Proc 1978 Annual Meeting American Astronomical Society (DPS)*, Pasadena, California (1978a)
- Haugstad, B S
- Turbulence in planetary occultations. I. A theoretical formulation, *Icarus* 35, 121-38 (1978b)
- Haugstad, B S
- Effects of the inhomogeneous background on radiation propagating through turbulent planetary atmospheres, *Radio Sci* 13, 3, 435-40 (1978c)
- Haugstad, B S
- Turbulence in planetary occultations. II. Effects on atmospheric profiles derived from Doppler measurements, *Icarus* 35, 410-21 (1978d)
- Haugstad, B S
- Turbulence in planetary occultations. III. Effects on atmospheric profiles derived from intensity measurements, *Icarus* 35, 422-35 (1978e)
- Haugstad, B S
- Turbulence in planetary occultations. IV. Power spectra of phase and intensity fluctuations, *Icarus* 37, 322-35 (1979a)

- Haugstad, B S
 Haugstad, B S
 Haugstad, B S
 V R Eshleman
 Howard, H T
 G Fjeldbo
 A J Kliore
 G S Levy
 D L Brunn
 R Dickinson
 R E Edelson
 W L Martin
 R B Postal
 B Seidel
 T T Sesplaukis
 D L Shirley
 C I Stelzried
 D N Sweetnam
 A I Zygielbaum
 P B Esposito
 J D Anderson
 I I Shapiro
 R D Reasenberg
 Hubbard, W B
 Hubbard, W B
 Hubbard, W B
 Hubbard, W B
 R E Nather
 D S Evans
 R G Tull
 D C Wells
 G W van Citters
 B Warner
 P Vanden Bout
 Hubbard, W B
 J R Jokipii
 Hubbard, W B
 D M Hunten
 A J Kliore
 Unpublished manuscript (1979b)
 - Turbulence in deep radio occultations, Paper accepted for publication in *Radio Sci.*, April 1981
 - On the wavelength dependence of the effects of turbulence on average refraction angles in occultations by turbulent planetary atmospheres, *Astrophys J* **229**, 393-8 (1979)
 - Venus: Mass, gravity field, atmosphere, and ionosphere as measured by the Mariner 10 dual-frequency system, *Science* **183**, 4131 (1974)
 Ray propagation in oblate atmospheres, *Icarus* **27**, 387-9 (1976)
 Wave optics of the central spot in planetary occultations, *Nature* **268**, 34-5 (1977)
 On the atmosphere with exponential turbulence, *Icarus* **39**, 473-8 (1979)
 The occultation of Beta Scorpii by Jupiter and Io, I, Jupiter, *Astron J* **77**, 41-59 (1972)
 Effects of turbulence on radio-occultation scale heights, *Astrophys J* **199**, L193-6 (1975)
 Effect of the Jovian oblateness on Pioneer 10/11 radio occultations, *Geophys Res Lett* **2**, 7, 265-8 (1975)

- Hubbard, W B
J R Jokipii
- Hubbard, W B
J R Jokipii
- Hubbard, W B
G V Coyne
T Gehrels
B A Smith
B H Zellner
- Hubbard, W B
J R Jokipii
B A Wilking
- Hubbard, W B
J R Jokipii
- Hunten, D M
M D McElroy
- Hunten, D M
J Veverka
- Ishimaru, A
- Jokipii, J R
- Jokipii, J R
W B Hubbard
- Keldysh, M V
- Keller, J B
- Keller, J B
- Stellar occultations by turbulent planetary atmospheres: A heuristic scattering model, *Icarus* **30**, 531-6 (1977a)
- Turbulent scattering in an exponential atmosphere: A wave-optical solution, *Astrophys J* **214**, 924-7 (1977b)
- Observations of Uranus occultation events, *Nature* **268**, 33-4 (1977)
- Stellar occultations by turbulent planetary atmospheres: A wave-optical theory including a finite scale height, *Icarus* **34**, 374-95 (1978)
- Comment on the paper "On the wavelength dependence..." by Haugstad and Eshleman, *Astrophys J* **229**, 399-401 (1979)
- The upper atmosphere of Venus. The regulus occultation reconsidered, *J Geophys Res* **73**, 4446-8 (1968)
- Stellar and spacecraft occultations by Jupiter: A critical review of derived temperature profiles. In: *Jupiter*, ed T Gehrels, Univ Arizona Press, Tucson, Ariz (1976)
- Effects of ray-bending on wave fluctuations. Paper presented at 1977 Annual Meeting of URSI, Stanford University, Stanford, Ca
- Turbulence and scintillations in the interplanetary plasma, *Ann Rev Astron Astrophys* **11**, 1-28 (1973)
- Stellar occultations by turbulent planetary atmospheres: The Beta Scorpii events, *Icarus* **30**, 537-50 (1977)
- Venus exploration with the automatic stations Venera 9 and Venera 10. Paper presented at the XIXth COSPAR meeting, Philadelphia, Pa (1976)
- *Proc Symp Appl Math* **13**, 227-46, Am Math Soc, Prov Rhode Isl (1962)
- Private communication, Stanford University, February 1977

Kliore, A
D L Cain
T W Hamilton

- Determination of some physical properties of the atmosphere of Mars from changes in the Doppler signal of a spacecraft on an Earth-occultation trajectory, JPL Techn Rept 32-674, JPL-California Institute of Technology (1964)

Kliore, A
D L Cain
G S Levy
V R Eshleman
G Fjeldbo
F D Drake

- Occultation experiments: Results of the first direct measurement of Mars' atmosphere and ionosphere, *Science* 149, 1243-8 (1965)

Kliore, A
G S Levy
D L Cain
G Fjeldbo
S I Rasool

- Atmosphere and ionosphere of Venus from Mariner 5 S-band radio occultation measurement, *Science* 158, 1683-8 (1967)

Kliore, A J
D L Cain
G Fjeldbo
B L Seidel
S I Rasool

- Preliminary results on the atmosphere of Io and Jupiter from Pioneer 10 S-band occultation experiment, *Science* 183, 323-4 (1974)

Kliore, A J
G Fjeldbo
B L Seidel
T T Sesplaukis
D W Sweetnam
P M Woiceshyn

- Atmosphere of Jupiter from the Pioneer 11 S-band occultation experiment: Preliminary results, *Science* 188, 474-6 (1975)

Kliore, A J
P M Woiceshyn

Structure of the atmosphere of Jupiter from Pioneer 10 and 11 radio occultation measurements. In: *Jupiter*, ed T Gehrels, Univ Arizona Press, Tucson, Ariz (1976)

Kliore, A J
P M Woiceshyn
W B Hubbard

Temperature of the atmosphere of Jupiter from Pioneer 10/11 radio occultations, *Geophys Res Lett* 3, 3, 113-16 (1976)

Kliore, A J
G Fjeldbo
I R Patel
D N Sweetnam
H B Holtz

Vertical structure of the ionosphere and upper neutral atmosphere of Saturn from the Pioneer radio occultation, *Science* 207, 446-9 (1980)

Kolosov, M A
O I Yakovlev
G P Yakovleva
A I Efimov

Fluctuations of radio waves and inhomogeneity of the refractive index of the Venusian atmosphere, *Kosm Issled* 8, 6, 882-8 (1970)

Kovalevsky, K
F Link

Diametre, aplatissement et propriétés optiques de la haute atmosphere de Neptune d'après l'occultation de l'étoile BD-17° 4388, *Astron Astrophys* 2, 398-412 (1969)

- Lawrence, R S
J W Strohbehn
- Lee, R W
- Lee, R W
- Lee, I C
J R Jokipii
- Lee, I C
J R Jokipii
- Liller, W
J I Elliot
J Veverka
I H Wasserman
C Sagan
- Link, F
- Lipa, B
I A Croft
- Lipa, B
G I Tyler
- Marov, M Ya
V S Avduevsky
N F Borodin
A P Ekonomov
V V Kerzhanovich
V P Lysov
B Ye Moshkin
M K Rozhdestvensky
O L Ryabov
- Mariner Stanford Group
- Martin, J M
G I Tyler
V R Eshleman
G E Wood
G F Lindal
- A survey of clear-air propagation effects relevant to optical communications, *Proc IEEE* **58**, 10, 1523-45 (1970)
- Remote probing using spatially filtered apertures, *J Opt Soc Amer* **64**, 10, 1295-1303 (1974)
- Private communication, Stanford University (1976)
- Strong scintillations in astrophysics, I The Markov approximation, its validity and application to angular broadening, *Astrophys J* **196**, 695-707 (1975a)
- Strong scintillations in astrophysics, III The fluctuations in intensity, *Astrophys J* **202**, 439-53 (1975b)
- The occultation of Beta Scorpii by Jupiter. III. Simultaneous high time-resolution records at three wavelengths, *Icarus* **22**, 82-104 (1974)
- Eclipse phenomena in Astronomy* chap 4, Springer, New York (1969)
- Refractive attenuation formulas for an unstable critical ray in a circularly symmetric medium, *Radio Sci* **10**, 6, 633-6 (1975)
- Statistical and computational uncertainties in atmospheric profiles from radio occultation: Mariner 10 at Venus, *Icarus* **39**, 192-208 (1979)
- Preliminary results on the Venus atmosphere from the Venera 8 descent module, *Icarus* **20**, 407-21 (1973)
- Venus: Ionosphere and atmosphere as measured by dual-frequency radio occultation of Mariner 5, *Science* **158**, 3809, 1678-83 (1967)
- A search for the radio occultation flash at Jupiter. Paper accepted for publication in *J Geophys Res*, October 1980

- Millis, R L
 L H Wasserman
 P V Birch
- Nicholson, P D
 D O Muhleman
- Orton, G
 A P Ingersoll
- Osawa, K
 K Ishimura
 M Shimizu
- Pannekoek, A
- Phinney, R A
 D L Anderson
- Rages, K
 J Veverka
 L Wasserman
 K C Freeman
- Salpeter, E E
- Sciff, A
 D B Kirk
 S C Sommer
 R E Young
 R C Blanchard
 D W Juergens
 J E Lepetich
 P F Intrieri
 J T Findlay
 J S Derr
- Tatarskii, V I
- Texas - Arizona Occultation Group
- Detection of rings around Uranus, *Nature* 267, 330-1 (1977)
- Independent radio occultation studies of Venus' atmosphere, *Icarus* 33, 89-101 (1978)
- Pioneer 10 and 11 and ground-based infrared data on Jupiter: The thermal structure and He-H₂ ratio. In: *Jupiter* ed T Gehrels. Univ Arizona Press, Tucson, Arizona (1976)
- Occultation of BD-17°4388 by Neptune on 7 April 1968. II. Observation at Okagama Station and the scale height of Neptune. *Tokyo Astron Bull* Second Series, 184, 2183-5 (1968)
- Über die Erscheinungen, welche bei einer Sternbedeckung durch einen Planeten auftreten, *Astron Nachr* 164, 6-10 (1903)
- On the radio occultation method for studying planetary atmospheres, *J Geophys Res (Space Phys)* 73, 5, 1819-27 (1968)
- The upper atmosphere of Neptune: An analysis of occultation observations, *Icarus* 23, 59-65 (1974)
- Interplanetary scintillations. I. Theory. *Astrophys J* 147, 2, 433-48 (1967)
- Structure of the atmosphere of Venus up to 110 kilometers: Preliminary results from the four Pioneer Venus entry probes. *Science* 203, 787-90 (1979)
- *The effects of the turbulent atmosphere on wave propagation*. Available from US Department of Commerce, National Technical Information Service, Springfield Virginia, Acc no TT68-50464 (1971)
- The occultation of Epsilon Geminorum by Mars: Analysis of McDonald data, *Astrophys J* 214, 934-45 (1977)

- Timofeeva, T S
O I Yakovlev
A I Efimov
- Radio wave fluctuation and turbulence of the nighttime Venusian atmosphere from radioscopy data of the space probe Venera 9, *Kosm Issled* 16, 2, 285-93 (1978)
- Trafton, L M
- A comment on Jovian greenhouse models, *Icarus* 19, 244-6 (1973)
- Tyler, G L
J P Brenkle
F A Komarek
A I Zygielbaum
- The Viking solar corona experiment, *J Geophys Res* 82, 28, 4335-40 (1977)
- Vakhnin, V M
- A review of the Venera-4 flight and its scientific program, *J Atmosph Sci* 25, 533-4 (1968)
- Vapillon, L
M Combes
J Lecacheux
- The β -Scorpii occultation by Jupiter, II The temperature and density profiles of the Jovian upper atmosphere, *Astron Astrophys* 29, 135-49 (1973)
- Veverka, J
L Wasserman
- The Regulus occultation light curves and the real atmosphere of Venus, *Icarus* 21, 196-8 (1974)
- Veverka, J
L Wasserman
C Sagan
- On the upper atmosphere of Neptune, *Astrophys J* 189, 569-75 (1974a)
- Veverka, J
L H Wasserman
J Elliot
C Sagan
W Liller
- The occultation of β Scorpii by Jupiter. I. The structure of the Jovian upper atmosphere, *Astron J* 79, 73-84 (1974b)
- Vinogradov, A P
U A Surkov
C P Florensky
- The chemical composition of the Venus atmosphere based on the data of the interplanetary Station Venera 4, *J Atmosph Sci* 25, 535-6 (1968)
- Wallace, L
M Prather
M J Belton
- The temperature structure of the atmosphere of Jupiter, *Astrophys J* 193, 481-93 (1974)
- Wasserman, L
J Veverka
- On the reduction of occultation light curves, *Icarus* 20, 322-45 (1973)
- Woo, R
- Observations of turbulence in the atmosphere of Venus using Mariner 10 radio occultation measurements, *J Atmosph Sci* 32, 6, 1084-90 (1975a)
- Woo, R
- Multifrequency technique for studying interplanetary scintillations, *Astrophys J* 201, 238-48 (1975b)

- Woo, R
- Radial dependence of solar wind properties deduced from Helios 1/2 and Pioneer 10/11 radio scattering observations, *Astrophys J* **219**, 727-39 (1978)
- Woo, R
A Ishimaru
- Remote sensing of the turbulence characteristics of a planetary atmosphere by radio occultation of a space probe, *Radio Sci* **8**, 2, 103-8 (1973)
- Woo, R
A Ishimaru
- Effects of turbulence in a planetary atmosphere on radio occultation, *IEEE Trans AP-22*, 4, 566-73 (1974)
- Woo, R
A Ishimaru
W B Kendall
- Observations of small-scale turbulence in the atmosphere of Venus by Mariner 5, *J Atmosph Sci* **31**, 1698-706 (1974)
- Woo, R
F C Yang
A Ishimaru
- Wave propagation in a random medium with inhomogeneous background, *Proc 1975 Annual Meeting URSI*, University of Colorado, Boulder
- Woo, R
F C Yang
A Ishimaru
- Structure of density fluctuations near the sun deduced from Pioneer 6 spectral broadening measurements, *Astrophys J* **210**, 593-602 (1976)
- Woo, R
F C Yang
A Ishimaru
- Probing the solar wind with radio measurements of the second moment field, *Astrophys J* **218**, 557-68 (1977)
- Woo, R
J W Armstrong
W B Kendall
- Measurements of turbulence in the Venus atmosphere deduced from Pioneer Venus multiprobe radio scintillations, *Science* **205**, 6, 87-9 (1979)
- Woo, R
A Ishimaru
F C Yang
- Radio scintillations during occultations by turbulent planetary atmospheres, *Radio Sci* **15**, 3, 695-703 (1980)
- Yaglom, A M
- *An introduction to the theory of stationary random functions*, Prentice-Hall, Englewood Cliffs, NJ (1962)
- Yakovlev, O I
A I Efimov
T S Timofeeva
K M Schvachkin
- Decimeter radio-wave fluctuations and energy flux during the descent of the Venera 7 and Venera 9 probes to the surface of Venus, *Kosm Issled* **12**, 1, 100-3 (1974)
- Young, A T
- Scintillations during occultations by planets. I. An approximate theory, *Icarus* **27**, 335-57 (1976)
- Young, P J
- Theory of the occultation of ϵ Gem by Mars, *Astron J* **82**, 1, 75-8 (1977)